MONITORING YEAST tRNA ADSORPTION BY QCM-D: AN OPPORTUNITY FOR OPTIMIZATION OF APTAMER SELECTION CONDITIONS

MONITORING YEAST tRNA ADSORPTION BY QCM-D: AN OPPORTUNITY FOR OPTIMIZATION OF APTAMER SELECTION CONDITIONS

BY JIETING SHANG, B.E.

A Thesis Submitted to the School of Graduate Studies in Partial Fulfillment of the Requirements for the Degree Master of Science

McMaster University MASTER OF SCIENCE (2014) Hamilton, Ontario (Chemical Engineering)

TITLE: Monitoring Yeast tRNA Adsorption by QCM-D: An Opportunity for Optimization of Aptamer Selection Conditions

AUTHOR: Jieting Shang

Pharmaceutical Engineering, B.E. (Tianjin University)

SUPERVISOR: Professor David Latulippe

NUMBER OF PAGES: 143

ABSTRACT

RNA aptamers that bind to a wide range of targets with high affinity and specificity have been identified via the *in vitro* systematic evolution of ligands by exponential enrichment (SELEX). However, the process is quite unpredictable due in part to binding that occurs not only on the targets themselves but also on any of the other functional groups, moieties, or surfaces. Recent modelling work has shown that this level of "background binding" is a key parameter in the performance of aptamer selection processes. One strategy to minimize the amount of background binding is to pre-block those possible binding sites with a non-amplifiable nucleic acid molecule, such as yeast tRNA. It is also known that binding buffer conditions have strong effect on the binding affinity of nucleic acids. However, there are no detailed studies and little quantitative information available to guide the design of aptamer selection processes. In this study, the binding ability of yeast tRNA, which has comparable size with most RNA aptamer libraries, on both silicon dioxide and poly (ethylene terephthalate glycol) (PET-G) surfaces was studied using Quartz Crystal Microbalance with Dissipation (QCM-D). Silicon dioxide surface is a commonly used substrate for QCM-D tests on the adsorption behaviour of different nucleic acid. PET-G is a commonly used polymer substrate for the fabrication of microfluidic devices, which are advanced techniques for aptamer selection. The presence of specific divalent cations, for example Mg^{2+} over Ca^{2+}, in binding buffers greatly enhanced

the binding of yeast tRNA on silicon dioxide surfaces and PET-G surfaces. Proper NaCl concentration (100 mM) and $MgCl_2$ concentration (5 mM) is necessary to enhance yeast tRNA binding on both surfaces. Yeast tRNA binding ability on silicon dioxide surfaces show more dependence on binding buffer pH than on PET-G surfaces.

TABLE OF CONTENTS

LIST OF FIGURES

LIST OF TABLES

ACKNOWLEDGEMENTS

It would not have been possible to finish my Master's of Applied Science degree at McMaster University without the help and support from my supervisor, committee members, my families, and friends.

Over the past two years, it is my great pleasure to work and study under Dr. David Latulippe's direction. He provided me excellent guidance, caring, patience, and encouraging atmosphere for doing research and study. It is an incredible experience in my life. His patience and wide knowledge provided me great guide in both research and study. David's mentorship has immeasurably influenced my personal development in my future career.

I acknowledge the members of Pelton research group for giving me complete access to their laboratory equipment and for sharing their technical expertise. I would like to thank Dr. Emily Cranston especially for her great advice and knowledgeable information about dealing with Quartz Crystal Microbalance with Dissipation (QCM-D) data analysis. I also thank Roozbeh Mafi from Dr. Pelton's research group for his kind help with the QCM-D measurement. He always provided me useful suggestions about the QCM-D technique. I appreciate the support and help for attenuated total reflection (ATR) analysis from Dr. Danielle Covelli—the research lab technician at the Biointerfaces Institute. The

administrative and technical staffs in the Chemical Engineering department were also extremely helpful.

I am truly blessed to have wonderful parents in China. They provided me incredible financial and spirit support. They were always supporting me and encouraging me with their best wishes. I also would like to thank my landlords—Connie and Jeff—who treat me as a family and offered me incredible company and support. Finally, I really appreciate about my boyfriend's endless love. He was always there cheering me up and stood by me through the good and bad times.

Chapter 1 Introduction

1.1 Introduction of Aptamer

Nucleic acid ligands, also termed as aptamers, are single-stranded DNA or RNA molecules that fold into unique three-dimensional structures that enable them to bind to a wide range of molecular targets including small molecules, proteins, and cells. The reported specificities and affinities of aptamers are comparable to those reported for monoclonal antibodies[1] . Aptamers are relatively stable under a wide range of buffer conditions and are resistant to physical or chemical degradation. Once the aptamer sequence is determined, it can be chemically synthesized at low cost.

Aptamer-binding sites include grooves and clefts that might be present on their target molecules, similar to the structures that act as binding sites for so called small-molecule drugs. This gives them highly specific, drug-like capabilities, such as antagonist activity, which can facilitate their integration into target validation and drug-screening programs. In addition, aptamers are more capable of penetrating tissues than other conventional ligands such as antibodies, because of their smaller sizes. Aptamers are also amenable to a wide variety of chemical modifications, such as radioscopic or fluorescent reporters and affinity

tags for molecular recognition. All these advantageous features made aptamers a promising alternative to antibodies and other protein-based ligands.

These properties led to a growing interest of different application of aptamers including chemical separation, biotechnology, environmental technology and therapeutics. Aptamers targeted to vascular endothelial growth factor -165[2] found utility in the treatment of wet macular degeneration initially. Later on, a range of targets against aptamers were found in bloodstream, such as thrombin, factor IXa and von Willebrand factor, or on cell surfaces such as epidermal growth factor receptor[3] . It may eventually be possible to use aptamers to access the targets inside tissues or cells by delivering either themselves or drugs across membrane. Particularly the utility in tumor immunotherapy, aptamers were found be able to inhibit the activity of mutation proteins in tumor cells. One such example is the receptor tyrosine kinase[4]. However, the *in vivo* application of such aptamers still remained to be estimated.

A numbers of studies have immobilized DNA or RNA aptamers onto chip-based biosensors for the detection of specific targets including nucleic acids, proteins, small molecules and inorganic cations. McCauley *et al.*[5] developed a chip-based biosensor which utilizes immobilized DNA and RNA aptamers to simultaneously detect and quantify levels of cancer-associated proteins (inosine monophosphate dehydrogenase II, vascular endothelial factor, basic fibroblast

growth factor) in the context of human serum and in cellular extracts. Xiao *et al.*[6] immobilized a methylene blue tagged, thrombin-binding DNA aptamer on a gold surface, which allows the electrochemical quantity detection of thrombin in blood serum. Swensen *et al.*[7] reported a Microfluidic Electrochemical Aptamer-based Sensor chip, which could continuously detect the small-molecule drug cocaine at near physiological, low micromolar concentrations directly in undiluted and unmodified blood serum.

Aptamers can also be effective affinity purification reagents. Romig *et al.*[8] immobilized a DNA-aptamer specific for human L-selectin to a chromatography support to create an affinity column. It was applied to efficiently purify a recombinant human L-selectin–Ig fusion protein from Chinese hamster ovary cell-conditioned medium. The fusion protein was efficiently bound to the column and efficiently eluted by gentle elution schemes. Application of the aptamer column as the initial purification step resulted in a 1500-fold purification with an 83% single step recovery. Cho *et al.*[9] developed a microbead-based affinity chromatography chip to separate and analyze hepatitis C virus RNA polymerase protein by immobilization of an RNA aptamer on beads.

Therefore, aptamers are attracting an increasing amount of interest in the development of chemical separation, biosensors, and clinic therapeutic applications.

1.2 Aptamer Selection Process

In 1990, two studies from the Szostak[10] and Gold[11] groups independently described an *in vitro* method for identifying aptamers that bind to a specific target. This method was called SELEX—Systematic Evolution of Ligands by Exponential Enrichment. It relies on the development of DNA synthesis methods which enable the generation of a large population of oligonucleotides, and polymerase chain reaction (PCR) which allows small numbers of molecules to be amplified into large amounts. It involves the progressive evolution of a combinatorial library of nucleic acid ligands to an enriched pool with high affinity to a particular target via repeated rounds of partitioning and amplification. With the development of aptamer technology in the last decades, various SELEX processes have been established that allowed various aptamers to be developed against a wide range of targets[12].

Traditional SELEX starts with a synthesised oligonucleotide library of double stranded DNA molecules (~100 bp) that feature a randomized sequence region flanked by constant regions. The latter are necessary for the amplification step. The starting library typically contains a few copies of between 1×10^{13} and 1×10^{15} molecules. In the case of DNA aptamer SELEX, the starting library is simply generated by thermal denaturation of the double stranded DNA molecules. In the case of RNA aptamer SELEX, the starting library is prepared by *in vitro*

transcription of the DNA templates with T7 RNA polymerase. During the selection process, a small fraction of the starting library binds to the target molecule at the given buffer and temperature conditions (Fig.1.2.1). The aptamers with properties to specifically bind to the targets can be separated from non-specific binding aptamers by various partition techniques such as membrane filtration, chromatography, surface plasma resonance, and electrophoresis[13] . Then the selected sequences are amplified to create a new pool that is used for the next selection round. To achieve the SELEX process, typically eight to fifteen cycles are usually needed[14,15]. Thus, the generation of aptamers by SELEX requires a significant investment of time, labour, and resources. Therefore, the SELEX technique needs to be improved urgently to achieve an efficient and reproducible aptamer selection process.

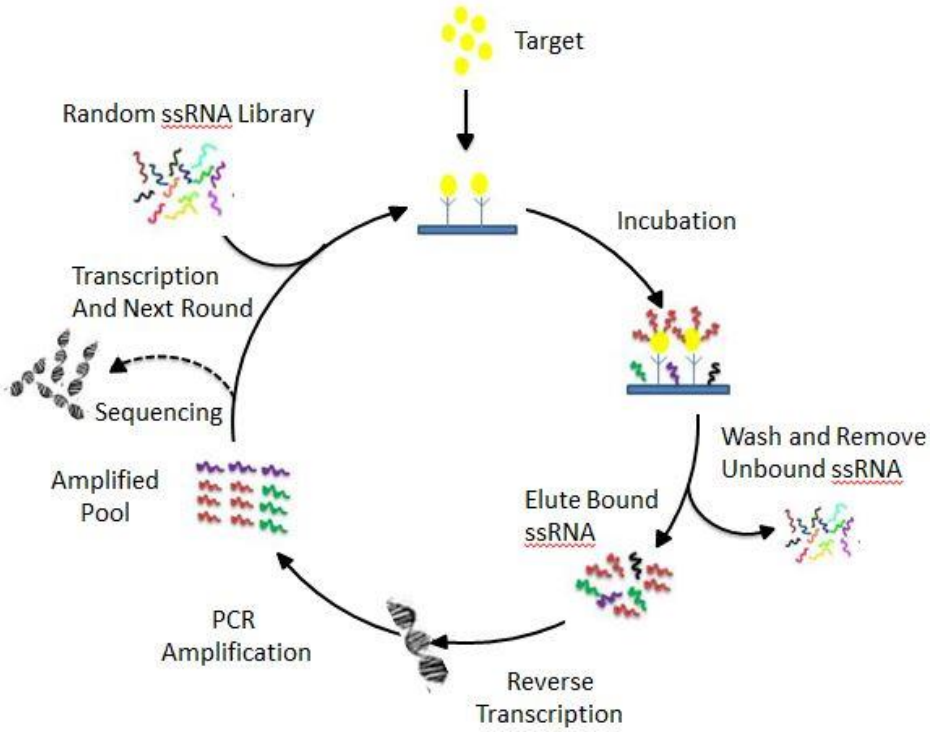

Fig.1.2.1. *In vitro* selection scheme: Aptamers for specific targets were separated from a huge randomized library (RNA library as an example) by a separation technique. The bound molecules are regenerated by amplification process for next selection process.

1.3 The Effect of Binding Buffer Conditions on SELEX

To date, a large number of DNA and RNA aptamers have been identified that bind to various molecule targets (Table S1)[12,16]. During SELEX process, temperature, incubation time, target concentration, DNA or RNA library concentration, and binding buffer condition will affect the aptamer binding behaviour and selection efficiency. However, only a few studies to date have

addressed quantity analysis about aptamer binding behaviour with different buffer conditions. Ahmad *et al.*[17] used a microfluidic selection process (M-SELEX) to examine the effect of the binding buffer pH on aptamer affinity. They successfully isolated three DNA aptamers against different protein targets with different isoelectric points through M-SELEX within only three cycles. The results showed that the binding buffer pH could dramatically influence the aptamer binding affinity by changing the target's net charges. Selection of aptamer against platelet derived growth factor B at the higher pH of 8.4, yielded an aptamer pool with lower affinity (K_d = 0.22 nM), while the selection performed at the lowest pH of 4.6, yielded the aptamer pool with the highest affinity (K_d = 0.044 nM). The dissociation constant (K_d) is commonly used as description of the affinity between aptamer and a target molecule. The smaller the dissociation constant, the more tightly bound the aptamer to its target molecule. Bridonneau *et al.*[18] found that binding affinity of the aptamer 15, which binds human nonpancreatic secretory phospholipase A2 (hnps-PLA2), decreased approximately ten-fold in the absence of Ca^{2+}. Since the 2'-NH_2 moiety of the purine nucleotides was an ionizable group with pKa of about 6.5, they found that RNA aptamer 15 had 10-times higher affinity against hnps-PLA2 at high pH. Carothers *et al.*[19] conducted parallel selection for *p*-amino phenylalanine (*p*AF) aptamers in four buffers with different concentrations of magnesium (1, 2.5, 5 and 10 mM), since magnesium concentration is significant to aptamer structure stability. They reported that the

pAF aptamer SELEX efficiency was highest at 2.5 mM magnesium concentration. By round ten, 25% of the total RNA in the 2.5 mM magnesium binding buffer exhibited binding, while 14%, 9%, and 2% of the total RNA in the 1, 5 and 10 mM magnesium bound the column. Therefore, fully understanding the influence of binding buffer condition on aptamer binding affinity is necessary in order to optimize aptamer SELEX process.

Moreover, optimizing the buffer conditions of aptamer selection could increase the likelihood to isolate specific aptamer. Topp *et al.*[20] developed an automated buffer testing protocol to test target-to-unselected RNA pool binding in 96 different buffer conditions, and concluded that binding buffer with divalent salt, such as $MgCl_2$ and $CaCl_2$, pH of 7.5 was the optimum binding buffer condition for aptamer SELEX process. They also pointed out that different monovalent salt would affect the aptamer binding affinity as well. Through analyzing the sensitive of thrombin-aptamer-binding sensor under different binding buffer conditions, Hianik *et al.*[21] found that increased concentration of Na^+ in binding buffer resulted in weakening of the binding of thrombin to the aptamers, due to shielding effect of Na^+. They also found that the method of aptamer immobilization, binding buffer pH, and the aptamer structure could influence the binding affinity of aptamers. Their results indicated that the aptamer-thrombin binding behavior acted best at binding buffer with pH of 7.5. Krauss *et al.*[22] found that K^+ markedly stabilizes thrombin-binding aptamer compared with Na^+.

Other than monovalent salt, divalent salt, and pH, the buffer species has also been found to affect aptamer binding to its target. Cho *et al.*[23] found that different selecting buffer base, such as tris (hydroxymethyl) aminomethane (Tris), phosphate buffered saline (PBS), and 4-(2-hydroxyethyl)-1-piperazineethanesulfonic acid (HEPES), influenced the binding strength in aptamer *in vitro* selection process. By using thermophoresis to separately determine the binding curve of thrombin aptamer and ATP aptamer in different buffer conditions (respective selection buffer, sodium citrate buffer and human serum), Baaske *et al.*[24] found that they all showed highest binding affinity in the buffer matched what was used for the selection process. They hypothesized that this behavior is due to the charge competition effects in other buffer conditions. Therefore, the efficiency of SELEX can be improved by adjusting the aptamer binding buffer condition, including the presence of divalent cations, concentration of monovalent salt, concentration of divalent salt, buffer species, and pH.

1.4 The Effect of Binding Buffer Conditions on Double Stranded DNA or RNA Adsorption Kinetics

Similar with DNA or RNA aptamer, the binding behavior of double stranded DNA or RNA was also influenced by binding buffer conditions. Vandeventer *et al*.[25] studied DNA adsorption kinetics to bare silica surface under

different buffer conditions through bulk depletion and quartz crystal microbalance (QCM) experiments. They found out that the amount of DNA adsorption increased with increasing KCl concentration, but decreased sharply with increasing pH. The authors also pointed out more DNA adsorbed to silica when a chaotropic salt was used. Nguyen *et al*.[26] monitored variations in frequency and dissipation energy using QCM-D and reported that the adsorbed DNA layer on silica surface was more rigid in the presence of divalent cations (Ca^{2+}) compared to monovalent cations (Na^{+}). Franchi *et al*.[27] found that the cations directly took part in the adsorption of nucleic acids to mineral surfaces, acting as a 'bridge' between the negative charges on the mineral surface and those of the phosphate groups of nucleic acids. Moreover, the divalent cations are more efficient than monovalent ones in mediating the nucleic acid adsorption. Cai *et al*.[28] pointed out that increasing pH could decrease the adsorption of DNA on clay minerals in some degree. By analyzing the measurement from QCM-D, Shen *et al.*[29] found that the presence of divalent cations (Ca^{2+}) in solutions greatly enhanced the deposition kinetics of RNA on bare silica surfaces, and made the deposited RNA more likely to be irreversible. They pointed out that solution pH affected the deposition behavior of RNA on silica surfaces as well. The release experiments which they furthermore performed indicated that detachment of RNA from silica surfaces was more significant in NaCl solutions than in $CaCl_2$ solutions at the same concentration. Therefore, it can be convinced that binding buffer with

variety ionic strength, different cations, and different pH can affect the binding behavior of both double-stranded and single-stranded nucleic acids.

1.5 The Influence of Non-specific Background Binding in SELEX

One of the tricky part for SELEX is to separate the specific binding aptamers from non-binding ones. However, the partition process of SELEX cannot remove all non-specific bound background aptamers from specific bound aptamers. Thus a fraction of unbound aptamers will be present in the next selection round.

Wang *et al.*[30] developed a mathematical model to address the influence of non-specific background binding on the efficiency of SELEX process. In the ideal case, in which only aptamers specifically bound to target molecules were recovered and transferred to next selection round, minimizing the target concentration could increase the selection efficiency. However, the fact was that no experimental separation process could perfectly separate the specific aptamers from non-specific bound background ones. This was extremely important when using lower target molecule concentrations, as the level of background binding could overwhelm and undermine the aptamer recovery which was used as the starting pool for next selection round. The authors compared two different selection methods with this mathematical model, and concluded that the one with

lower background binding offered dramatic advantage to improve the SELEX efficiency. It not only allowed greater flexibility in experiment design because it could tolerate much wider range of target concentrations, but also could generate higher affinity aptamers in few selection rounds. Furthermore, Latulippe *et al.*[31] designed a reusable PET-G microcolumn process for the efficiency selection of RNA aptamers for multiple target molecules. At the beginning of each experiment, yeast tRNA in binding buffer was introduced to block any possible non-target binding sites in microcolumn. However, the quantitative polymerase chain reaction (qPCR) analysis results showed that there were still countable amount of non-target-bound oligonucleotides went into next selection round together with target-bound aptamers after partition process, even when the measurement was taken in the empty microcolumn without any target molecule immobilized on the surface. These findings emphasizes that minimizing the background binding is significant to increase the SELEX efficiency and need to be fully understood.

However, there is no realistic separation process to totally separate the specific target-bound aptamer from non-specific background bound molecules. The easier way to minimize the background binding is to enhance the yeast tRNA background blocking ability in order to avoid any non-specific molecule binding to the surface. Since the binding buffer has great influence on the binding behaviour of nucleic acids including both double stranded and single stranded DNA and RNA, it is necessary to understand whether pH, monovalent salt

identity, monovalent salt concentration, divalent salt identity, and divalent salt concentration will affect the yeast tRNA blocking behaviour on both silicon dioxide surfaces and PET-G surfaces.

1.6 Measuring the Yeast tRNA Binding Behaviour Using QCM-D

In order to better understand the yeast tRNA binding behavior onto SiO_2 and PET-G surfaces under a wide range of binding buffer conditions, QCM-D was employed. QCM-D is a highly sensitive mass and dissipation measuring device. Its resonance frequency decreases linearly with the increase of adsorption mass on a quartz crystal surface, Its additional measurement of damping in the crystal oscillation, called dissipation is related to viscoelastic properties[32].

QCM-D has been confirmed as an advanced equipment to study nucleic acids' adsorption behavior under different buffer conditions. Sato *et al.*[33] invested the adsorption of oligonucleotides onto cellulose surfaces using QCM-D. The authors pointed out that Boese and Breaker's cellulose binding oligonucleotide showed higher maximum adsorption onto cellulose, particularly at high Ca^{2+} strength conditions (100 mM $CaCl_2$). Shen *et al.*[29] examined the deposition kinetics of RNA on silica surfaces under a wide range of environmental related buffer conditions with a wide range of monovalent salt, divalent salt, ionic strength, and pH using QCM-D. The authors found that the deposition rate was

higher when the buffers contained high concentration of Ca^{2+} at lower pH (pH=6.0) than the buffers contained single monovalent salt. Michanek *et al*.[34] used QCM-D to compare the binding ability of yeast tRNA onto two different bilayers. Nguyen *et al*.[26] found that the adsorbed plasmid DNA layer was more rigid in the presence of divalent salt cations (Ca^{2+}) compared to monovalent cations (Na^{+}), which was modeling from QCM-D measurement results.

Since the QCM-D is a highly sensitive mass measuring device, they can monitor DNA or RNA aptamer *in vitro* selection process due to the mass change and evaluate the affinity constant of the selected aptamers as well. Fukusho *et al*.[35] used the Quartz Crystal Microbalance (QCM) to select RNA aptamers which could specially bind to Rev peptide by designing a simple α-helical peptide QCM sensor model. They successfully achieved the selection within seven rounds due to the high sensitivity of QCM. They also measured the association constant of Rev peptide targeted RNA aptamer afterwards. Based on this, the authors[36] further improved the QCM SELEX process by immobilizing all spots on Au QCM sensors with N-peptide which was claimed has higher ability for binding RNA aptamers. Through the analysis of QCM frequency shift, they furthermore concluded the preference sequence of RNA aptamer to Rev peptide.

As a well-established technique, QCM-D has become an incredible instrument to quantify relative small molecule adsorption (like ng/cm^2) and

detachment at the solid-liquid interface in real time due to its high sensitive and accuracy. To illustrate the influence of binding buffer conditions on yeast tRNA background blocking during aptamer SELEX process, QCM-D was employed in this study. Two different QCM-D sensor surface—silicon dioxide and PET-G – as the background binding material were used in measurements.

Numerous of studies have used silicon dioxide surface for DNA or RNA binding studies[37,38,39], it is a good starting surface to roughly determine the binding behaviour of yeast tRNA under various binding buffers. Moreover Indest *et al*.[40] measured the adsorption behaviour of human serum albumin (HSA) on differently modified poly (ethylene terephthalate) (PET) coated surface with QCM, which provided the possibility to measure the yeast tRNA binding ability on PET-G surfaces with QCM-D. PET-G is also a commonly used substrait for microfluid devices which was used as an advanced technique for aptamer *in vitro* selection[31]. Therefore, it is necessary and significant to measure the yeast tRNA binding behaviour on PET-G surfaces with QCM-D.

In this study, the binding ability of yeast tRNA onto silicon dioxide surfaces and PET-G surfaces were experimentally characterized using QCM-D. The effect of different monovalent cations, different divalent cations, variety cation strength, and different pH of binding buffer conditions on yeast tRNA adsorption behavior were studied. The knowledge gained from this study can be

further used to optimize the DNA or RNA aptamer *in vitro* selection process by minimizing non-specific background binding.

Chapter 2 Detailed Summary of Published SELEX Buffer Conditions

In order to determine the binding buffer conditions needed to be tested, binding buffer conditions used in eighty-five previous aptamer selection studies (Table S-1) were summarized. It apperared that in these literatures, the binding buffers for aptamer selection process were mostly chosen based on previous experience. There is little quantified analysis about whether a specific cation and its concentration in binding buffer can affect the selection performance. Therefore, it is significantly necessary to quantify the effect of binding buffer conditions on yeast tRNA binding to silicon dioxide and PET-G surfaces in order to maximize its pre-blocking ability before aptamer *in vitro* selection process.

2.1 Monovalent Salt Conditions

More than half (56%) of the reviewed studies used sodium chloride (NaCl) as monovalent salt in binding buffers for SELEX (Fig. 2.1). Potassium chloride (KCl) was an alternative monovalent salt in binding buffers, but sometimes used at low concentration (from 1 mM to 5 mM) together with high concentration of NaCl (from 100 mM to 450 mM). Only 1% of the reviewed studies used LiCl as the monovalent salt in binding buffer. 6% of these eighty-five studies did not use any monovalent salt in their binding buffers. Various concentrations of single NaCl or KCl as monovalent salt were also used in the binding buffers (Fig. 2.2

and Fig. 2.3). Almost half (44%) of the reviewed studies set the concentration of NaCl in binding buffers ranging from 100 mM to 150 mM, while 15% of them used 1 mM to 50 mM as the NaCl concentration, and 21% of them used 200 mM to 250 mM as the NaCl concentration in binding buffers. Only a small percent of the reviewed studies used higher concentration of NaCl (from 300 mM to 1000 mM) in binding buffers for aptamer *in vitro* selection. 41% of the reviewed SELEX studies used 1 mM to 5 mM KCl together with NaCl as monovalent salt in binding buffers. 21% of the reviewed SELEX process used 50 mM KCl in the binding buffers. 23% of them set the concentration of KCl ranging from 100 mM to 150 mM, while only 18 % of the reviewed SELEX processes used higher KCl concentration ranging from 300 mM to 1000 mM.

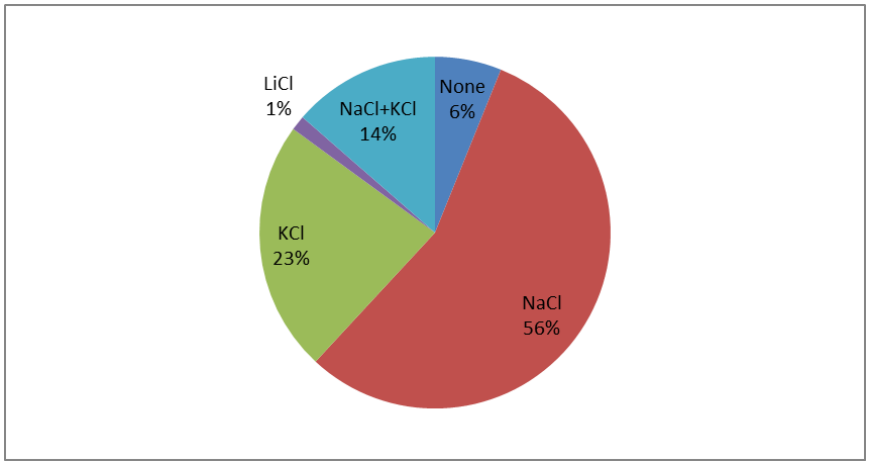

Fig.2.1. Comparison of monovalent salt type in SELEX binding buffers from eighty-five different studies found in the literature; see Table S1 in the Appendix for detailed summary of the exact buffer composition.

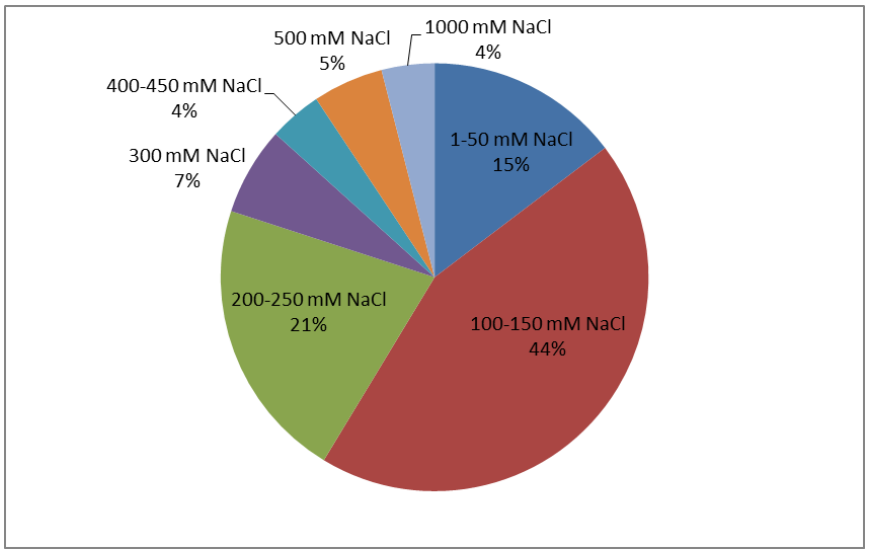

Fig.2.2. Comparison of sodium chloride concentration in SELEX binding buffers from sixty different studies found in the literature; see Table S1 in the Appendix for detailed summary of the exact buffer composition.

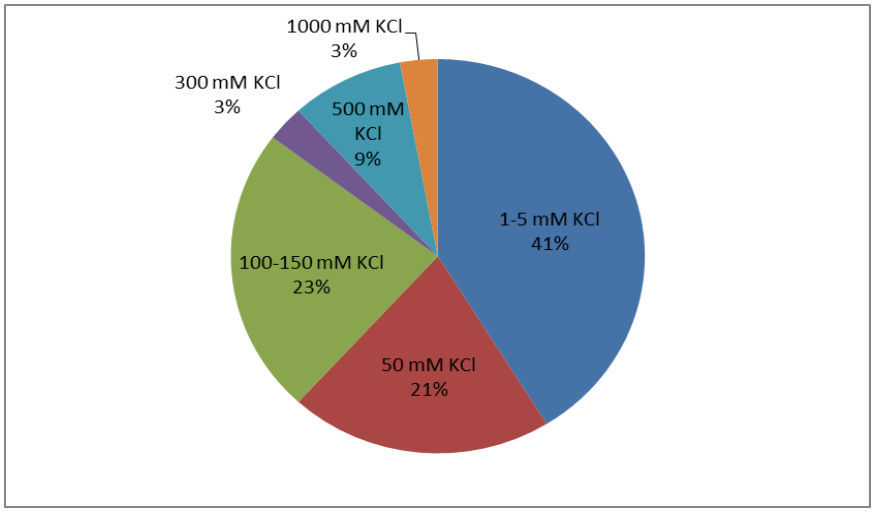

Fig.2.3. Comparison of potassium chloride concentration in SELEX binding buffers from thirty-one different studies found in the literature; see Table S1 in the Appendix for detailed summary of the exact buffer composition.

2.2 Divalent Salt Conditions

Divalent salt was reported acting as the "bridge" between nucleic acid and target molecule[27], which is significant in improving the binding affinity of aptamers. The interaction between oligonucleotide and divalent cation reduces the negative charges of oligonucleotides and results in the less repulsion between aptamer and its target molecule. Since the RNA backbone is polyanionic, the negative-negative charge repulsion may inhibit formation of compelete structures in the absence of counterions. Divalent cations can help screen this charge and enable the backbone to fold closer to it[41]. Mg^{2+} was the most often (72%) used divalent cation in these 85 reviewed studies, while 17% reviewed SELEX studies

used Ca^{2+} instead (Fig 2.4). The other 4% and 2% of the reviewed studies used $ZnCl_2$ and $MnCl_2$ as divalent salt in binding buffers. Only 5% of the studies did not contain any divalent salt in binding buffers.

Moreover, different concentrations of divalent salt in binding buffers were used in aptamer SELEX processes. From present reviewed studies, the $MgCl_2$ concentration varied from 0.5 mM to 100 mM (Fig. 2.5). Most studies used a $MgCl_2$ concentration of 1 mM (24%), 5 mM (39%), or 10 mM (14%). Interestingly, 1 mM magnesium concentration is consistent with the amount of free magnesium that is present *in vivo*.

The concentration of $CaCl_2$ used in binding buffers ranged from 0.3 mM to 5 mM (Fig 2.6). 7% of the reviewed studies set the $CaCl_2$ concentration at 0.3 mM. 43% of the reviewed studies used 1 mM as the concentration of $CaCl_2$. 14% of the reviewed studies used 2 mM $CaCl_2$ in binding buffers, while 36% of them used 5 mM $CaCl_2$ in binding buffers.

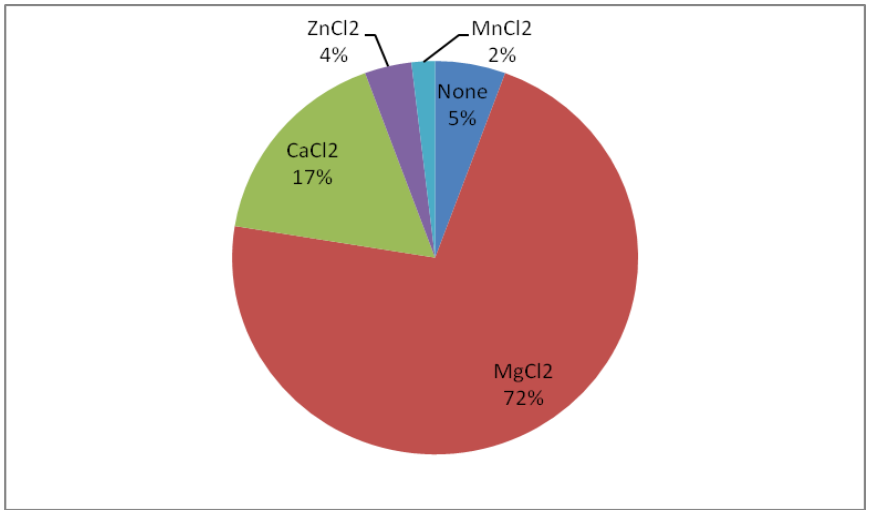

Fig.2.4. Comparison of divalent salt type in SELEX binding buffers from eighty-five different studies found in the literature; see Table S1 in the Appendix for detailed summary of the exact buffer.

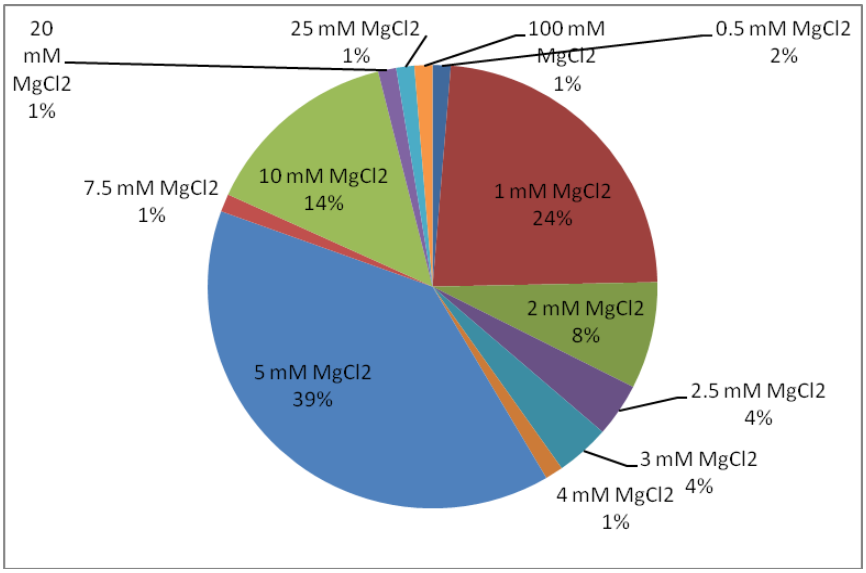

Fig.2.5. Comparison of magnesium chloride concentration in SELEX binding buffers from sixty-one different studies found in the literature; see Table S1 in the Appendix for detailed summary of the exact buffer composition.

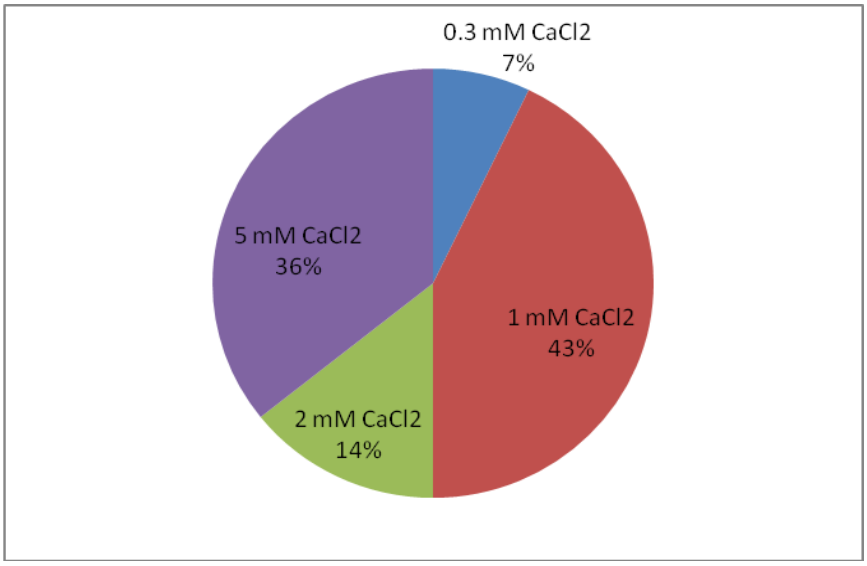

Fig.2.6. Comparison of calcium chloride concentration in SELEX binding buffers from fifteen different studies found in the literature; see Table S1 in the Appendix for detailed summary of the exact buffer composition.

2.3 pH conditions

It is known that pH influenced binding affinity of both single stranded and double stranded nucleic acids. Most of the SELEX processes (85%) used binding buffers at pH between 7.4 to 7.6 (Fig. 2.7). 3% of the reviewed studies used binding buffers with pH of 6.4. 7% of reviewed aptamer selection processes used binding buffers with pH ranging from 7.0 to 7.3. 5% of them used binding buffers with pH ranging from 8.0 to 8.5.

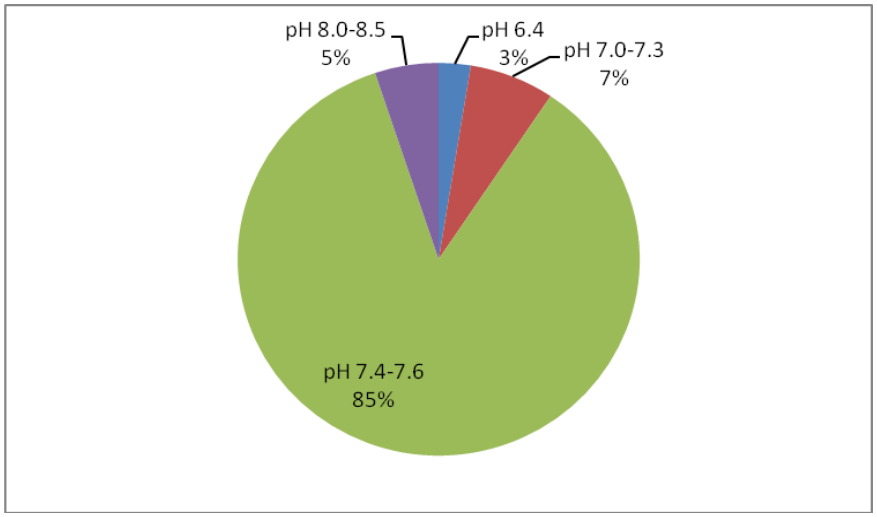

Fig.2.7. Comparison of pH values of SELEX binding buffers from eighty-five different studies found in the literature; see Table S1 in the Appendix for detailed summary of the exact buffer composition

Chapter 3: Materials and Methods

3.1 Yeast tRNA Preparation

Yeast tRNA is the transfer RNA purified from brewer's yeast. Previous studies have used it as a carrier in nucleic acid purification[42] as well as a non-amplifiable blocker molecule in aptamer selection studies[31]. It is a single stranded RNA molecule, typically 73 to 94 nucleotides (nt) in length. It serves as the carrier to bring amino acid sequence to ribosome for protein synthesis, which was directed by message RNA in a cell. Yeast tRNA has the typical cloverleaf structure which is a common RNA tertiary structure motif.

When working with yeast tRNA, care must be taken to create a ribonuclease (RNase)-free environment[43]. Ribonuclease (RNase), which can catalyze the degradation of RNA into smaller components, is stable and thus special processing steps were required to inactivate them. To ensure the experiment can be successful, it is important to maintain a ribonuclease-free environment. Milli-Q ultrapure water, which is from Millipore purification system, was treated by adding diethyl pyrocarbonate (DEPC) (Biosciences), to a final concentration 0.1%[44] and incubating the solution at 37 ℃ overnight. DEPC destroys the enzymatic activity of RNase by binding to the active site. The DEPC treated Milli-Q water (DEPC-H_2O) was then autoclaved at 120 ℃ for 20 min to

inactivate the DEPC. All the nucleic acid solutions were prepared in DEPC treated Milli-Q water in order to minimize the occurrence of degradation. Additionally, sterile, disposal plasticware was used to store the solutions. Any non-disposal glassware were firstly soaked in 0.1% DEPC-treated Milli-Q water overnight[45].

The QCM-D experiments were performed with yeast tRNA from approximate 60-90 nt in size, which was purchased from Invitrogen Life Technologies. Stock solution of yeast tRNA at the concentration of 10 μg/μL was prepared as follows. 2.5 mL DEPC treated Milli-Q water was added to the vial containing 25 mg yeast tRNA powder, and dissolved it gently. Then 250 μL of the yeast tRNA stock solution was aliquoted into ten Eppendorf tubes and stored at -20 ℃. Storage at this temperature is sufficient to maintain yeast tRNA integrity for over 2 years[46].

3.2 RNA Library Preparation

GSN70 RNA Library[31] was also used as comparison to confirm that yeast tRNA was a suitable material to block the background in aptamer SELEX process. It was prepared as follows. One vial containing about 7.2 mg (24 copies of 5×10^{15} RNA library) of GSN70 library was centrifuged at 4 ℃ for 30 min. The pellet was then rinsed with 1 mL of 70% ethanol (Commercial Alcohol) gently, and

centrifuged at 4 ℃ for another 5 min. The ethanol was completed removed from pellet using pipette. Then the pellet was re-suspended in 1 mL DEPC treated Milli-Q water to a final concentration of 7.2 μg/μL and aliquoted into four Eppendorf tubes (250 μL per tube) and stored at -20 ℃ for further experiment.

3.3 RNA Denaturing Gel Electrophoresis

8% denaturing vertical gel[47] and a low range ssRNA ladder purchased from New England Biolabs (NEB), were used to detect the length, concentration, and integrity of the yeast tRNA and GSN 70 RNA Library[31].

3.3.1 8% Denaturing Gel Preparation

Denaturing polyacrylamide gel stock solution was made by mixing 250 g of urea (EMD), 50 mL of 10×TBE buffer (Tris/Boric Acid/EDTA Buffer, 1×Solution: 89 mM Tris, 89 mM boric acid, 2 mM EDTA, pH 8.4, purchased from Bio-Rad), 132.5 mL of 30% Acrylamide/Bis Solution (Bio-Rad) and Milli-Q water together to the total volume of 500 mL. The solution was then stirred to dissolve with a stir bar and heated briefly in a 60℃ water bath. Two gels were made at the same time by adding 75 μL of 10% ammonium persulfate (APS, Bio-Rad) and 7.5 μL of Tetramethylethylenediamine (TEMED) (Fisher BioReagents)

to 15 mL of denaturing gel stock solution. The final concentration of urea in the gel was 8 M. Vertical gels were prepared by immediately pouring 7 mL of thoroughly mixed gel solution between the gel plates (Bio-Rad), inserting a 11-well comb, and allowing the gel to polymerize at room temperature for 1 hour.

3.3.2 Gel Loading RNA Sample Preparation

To prepare a gel loading RNA sample, 5 μL RNA solution and 5 μL 2×RNA loading buffer (NEB) were mixed in 1.5 mL Eppendorf tube. Then gel loading RNA samples were heated in 65 ℃ water bath for 5 min, and chilled on ice for at least 5 min.

3.3.3 8% Denaturing Gel Electrophoresis

Gels were loaded into a Mini-Sub Cell GT electrophoresis system (Bio-Rad) that had been pre-filled with 230 mL of 0.5×TBE buffer. The comb was then gently removed from the gel to expose the wells. Each well of the gel was rinsed with 0.5×TBE buffer before loading any samples. The low range ssRNA ladder was loaded into at least one well of the gel as a reference marker. The ladder consists of 6 fragments ranging from 50 to 1,000 nt. The RNA samples were then loaded into the other wells one by one. The majority of the gels were run for 45

min at 180 V using a PowerPac Basic power supply (Bio-Rad) until the indicator dye in the ladder running to the bottom of the gel.

3.3.4 Gel Stain after Electrophoresis

The gels were stained with 50 mL of SYBR® Safe working solution (Invitrogen), prepared by a 10,000:1 dilution of the stock solution with 1×TBE buffer, for 30 min on a shaker platform. The gels and staining solution were protected from light by covering it with aluminum foil. Gel images were captured using a Typhoon 9400 scanner (GE Healthcare) and analyzed using ImageQuant 5.2 software.

3.4 Buffers in QCM-D Experiments

3.4.1 Binding Buffers

To prepare the various buffer solutions that were required for this work, the following five stock solutions were prepared:

- 500 mM Tris (Tris(hydroxymethyl)aminomethane, Bio-Rad) in DEPC-H_2O
- 2500 mM NaCl (Fisher Science) in DEPC-H_2O

- 2500 mM KCl (EMD) in DEPC-H_2O
- 50 mM $MgCl_2$ (Fisher Science) in DEPC-H_2O
- 50 mM $CaCl_2$ (Fisher Science) in DEPC-H_2O

Any binding buffer composition with desired salt type and concentration was made by diluting these stock solutions with DEPC-H_2O. All the binding buffers were prepared 24 hours before each measurement in case of contamination. The pH was adjusted with 0.1 mM HCl (Fisher Science) in DEPC-H_2O or 0.1 mM NaOH (Fisher Science) in DEPC-H_2O.

A total of fourteen different buffers were prepared; details on the composition of each one are shown in Table 3.4.1.

Table 3.4.1 Binding Buffer for QCM-D Experiments on Silicon Dioxide Surfaces

Binding Buffer	Buffer Base	NaCl (mM)	KCl (mM)	$MgCl_2$ (mM)	$CaCl_2$ (mM)	pH
A	25 mM Tris	100	-	-	-	7.5
B	25 mM Tris	100	-	0.2	-	7.5
C	25 mM Tris	100	-	1	-	7.5
D	25 mM Tris	100	-	5	-	7.5
E	25 mM Tris	100	-	25	-	7.5
F	25 mM Tris	100	-	5	-	6.5
G	25 mM Tris	100	-	5	-	8.5
H	25 mM Tris	25	-	5	-	7.5
I	25 mM Tris	400	-	5	-	7.5
J	25 mM Tris	-	100	5	-	7.5
K	25 mM Tris	100	-	-	0.2	7.5
L	25 mM Tris	100	-	-	1	7.5
M	25 mM Tris	100	-	-	5	7.5
N	25 mM Tris	100	-	-	25	7.5

A subset of these fourteen buffers was used to investigate the effects of buffer composition. For example, the influence of the divalent cation on yeast tRNA binding to a silicon dioxide surface was measured by comparing the QCM-D results for binding buffers A, D, and M (see Table 3.4.2).

Table 3.4.2 Binding Buffers to Measure the Influence of Divalent Salt on Yeast tRNA Binding to SiO_2 Surfaces and PET-G surfaces

Binding Buffer	Buffer Base	NaCl (mM)	KCl (mM)	$MgCl_2$ (mM)	$CaCl_2$ (mM)	pH
A	25 mM Tris	100	-	-	-	7.5
D	25 mM Tris	100	-	5	-	7.5
M	25 mM Tris	100	-	-	5	7.5

The influence of divalent salt ($MgCl_2$ and $CaCl_2$) concentration on yeast tRNA binding to a silicon dioxide surface was measured by comparing the QCM-D results for binding buffers B, C, D, E, K, L, M, N(see Table 3.4.3):

Table 3.4.3 Binding Buffers to Measure the Influence of Divalent Salt Concentration on Yeast tRNA Binding to SiO_2 Surfaces and PET-G surfaces

Binding Buffer	Buffer Base	NaCl (mM)	KCl (mM)	$MgCl_2$ (mM)	$CaCl_2$ (mM)	pH
B	25 mM Tris	100	-	0.2	-	7.5
C	25 mM Tris	100	-	1	-	7.5
D	25 mM Tris	100	-	5	-	7.5
E	25 mM Tris	100	-	25	-	7.5
K	25 mM Tris	100	-	-	0.2	7.5
L	25 mM Tris	100	-	-	1	7.5
M	25 mM Tris	100	-	-	5	7.5
N	25 mM Tris	100	-	-	25	7.5

The influence of different monovalent salt (NaCl and KCl) on yeast tRNA binding on a silicon dioxide surface was measured by comparing the QCM-D results for binding buffers D and J (see Table 3.4.4).

Table 3.4.4 Binding Buffers to Measure the Influence of Monovalent Salt on Yeast tRNA Binding to SiO_2 Surfaces and PET-G surfaces

Binding Buffer	Buffer Base	NaCl (mM)	KCl (mM)	$MgCl_2$ (mM)	$CaCl_2$ (mM)	pH
D	25 mM Tris	100	-	5	-	7.5
J	25 mM Tris	-	100	5	-	7.5

The effect of monovalent salt (NaCl) concentration on yeast tRNA binding on a silicon dioxide surface was measured by comparing the QCM-D results for binding buffers D, H, and I(see Table 3.4.5).

Table 3.4.5 Binding Buffers to Measure the Influence of Monovalent Salt (NaCl) Concentration on Yeast tRNA Binding to SiO_2 Surfaces

Binding Buffer	Buffer Base	NaCl (mM)	KCl (mM)	$MgCl_2$ (mM)	$CaCl_2$ (mM)	pH
D	25 mM Tris	100	-	5	-	7.5
H	25 mM Tris	25	-	5	-	7.5
I	25 mM Tris	400	-	5	-	7.5

The effect of different binding buffer pH on yeast tRNA binding on a silicon dioxide surface was measured by comparing the QCM-D results for binding buffers D, F, and G (see Table 3.4.6) using QCM-D.

Table 3.4.6 Binding Buffers to Measure the Influence of Binding Buffer pH on Yeast tRNA Binding to SiO_2 Surface and PET-G surfaces

Binding Buffer	Buffer Base	NaCl (mM)	KCl (mM)	$MgCl_2$ (mM)	$CaCl_2$ (mM)	pH
D	25 mM Tris	100	-	5	-	7.5
F	25 mM Tris	100	-	5	-	6.5
G	25 mM Tris	100	-	5	-	8.5

For the experiments with PET-G surface, an additional seven buffers were used (see Table 3.4.7).

Table 3.4.7 Binding Buffer for QCM-D Experiments on PET-G surface

Binding Buffer	Buffer Base	NaCl (mM)	KCl (mM)	$MgCl_2$ (mM)	$CaCl_2$ (mM)	pH
O	25 mM Tris	25	-	-	-	7.5
P	25 mM Tris	400	-	-	-	7.5
Q	25 mM Tris	-	25	-	-	7.5
R	25 mM Tris	-	100	-	-	7.5
S	25 mM Tris	-	400	-	-	7.5
T	25 mM Tris	-	25	5	-	7.5
U	25 mM Tris	-	400	5	-	7.5

The influence of divalent salt on yeast tRNA binding on a PET-G surface was measured by comparing the QCM-D results for binding buffers A, D, and M (see Table 3.4.2):

The influence of divalent salt ($MgCl_2$ and $CaCl_2$) concentration on yeast tRNA binding on a PET-G surface was measured by comparing the QCM-D results for binding buffers B, C, D, E, K, L, M, N(see Table 3.4.3):

The influence of different monovalent salt (NaCl and KCl) on yeast tRNA binding on a PET-G surface was measured by comparing the QCM-D results for binding buffers D and J (see Table 3.4.4).

The effect of monovalent salt (NaCl and KCl) concentration on yeast tRNA binding on a PET-G surface was measured by comparing the QCM-D results for binding buffers D, H, I, A, O, P, Q, R, S, T, J, and U(see Table 3.4.8).

Table 3.4.8 Binding Buffers to Measure the Influence of Monovalent Salt Concentration on Yeast tRNA Binding to PET-G Surfaces

Binding Buffer	Buffer Base	NaCl (mM)	KCl (mM)	$MgCl_2$ (mM)	$CaCl_2$ (mM)	pH
D	25 mM Tris	100	-	5	-	7.5
H	25 mM Tris	25	-	5	-	7.5
I	25 mM Tris	400	-	5	-	7.5
A	25 mM Tris	100	-	-	-	7.5
O	25 mM Tris	25	-	-	-	7.5
P	25 mM Tris	400	-	-	-	7.5
Q	25 mM Tris	-	25	-	-	7.5
R	25 mM Tris	-	100	-	-	7.5
S	25 mM Tris	-	400	-	-	7.5
T	25 mM Tris	-	25	5	-	7.5
J	25 mM Tris	-	100	5	-	7.5
U	25 mM Tris	-	400	5	-	7.5

The effect of different pH of binding buffers on yeast tRNA binding on a PET-G surface was measured by comparing the QCM-D results for binding buffers D, F, and G(see Table 3.4.6)

3.4.2 Elution Buffers

Elution buffer was required to elute the yeast tRNA from the QCM-D sensor surfaces. In order to minimize the buffer effect in QCM-D experiment, various elution buffers were tested by comparing their QCM-D frequency signal to that obtained for binding buffer in the absence of yeast tRNA. 25 mM Tris, 8 mM Ethylenediamine Tetraacetic Acid (EDTA) (Fisher Science), pH 8.0 was used for yeast tRNA binding on silicon dioxide surface experiments. 25 mM Tris, 10 mM EDTA, pH 8.5 was used for yeast tRNA binding on PET-G surface experiments. EDTA has the ability to sequester metal ions, such as Ca^{2+}, and Mg^{2+}, in the binding buffer from yeast tRNA. Therefore, the bound yeast tRNA on a silicon dioxide surface or PET-G surface can be efficiently eluted using such elution buffer.

3.5 QCM-D Measurement

3.5.1 The Principle of QCM-D

Yeast tRNA binding measurements were performed with an E4 QCM-D instrument (Q-sense). QCM-D experiments were performed with quartz sensor crystals supplied by Q-sense. These quartz crystals were AT-cut quartz with gold on the active surface in 14 mm diameter (Fig. 3.5.1). The fundamental frequency

(f_0) of quartz crystals is approximately 5 MHz, and the sensitivity constant (C) is 0.177 mg/m^2 Hz[32]. The yeast tRNA adsorption measurements were performed with two kinds of quartz crystal sensors. One kind of sensors were coated with silicon dioxide (300 nm), and the other kind of sensors were coated with PET-G (300 nm). The sensors have three layers from bottom to top, which are quartz, Au, and coated material such as silicon dioxide or PET-G.

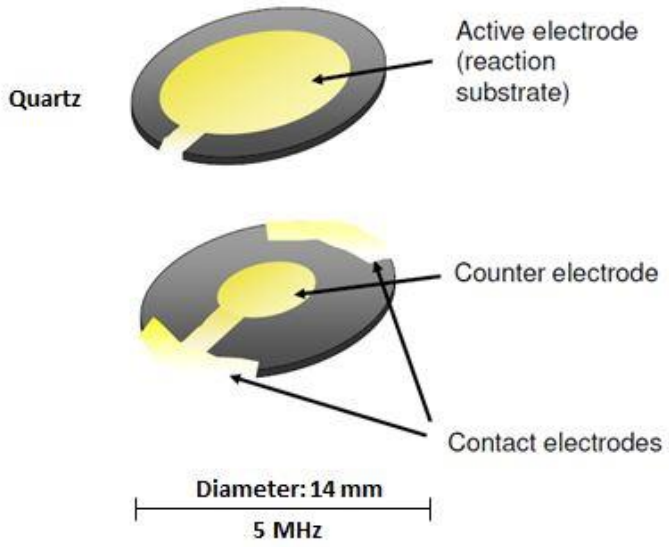

Fig.3.5.1. QCM-D sensors[48]

The QCM-D simultaneously measures the change in frequency (Δf) and the change in dissipation (ΔD) of a quartz crystal sensor whose surface is in contact with an adsorbing medium. The change in frequency (Δf) can be

converted into a change in adsorption mass per unit area (Γ_s) on the sensor surface using the Sauerbrey equation (equation 1) when the film is rigid[49].

$$\Gamma_s = -\frac{C\Delta f}{n} \tag{1}$$

where C is a device constant which is only related to quartz. n is the overtone number (1, 3, 5, 7, 9, 11, and 13) which is the natural resonance or vibration frequency of QCM-D system.

The dissipation provides a measurement of the viscoelasticity of the adsorbed film (equation 2)[33] on the sensor surface. A small dissipation implies a rigid film, while a large dissipation means a more loosely bound and softer extended film.

$$D = \frac{E_{dissipation}}{2\pi E_{stored}} \tag{2}$$

where $E_{dissipation}$ is the dissipated energy during one oscillation cycle and E_{stored} is the total energy stored in the oscillation.

In this study, the change in adsorption mass on both silicon dioxide sensor surface and PET-G sensor surface can be calculated by the Sauerbrey equation because the shift of dissipation was found to be small and close to zero (Fig.4.2.5

and Fig.4.4.2). Therefore, the change of frequency (Δf) is negatively proportional to the adsorbed yeast tRNA mass per unit area on sensor surface.

The frequency changing rate of yeast tRNA (k_f) can be determined from the slope of the linear portion of the change in resonance frequency Δf_5 versus time curve[50]:

$$k_f = \frac{d\Delta f_5}{dt} \tag{3}$$

where t is the binding time (min), and Δf_5 is the change of frequency at overtone 5. The unit of k_f is Hz/min.

Combining equations 1 and 3 enables an estimate of the binding mass rate (k_m) as shown as Equation 4:

$$k_m = -\frac{C}{n}\frac{d\Delta f_5}{dt} \tag{4}$$

Therefore, the binding mass rate (k_m) is negatively proportional to the frequency changing rate (k_f). In this study, negative value of the change of frequency rate (equation 3) is used to represent the yeast tRNA adsorption mass rate on a sensor surface.

3.5.2 Measurements of Yeast tRNA Binding Behavior by QCM-D

The starting DNA or RNA library concentration in SELEX process is typically at about 0.17 mg/mL[51]. 5 μM (~0.198 mg/mL) yeast tRNA can be clearly detected by gel electrophoresis (Fig.4.1.1), and binding to silicon dioxide surfaces and PET-G surfaces with the frequency shift using QCM-D (Fig.4.2.4 and Fig.4.4.1) Therefore, the concentration of yeast tRNA was kept at 5 μM in each binding buffer conditions during QCM-D measurements.

Before and after each adsorption experiment, the QCM-D instrument was cleaned by pumping approximately 20 mL of 2% Hellmanex II (HellmaAnalytics) via peristaltic pump (Ismatec IPC-N 4) through the QCM-D system at 30 ℃, followed by pumping 100 mL of Milli-Q water through the system. Finally the standard Q-Sense flow module was dried with pumping air through the equipment for 10 min.

In this study, yeast tRNA binding was examined on both silicon dioxide coated QCM-D sensors and PET-G coated QCM-D sensors. Before and after each adsorption experiment, the silicon dioxide coated sensors were treated in a UV/ozone Procleaner chamber (Bioforce Nanosciences) for 10 min, immersed into a 2% Sodium Dodecyl Sulfate (SDS) (Fisher Science) solution for 30 min at room temperature, rinsed with Milli-Q water, dried with nitrogen gas, and then oxidized for 20 min in the UV/ozone chamber. For the PET-G coated QCM-D

sensors, the cleaning process before and after each experiment was as follows. The PET-G sensors were immersed in a 1% Deconex 11 (Borer) solution for 30 min at 30 ℃, rinsed with Milli-Q water, kept in Milli-Q water for at least 2 hours, rinsed with 99% ethanol, and then dried with nitrogen gas. One QCM-D sensor can only be used for several times. After the frequency noise, which is a significant quantity to represent the frequency stability of a QCM-D sensor, increased up to over 1 Hz and a stable baseline could not be reached after running 40 min buffer through QCM-D system, the accuracy and sensitivity of QCM-D sensors decreased dramatically, so that the sensors cannot be used to measure yeast tRNA binding behavior anymore.

All the binding buffers and elution buffers were sonicated for at least 40 min to degas before running experiments using QCM-D. The yeast tRNA was pipetted into the sonicated binding buffers at concentration of 5 μM. All experiments were performed at 25 ℃ with 150 μL/min of flow rate.

As shown in Fig.3.5.2, the traditional setup of the QCM-D experiment was improved by the use of a three way switching valve (IDEX Health & Science) (Fig.3.5.3) to enable simple change from one solution to another. Moreover, the three way switching valve decreases the opportunity of pumping air into QCM-D system when changing from one solution to another, since air bubble can make the frequency change dramatically and influence the accurancy of experiment.At

the start of each experiment, one of the inlet tubes (Q-Sense) from switching valve was immersed in a 50 mL centrifuge tube filled with binding buffer, while the other inlet tube was immersed in 50 mL centrifuge tube filled with 5 μM yeast tRNA in binding buffer. For each adsorption experiment the sequence of steps was as follows:

(1) Binding buffer was pumped through until the baseline frequency drift was less than 0.1 Hz over 10 min;

(2) The valve was switched from binding buffer to 5 μM yeast tRNA in binding buffer and pumped through for approximate 50 min to 60 min;

(3) Move the inlet tube that was immersed in binding buffer into another 50 mL centrifuge tube filled with elution buffer;

(4) The valve was switched from 5 μM yeast tRNA in binding buffer to elution buffer and pumped through this solution for at least 15 min until the frequency drift was less than 0.1 Hz for about 5 min;

(5) Move the inlet tube which was immersed in binding buffer containing 5 μM yeast tRNA to another binding buffer solution;

(6) Replace solutions as necessary and then start new experiment with another binding buffer condition continuesely.

For every experiment with yeast tRNA solution, a 'blank experiment' was also performed at the same time in another QCM-D chamber with the exact same QCM-D sensor, but instead of injecting yeast tRNA into the system, the same binding buffer without any yeast tRNA was used. Same elution buffer was then injected at the same moment with yeast tRNA adsorption experiment explained previously.

The first overtone and overtone 9, 11, 13 are not used in QCM-D data analysis because of their bigger noise and less accurancy. Instead, overtone 3, 5, and 7 are commonly used. The change of frequency at overtone 5 (Δf_5) was chosen for experiment analysis through this study, due to its less noise. The adsorption experiments are analyzed by plotting the change of frequency at overtone 5 (Δf_5) versus time (t) and comparing the results to the 'blank experiment' and also to experiments conducted with different buffer compositions. The change of frequency versus time curve were finally converted to the negative frequency changing rate (k_f) by equation 3 to illustrate the yeast tRNA binding rates under different binding buffer conditions.

A

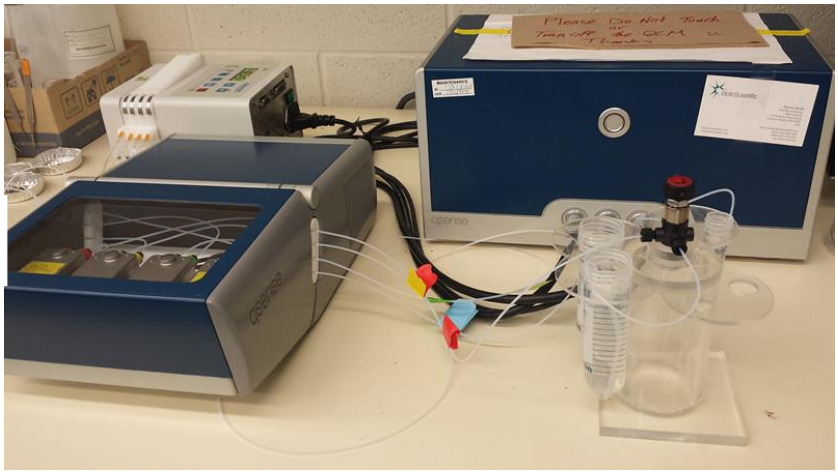

B

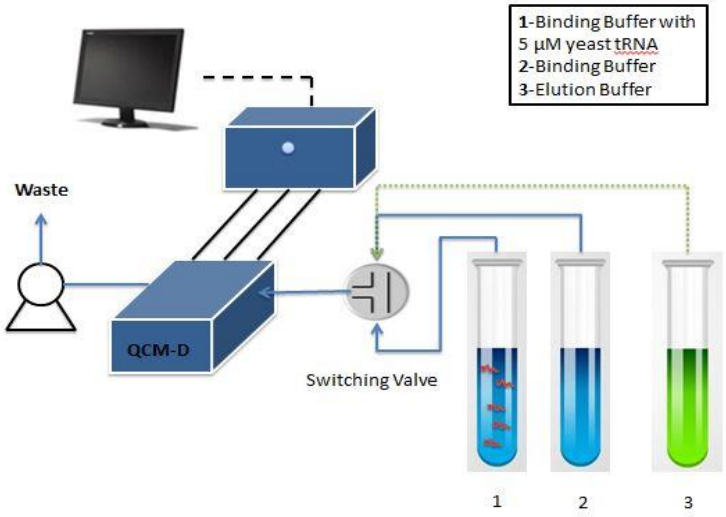

Fig.3.5.2. Panel A – The actual set of QCM-D experiment with Three Channel Switching Valve;

Panel B – The model of QCM-D experiment with Three Channel Switching Valve: Quartz crystal sensors were put into the temperature controlled QCM-D chambers with liquid inlet and outlet. The outlet tube was connected with a peristaltic pump (Ismatec IPC-N 4) The inlet tube was connected with a three channel switching valve (IDEX Health & Science).

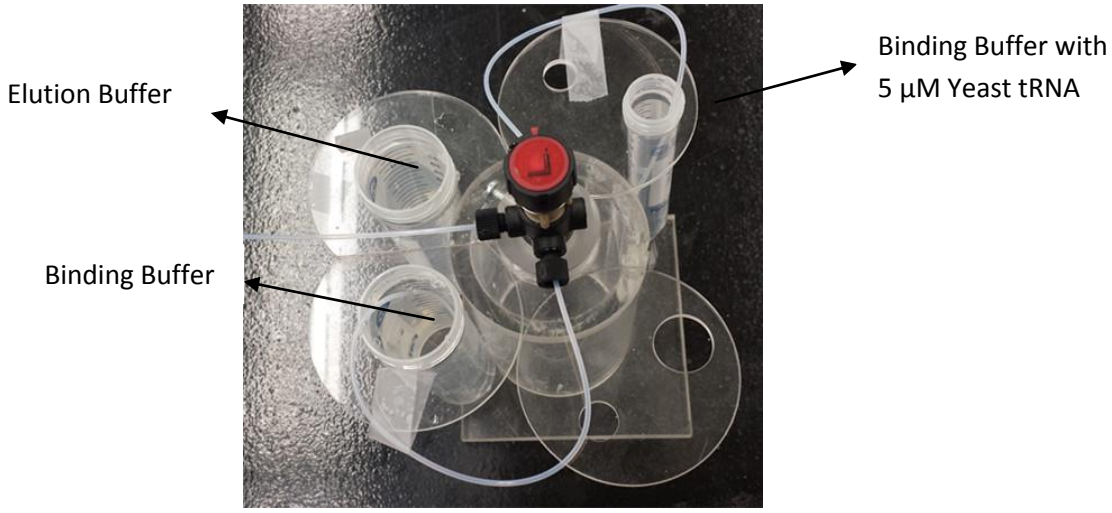

Fig.3.5.3. The Three Channel Switching Valve: The middle tube was connected with QCM-D. The lower tube was immersed into binding buffer. The upper tube was immersed into the same binding buffer with 5 µM yeast tRNA.

3.6 Surface Characterization Test with Fourier Transform Infrared Microscope

The PET-G coated QCM-D sensor surface was custom prepared by Q-sense. In order to confirm the properties of the surface, the attenuated total reflection (ATR) model of Fourier Transform Infrared Microscope HYPERION 3000 (Bruker) was used[52]. ATR is an advanced technique using infrared spectroscopy to identify the chemical propertities of sample directly in the solid or liquid state without further preparation. A PET-G QCM-D sensor was placed on the measuring plane. The pure gold surface was used as background measurement in the test. After the PET-G coated QCM-D sensor position was defined in the

visual image of microsope, a beam of infrared light was passed through the ATR tip, which was made by germanium with a high refraction index.

This total internal reflection formed the evanescent wave which extended into the sample. The beam which exited out of the crystal was collected by a detector. Through the adsorption versus wavelength curve, chemical functional group in the sample can be identified, with which its chemical structure can be determined.

Chapter 4 Results and Discussion

4.1 Yeast tRNA Characterization

The purity of yeast tRNA (Invitrogen) was evaluated using the Nanodrop spectrophotometer (Fisher Scientific). The A_{260}/A_{280} ratio for the yeast tRNA was 2.0, indicating that the yeast tRNA solution was not contaminated by proteins[53]. To determine the integrity of yeast tRNA, gel electrophoresis analysis was performed using a low range ssRNA ladder (NEB) and GSN70 RNA library[31] as size markers. As shown in Fig 4.1.1, there were four clear bands associated with the yeast tRNA sample (Lane 2). A sharp band was observed at the same position as the GSN70 RNA library (Lane 3) that was reported to be 120 nt in size[31]. Three other broad bands were around 70 nt, 80 nt, and 40 nt. Thus, the yeast tRNA had a reasonably high purity and similar size to a typical RNA library and thus is well suited to be used as a background pre-blocking molecule before aptamer SELEX processes. In this work, it was used in the QCM-D experiments to evaluate the influence of the binding buffer conditions on the yeast tRNA binding ability on silicon dioxide and PET-G surfaces.

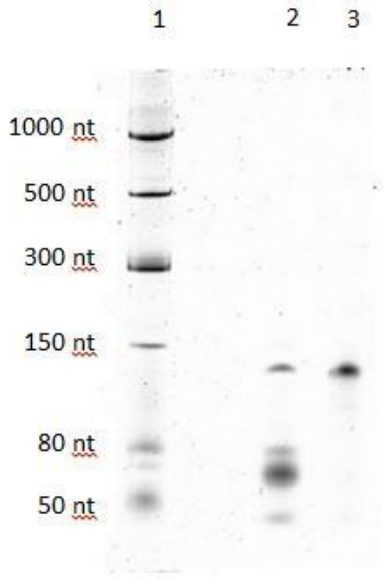

Fig.4.1.1. 8% denaturing gel electrophoresis image of yeast tRNA and RNA library. Lane 1 - 5 µL of low range ssRNA ladder (NEB); Lane 2 - 5 µL of yeast tRNA (Invitrogen) at 5 µM concentration; Lane 3 - 5 µL of GSN70 RNA Library[31]

4.2 Yeast tRNA Binding Behavior on Silicon Dioxide Surface

4.2.1 Influence of Different Divalent Cation in Binding Buffers

Fig 4.2.1 presents the real-time frequency shifts in the experiment of yeast tRNA binding to silicon dioxide surfaces with binding buffer composition of 25 mM Tris, 100 mM NaCl, and 5 mM $MgCl_2$ at pH 7.5. The x-axis shows the run time in minutes while the y-axis shows the change of silicon dioxide QCM-D sensor frequency (overtone 5). For the first 10 minutes of run time ('step 1' in Fig.4.2.1 – Panel A), just the binding buffer was pumped through the QCM-D

sensor to monitor for a stable baseline signal. Then the valve was switched to pump the yeast tRNA solution (5 μM in binding buffer) into the sensor. The downward shift of frequency change indicates an increase in mass on the sensor surface according to equation 1, which was caused by the binding of yeast tRNA on silicon dioxide surfaces. After approximately 60 minutes, the valve was switched to the elution buffer (25 mM Tris, 8 mM EDTA, pH 8.0) and a rapid change in the frequency was observed. The change in frequency returned back to zero suggesting that the bound yeast tRNA was eluted from the QCM-D sensor surface.

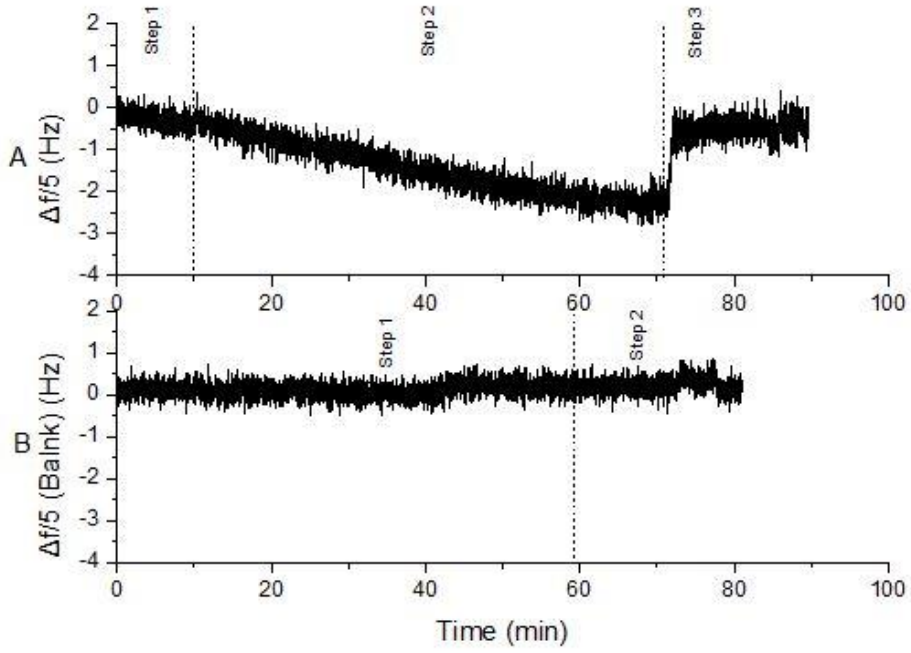

Fig.4.2.1. Frequency shift divided by the fifth overtone (Δf/5) as a function of run time for yeast tRNA binding to silicon dioxide under binding buffer—25 mM Tris, 100 mM NaCl, 5 mM MgCl2, pH 7.5.

Panel A - Experiments with yeast tRNA solution: The dashed line at approximately 10 min marks the change from binding buffer to 5 μM yeast tRNA solution in binding buffer; the dashed line at approximately 72 min marks the change from yeast tRNA solution in binding buffer to elution buffer (25 mM Tris, 8 mM EDTA, pH 8.0).

Panel B – 'Blank' experiment without any yeast tRNA: The dashed line at approximately 60 min marks the change from binding buffer to elution buffer (25 mM Tris, 8 mM EDTA, pH 8.0)

In order to confirm that the frequency shift measured by the QCM-D instrument actually represented the yeast tRNA first binding and then eluting from the silicon dioxide surface, a series of samples were collected and then analyzed by gel electrophoresis (see Fig 4.2.2). The samples were collected from the pump waste outlet stream first immediately after switching to the elution buffer and then

at 2 minute intervals; a total of eight samples were collected (Lanes 3 through 10 in Fig 4.2.2). The band intensity decreased gradually after running elution buffer for 2 min and 4 min. Yeast tRNA can be rarely detected after running elution buffer for more than 6 min, which appears to coincide with the change in frequency as measured by QCM-D (see Fig 4.2.1 – Panel A).

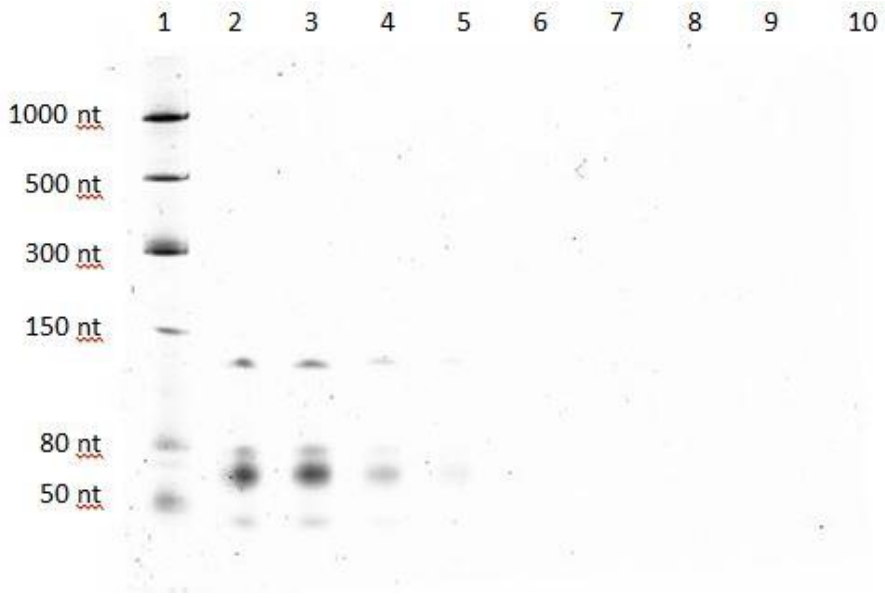

Fig.4.2.2. 8% denaturing gel electrophoresis image of samples collected during experiment corresponding to results in Fig.4.2.1. Lane 1 - 5 µL low range ssRNA ladder (NEB); Lane 2 – 5 µL of stock solution of 5 µM yeast tRNA solution in binding buffer (25 mM Tris, 100 mM NaCl, 5 mM $MgCl_2$, pH 7.5); Lane 3 - 5 µL of sample collected from pump waste after running elution buffer for 0 min; Lanes 4 through 10 - 5 µL of sample collected from pump waste after running elution buffer for 2, 4, 6, 8, 10, 12, and 14.

As shown in Fig.4.2.1- Panel B, QCM-D frequency did not shift down, but continued as stable if there was no yeast tRNA in binding buffers. Thus, the binding of yeast tRNA onto silicon dioxide surfaces and elution of yeast tRNA

from surfaces could be both detected accurately using QCM-D in real time via the monitoring of resonant frequency.

During the yeast tRNA binding experiment, the change of dissipation was less than 0.5×10^{-6} (see Fig.4.2.5 – Panel A), indicating that yeast tRNA layer binding on the silicon dioxide surface was stable and did not aggregate under the studied binding buffer condition[54,55,56] . Therefore, the frequency shift is negatively proportional to the change of deposited mass on surfaces which can be quantified by the Sauerbrey equation (equation 1). Thus, the negative rate of frequency shift is equivalent to the rate of yeast tRNA binding mass on surface, which can be quantified by equation 3. The yeast tRNA binding rates could be compared by a simple analysis of the frequency change with time via linear regression; however the typical response was non-linear over the entire run time and thus sub-intervals were used to analyze the change in binding rate over time. In order to determine the best sub-interval to compare the different buffer conditions, the binding rates were calculated for 2.5, 5, and 10 minutes. A comparison of the results was shown in Fig 4.2.3 for the data from Fig 4.2.1 – Panel A. The error bar for each calculation was determined from the Analysis of Variance (ANOVA analysis). The binding rates corresponding to 2.5 min and 5 min were quite sensitive to the noise of the QCM-D measurement as indicated by the larger error bars and several negative results. The binding rates calculated every 10 min were less sensitive to the random fluctuations and thus better

represented the change in binding rate with time. Thus, the 10 min interval was used for all subsequent calculations.

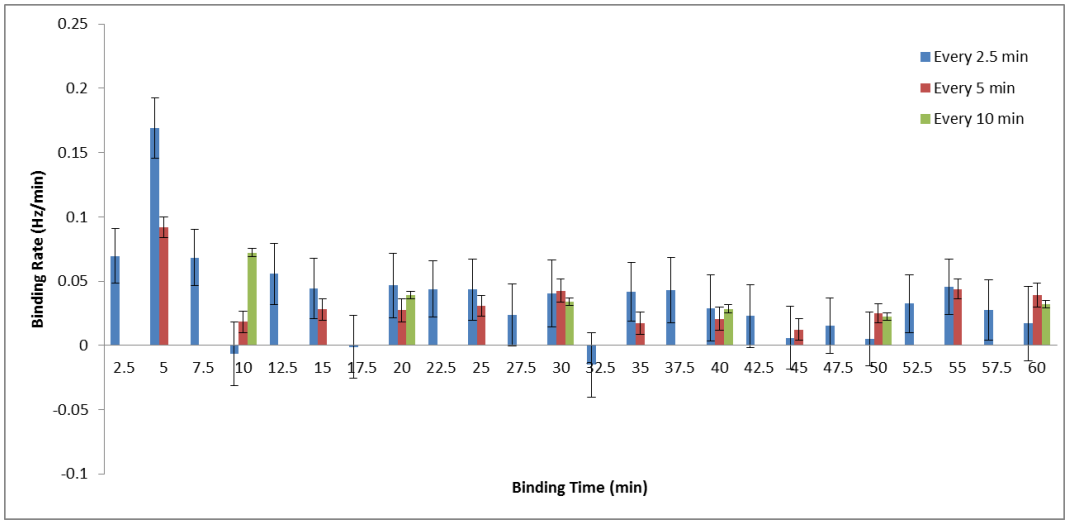

Fig.4.2.3. Comparison of different time intervals for analyzing the frequency shift results from Fig 4.2.1 – Panel A according to Equation 3.

The real-time frequency shifts in the experiments of yeast tRNA binding to the silicon dioxide surface are shown in Fig.4.2.4 – Panel A. The measurements were taken under three different binding buffer conditions which either included $MgCl_2$ or $CaCl_2$ as divalent salt, or did not contain any divalent salt. For each single measurement, the establishment of a stable frequency baseline while binding buffer was flown over the QCM-D sensor was verified before any experiments were started. Then a 5 μM yeast tRNA solution prepared in the same binding buffer was injected for approximate 50 min to 60 min. Typically, this caused a significant change in the frequency. Next yeast tRNA was eluted from

the surface using elution buffer – 25 mM Tris, 8 mM EDTA, pH 8.0. Following that, another measurement in different binding buffer condition was performed.

QCM-D experiments with yeast tRNA-free solutions were conducted to examine whether the buffer effect was important for binding behavior measurements. The changes in frequency (Fig.4.2.4 – Panel B) and dissipation (Fig.4.2.5 – Panel B) were negligible when the solutions were changed from binding buffers (25 mM Tris, 100 mM NaCl, pH 7.5; 25 mM Tris, 100 mM NaCl, 5 mM $MgCl_2$, pH 7.5; 25 mM Tris, 100 mM NaCl, 5 mM $CaCl_2$, pH 7.5) to elution buffer (25 mM Tris, 8 mM EDTA, pH 8.0). For example, when the valve was switched from binding buffer – 25 mM Tris, 100 mM NaCl, 5 mM $MgCl_2$, pH 7.5 (‘step 1’ in Fig.4.2.5 – Panel B) – to elution buffer – 25 mM Tris, 8 mM EDTA, pH 8.0 (‘step 2’ in Fig.4.2.5 – Panel B), a change of 0.2 Hz in frequency and a change of 0.1×10^{-6} in associated dissipation were observed. Both changes were not higher than the inherent drift of QCM-D baseline. Therefore, under these specific conditions, the binding mass of yeast tRNA can be quantified via QCM-D without the need to consider buffer effects.

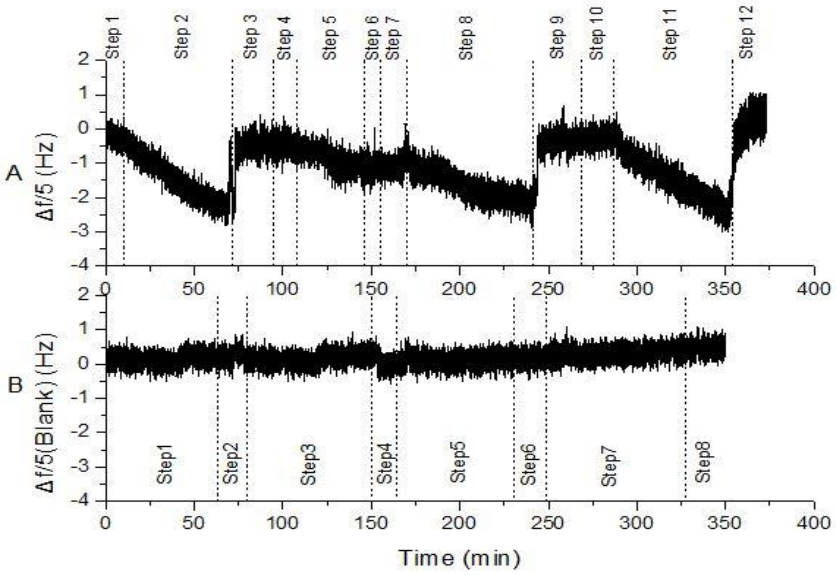

Fig.4.2.4. Frequency shift divided by the fifth overtone (Δf/5) as a function of time for yeast tRNA binding to silicon dioxide sensor under binding buffer conditions with or without divalent salt ($CaCl_2$ or $MgCl_2$) at 5 mM concentration.
Panel A – Experiments with yeast tRNA solution: Step 1 - Binding buffer (25 mM Tris, 100 mM NaCl, 5 mM $MgCl_2$, pH 7.5); Step 2 – 5 μM yeast tRNA in same binding buffer as Step 1; Step 3 - Elution buffer (25 mM Tris, 8 mM EDTA, pH 8.0); Step 4 - Binding buffer (25 mM Tris, 100 mM NaCl, pH 7.5); Step 5 – 5 μM yeast tRNA in same binding buffer as Step 4; Step 6 (same as Step 3) - Elution buffer (25 mM Tris, 8 mM EDTA, pH 8.0); Step 7 - Binding buffer (25 mM Tris, 100 mM NaCl, 5 mM $CaCl_2$, pH 7.5); Step 8 – 5 μM yeast tRNA in same binding buffer as Step 7; Step 9 (same as Step 3) - Elution buffer (25 mM Tris, 8 mM EDTA, pH 8.0); Step 10 (same as Step 1) - Binding buffer (25 mM Tris, 100 mM NaCl, 5 mM $MgCl_2$, pH 7.5); Step 11 (same as Step 2) – 5 μM yeast tRNA in same binding buffer as Step 10; Step 12 (same as Step 3) - Elution buffer (25 mM Tris, 8 mM EDTA, pH 8.0).

Panel B – 'Blank' experiments without any yeast tRNA: Step 1 - Binding buffer (25 mM Tris, 100 mM NaCl, 5 mM $MgCl_2$ pH 7.5); Step 2 - Elution buffer (25 mM Tris, 8 mM EDTA, pH 8.0); Step 3 - Binding buffer (25 mM Tris, 100 mM NaCl, pH 7.5); Step 4 (same as Step 2) - Elution buffer (25 mM Tris, 8 mM EDTA, pH 8.0); Step 5 - Binding buffer (25 mM Tris, 100 mM NaCl, 5 mM $CaCl_2$, pH 7.5); Step 6 (same as Step 2) - Elution buffer (25 mM Tris, 8 mM EDTA, pH 8.0); Step 7 (same as Step 1) - Binding buffer (25 mM Tris, 100 mM NaCl, 5 mM $MgCl_2$, pH 7.5); Step 8 (same as Step 2) - Elution buffer (25 mM Tris, 8 mM EDTA, pH 8.0).

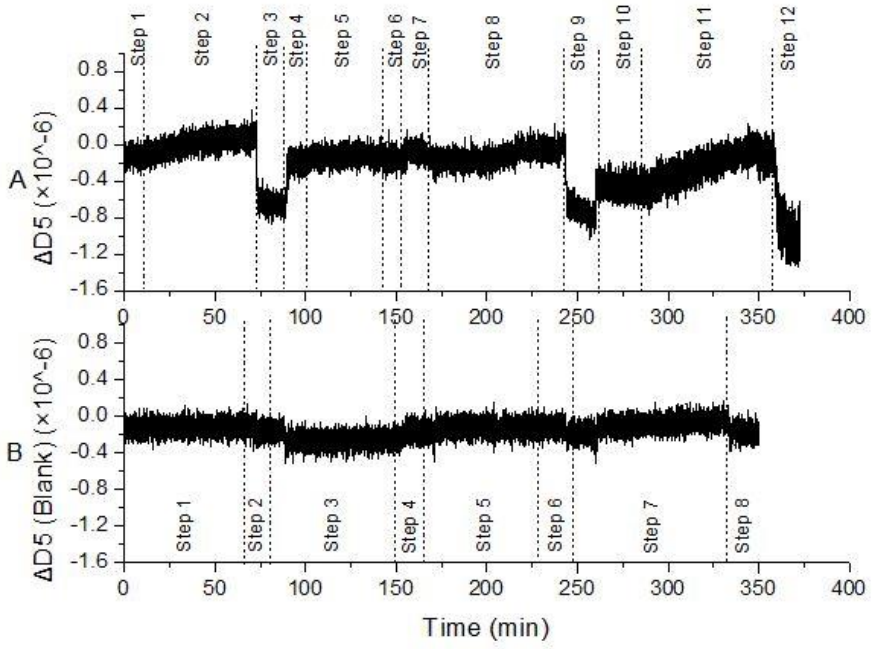

Fig.4.2.5. Associated dissipation shift (ΔD_5) as a function of time for the same experimental conditions as detailed in Fig 4.2.4.

Fig.4.2.4 – Panel A showed that yeast tRNA hardly bond to bare silicon dioxide surfaces when the binding buffer did not contain any divalent salt ('step 4' to 'step 6'). After added $CaCl_2$ in the binding buffer, the binding ability of yeast tRNA was enhanced slightly. The yeast tRNA showed enhanced binding onto silicon dioxide surface when added $MgCl_2$ in the binding buffer. The measurements of yeast tRNA binding to silicon dioxide surfaces in binding buffer with $MgCl_2$ (25 mM Tris, 100 mM NaCl, 5 mM $MgCl_2$, pH 7.5) were performed both at the beginning and the end. The consistency of these two measurements indicated that the yeast tRNA binding ability on silicon dioxide was only

influenced by different binding buffer conditions. Thus different yeast tRNA binding behaviors were not due to change in the sensor itself. Favorable binding rates (calculated every 10 min in Table S-2) of yeast tRNA on silicon dioxide surface under different binding buffer conditions were further obtained from equation 3 and provided in Fig 4.2.6. Binding rates tended to increase when the binding buffer contained divalent cations either Ca^{2+} or Mg^{2+}, and increased most significantly when the binding buffers contained Mg^{2+}. Such results can be approved by previous studies about ionic requirement on RNA binding[57]. Therefore, divalent salt in binding buffers is necessary for yeast tRNA binding on silicon dioxide surfaces. However, yeast tRNA binding preferred Mg^{2+} rather than Ca^{2+}as the bridge to bring yeast tRNA backbone to silicon dioxide surfaces.

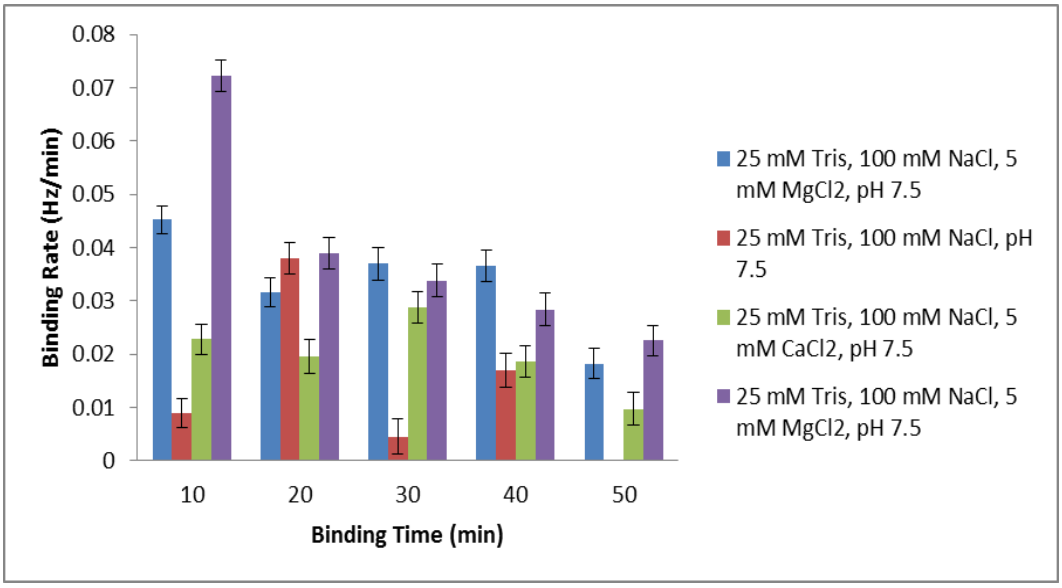

Fig.4.2.6. Binding Rates of yeast tRNA on silicon dioxide surface obtained every 10 min under binding buffer conditions, which either included Mg^{2+} or Ca^{2+}, or did not contain any divalent cations: 25 mM Tris, 100 mM NaCl, 5 mM $MgCl_2$, pH 7.5 (blue bars and purple bars), 25 mM Tris, 100 mM NaCl, 5 mM $CaCl_2$, pH 7.5 (green bars), 25 mM Tris, 100 mM NaCl, pH 7.5 (red bars).

4.2.2 Influence of Divalent Cation Concentration in Binding Buffers

As discussed previously, the presence of divalent cation in binding buffer, Mg^{2+} or Ca^{2+}, was significant for yeast tRNA binding to the bare silicon dioxide surfaces. Although 39% of sixty-one previous reviewed literatures used Mg^{2+} at concentration of 5 mM, there were still numbers of study which selected aptamer at other Mg^{2+} concentration ranging from 0.3 mM to 25 mM (Fig. 2.5). Various concentrations of Ca^{2+}in binding buffer were also used in fifteen previous SELEX process (Fig.2.6). Fig.2.6 revealed that 43% of the reviewed studies used 1 mM

$CaCl_2$ in binding buffers, while 36% used 5 mM $CaCl_2$ in binding buffers. In that case, it is necessary and significant to measure the influence of divalent salt concentration (both $MgCl_2$ and $CaCl_2$) on yeast tRNA binding ability to a silicon dioxide surface.

The most often used divalent concentrations in binding buffers are 1 mM and 5 mM (Fig.2.5 and Fig.2.6). Moreover, 1 mM magnesium concentration is consistent with the amount of free magnesium that is present *in vivo*. Therefore, the binding ability of yeast tRNA onto silicon dioxide surfaces under binding buffer with different concentration of $MgCl_2$ ranging from 0.2 mM, 1 mM, 5 mM, to 25 mM were measured using QCM-D (Fig.4.2.7 – Panel A). The concentration of yeast tRNA in each binding buffer was fixed the same at 5 μM, and all the other buffer conditions including Tris base (25 mM), NaCl concentration (100 mM), pH value (7.5), were kept consistent in all measurements as well. In other words, the only variable parameter was the concentration of $MgCl_2$ throughout the experiment. After each single yeast tRNA binding measurement, the surface-bound yeast tRNA was eluted from the silicon dioxide sensor surface with elution buffer (25 mM Tris, 8 mM EDTA, pH 8.0), following which another measurement with different binding buffer condition started. The rapid frequency shift when changing from elution buffer – 25 mM Tris, 8 mM EDTA, pH 8.0 (‘step 9’ in Fig.4.2.7 – Panel A) to binding buffer – 25 mM Tris, 100 mM NaCl, 25 mM $MgCl_2$, pH 7.5 (‘step 10’ in Fig.4.2.7 – Panel A) shown in Fig 4.2.7 –

Panel A was compatible with the corresponding 'blank' experiment without any yeast tRNA pumped into QCM-D (Fig 4.2.7 – Panel B from 'step 6' to 'step 7'). It indicated that the frequency shift was only caused by buffer effect, and not related to yeast tRNA binding. As shown in Figure 4.2.7 – Panel A, yeast tRNA rarely bound to silicon dioxide surfaces at low $MgCl_2$ concentration - 0.2 mM ('step 2' in Fig.4.2.7 – Panel A). It began to bind to the sensor surface after increasing the $MgCl_2$ concentration to 1 mM ('step 5' in Fig.4.2.7 – Panel A). The binding rates (calculated every 10 min) increased with increasing Mg^{2+} strength from 0.2 mM to 5 mM in the binding buffers, however, declined when increasing the $MgCl_2$ concentration from 5 mM to 25 mM (Fig.4.2.8). Moreover, it is observed that yeast tRNA showed largest binding rates when the Mg^{2+} concentration was fixed at 5 mM (see Table S-3). At each concentration, the binding rates decreased gradually with the increasing binding time, indicating that the silicon dioxide QCM-D sensor surface was gradually covered by yeast tRNA . Thus, the optimizing concentration of $MgCl_2$ in binding buffers is 5 mM in order to enhance the yeast tRNA binding to silicon dioxide surfaces.

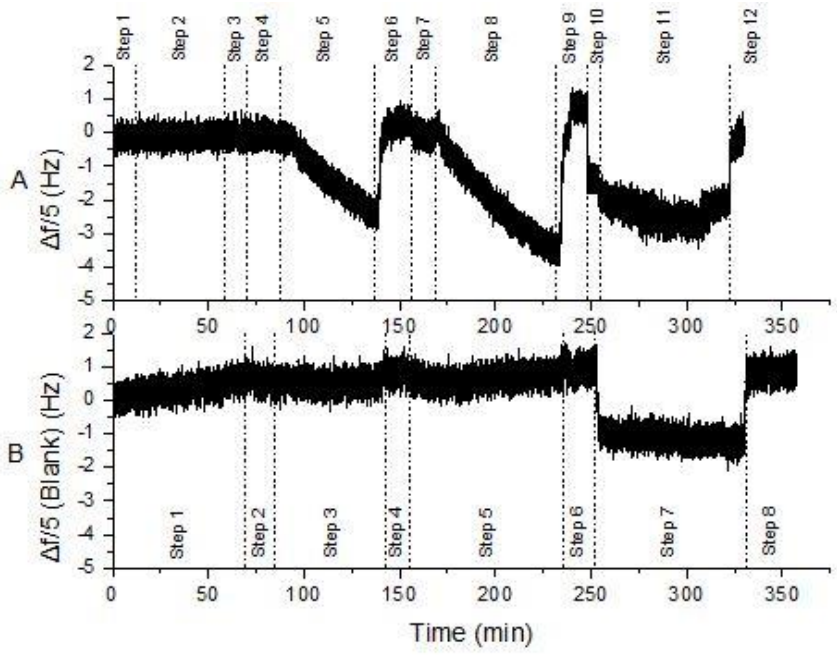

Fig.4.2.7. Frequency shift divided by the fifth overtone (Δf/5) as a function of time for yeast tRNA binding to silicon dioxide sensor under binding buffer conditions with different concentration of $MgCl_2$ (0.2 mM, 1 mM, 5 mM, and 25 mM). Panel A – Experiments with yeast tRNA solution: Step 1 - Binding buffer (25 mM Tris, 100 mM NaCl, 0.2 mM $MgCl_2$, pH 7.5); Step 2 – 5 μM yeast tRNA in same binding buffer as Step 1; Step 3 - Elution buffer (25 mM Tris, 8 mM EDTA, pH 8.0); Step 4 - Binding buffer (25 mM Tris, 100 mM NaCl, 1 mM $MgCl_2$, pH 7.5); Step 5 – 5 μM yeast tRNA in same binding buffer as Step 4; Step 6 (same as Step 3) - Elution buffer (25 mM Tris, 8 mM EDTA, pH 8.0); Step 7 - Binding buffer (25 mM Tris, 100 mM NaCl, 5 mM $MgCl_2$, pH 7.5); Step 8 – 5 μM yeast tRNA in same binding buffer as Step 7; Step 9 (same as Step 3) - Elution buffer (25 mM Tris, 8 mM EDTA, pH 8.0); Step 10 (same as Step 1) - Binding buffer (25 mM Tris, 100 mM NaCl, 25 mM $MgCl_2$, pH 7.5); Step 11 (same as Step 2) – 5 μM yeast tRNA in same binding buffer as Step 10; Step 12 (same as Step 3) - Elution buffer (25 mM Tris, 8 mM EDTA, pH 8.0).

Panel B – 'Blank' experiments without any yeast tRNA: Step 1 - Binding buffer (25 mM Tris, 100 mM NaCl, 0.2 mM $MgCl_2$, pH 7.5); Step 2 - Elution buffer (25 mM Tris, 8 mM EDTA, pH 8.0); Step 3 - Binding buffer (25 mM Tris, 100 mM NaCl, 1 mM $MgCl_2$ pH 7.5); Step 4 (same as Step 2) - Elution buffer (25 mM Tris, 8 mM EDTA, pH 8.0); Step 5 - Binding buffer (25 mM Tris, 100 mM NaCl, 5 mM $MgCl_2$, pH 7.5); Step 6 (same as Step 2) - Elution buffer (25 mM Tris, 8 mM EDTA, pH 8.0); Step 7 (same as Step 1) - Binding buffer (25 mM Tris, 100 mM NaCl, 25 mM $MgCl_2$, pH 7.5); Step 8 (same as Step 2) - Elution buffer (25 mM Tris, 8 mM EDTA, pH 8.0).

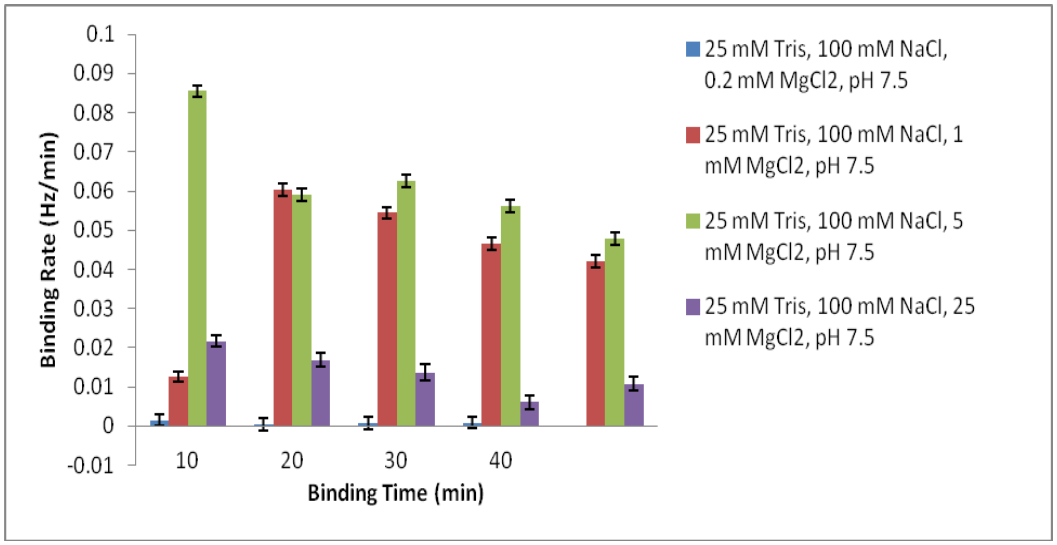

Fig.4.2.8. Binding Rates of yeast tRNA on silicon dioxide surface obtained every 10 min under binding buffer conditions, which included different concentration of $MgCl_2$: 25 mM Tris, 100 mM NaCl, 0.2 mM $MgCl_2$, pH 7.5 (blue bars), 25 mM Tris, 100 mM NaCl, 1 mM $MgCl_2$, pH 7.5 (red bars), 25 mM Tris, 100 mM NaCl, 5 mM $MgCl_2$, pH 7.5 (green bars), 25 mM Tris, 100 mM NaCl, 25 mM $MgCl_2$, pH 7.5 (purple bars).

Binding ability of yeast tRNA on bare silicon dioxide surfaces with different $CaCl_2$ concentration was measured using QCM-D, which was presented in Fig.4.2.9. The rapid frequency shift at approximate 250 min in Fig.4.2.9 – Panel A was caused by buffer effect while changing from elution buffer – 25 mM Tris, 8 mM EDTA, pH 8.0 (‘step 9’ in Fig.4.2.9 – Panel A) to binding buffer – 25 mM Tris, 100 mM NaCl, 25 mM $CaCl_2$, pH 7.5 (‘step 10’ in Fig.4.2.9 – Panel A). It was compatible with the frequency shift at approximate 250 min in Fig.4.2.9 – Panel B, which was caused by changing from the same elution buffer – 25 mM Tris, 8 mM EDTA, pH 8.0 (‘step 6’ in Fig.4.2.9 – Panel B) to the same binding

buffer – 25 mM Tris, 100 mM NaCl, 25 mM $CaCl_2$, pH 7.5 ('step 7' in Fig.4.2.9 – Panel B). Therefore, the frequency shift was caused by the buffer effect, and not related to any yeast tRNA binding behavior.

Compared with binding buffers with Mg^{2+} as divalent cations, the binding abilities of yeast tRNA in binding buffers with Ca^{2+} were weaker at each concentration (0.2 mM, 1 mM, 5 mM, and 25 mM). The binding rates (calculated every 10 min) of yeast tRNA in binding buffers with 0.2 mM $CaCl_2$, and 1 mM $CaCl_2$ (see Table S-4) were close to the ones in binding buffer without any divalent salt - 25 mM Tris, 100 mM NaCl, pH 7.5 (see Table S-1). Thus, the low concentration of $CaCl_2$ did not improve yeast tRNA binding ability onto silicon dioxide surfaces. Moreover, the binding rates did not increase significantly with the increasing concentration of $CaCl_2$ (Fig.4.2.10). Even the highest binding rate of yeast tRNA on silicon dioxide in the binding buffer with 25 mM $CaCl_2$ only reached up to (0.0412 ± 0.0023) Hz/min (see Table S-4), which was approximate 20 times smaller than the largest yeast tRNA binding rate in binding buffer containing 5 mM $MgCl_2$ (0.8557 ± 0.0014) Hz/min (see Table S-3). Although the binding rates of yeast tRNA increased slightly with the increasing concentration of $CaCl_2$, it is still not significant to contain Ca^{2+} in the binding buffers in order to enhance yeast tRNA binding ability to bare silicon dioxide surfaces.

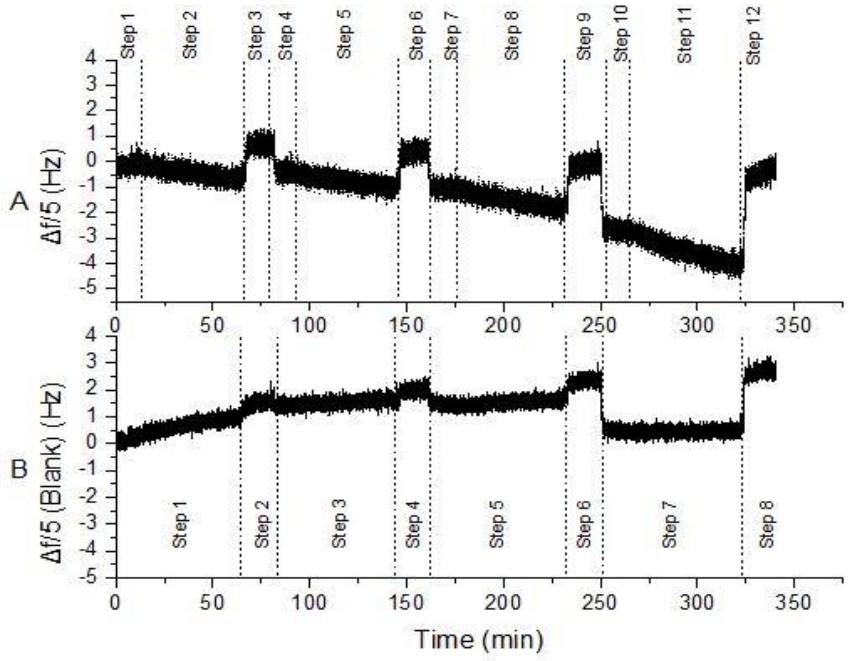

Fig.4.2.9. Frequency shift divided by the fifth overtone (Δf/5) as a function of time for yeast tRNA binding to silicon dioxide sensor under binding buffer conditions with different concentration of $CaCl_2$ (0.2 mM, 1 mM, 5 mM, and 25 mM). Panel A – Experiments with yeast tRNA solution: Step 1 - Binding buffer (25 mM Tris, 100 mM NaCl, 0.2 mM $CaCl_2$, pH 7.5); Step 2 – 5 μM yeast tRNA in same binding buffer as Step 1; Step 3 - Elution buffer (25 mM Tris, 8 mM EDTA, pH 8.0); Step 4 - Binding buffer (25 mM Tris, 100 mM NaCl, 1 mM $CaCl_2$, pH 7.5); Step 5 – 5 μM yeast tRNA in same binding buffer as Step 4; Step 6 (same as Step 3) - Elution buffer (25 mM Tris, 8 mM EDTA, pH 8.0); Step 7 - Binding buffer (25 mM Tris, 100 mM NaCl, 5 mM $CaCl_2$, pH 7.5); Step 8 – 5 μM yeast tRNA in same binding buffer as Step 7; Step 9 (same as Step 3) - Elution buffer (25 mM Tris, 8 mM EDTA, pH 8.0); Step 10 (same as Step 1) - Binding buffer (25 mM Tris, 100 mM NaCl, 25 mM $CaCl_2$, pH 7.5); Step 11 (same as Step 2) – 5 μM yeast tRNA in same binding buffer as Step 10; Step 12 (same as Step 3) - Elution buffer (25 mM Tris, 8 mM EDTA, pH 8.0).

Panel B – 'Blank' experiments without any yeast tRNA: Step 1 - Binding buffer (25 mM Tris, 100 mM NaCl, 0.2 mM $CaCl_2$, pH 7.5); Step 2 - Elution buffer (25 mM Tris, 8 mM EDTA, pH 8.0); Step 3 - Binding buffer (25 mM Tris, 100 mM NaCl, 1 mM $CaCl_2$ pH 7.5); Step 4 (same as Step 2) - Elution buffer (25 mM Tris, 8 mM EDTA, pH 8.0); Step 5 - Binding buffer (25 mM Tris, 100 mM NaCl, 5 mM $CaCl_2$, pH 7.5); Step 6 (same as Step 2) - Elution buffer (25 mM Tris, 8 mM EDTA, pH 8.0); Step 7 (same as Step 1) - Binding buffer (25 mM Tris, 100 mM NaCl, 25 mM $CaCl_2$, pH 7.5); Step 8 (same as Step 2) - Elution buffer (25 mM Tris, 8 mM EDTA, pH 8.0).

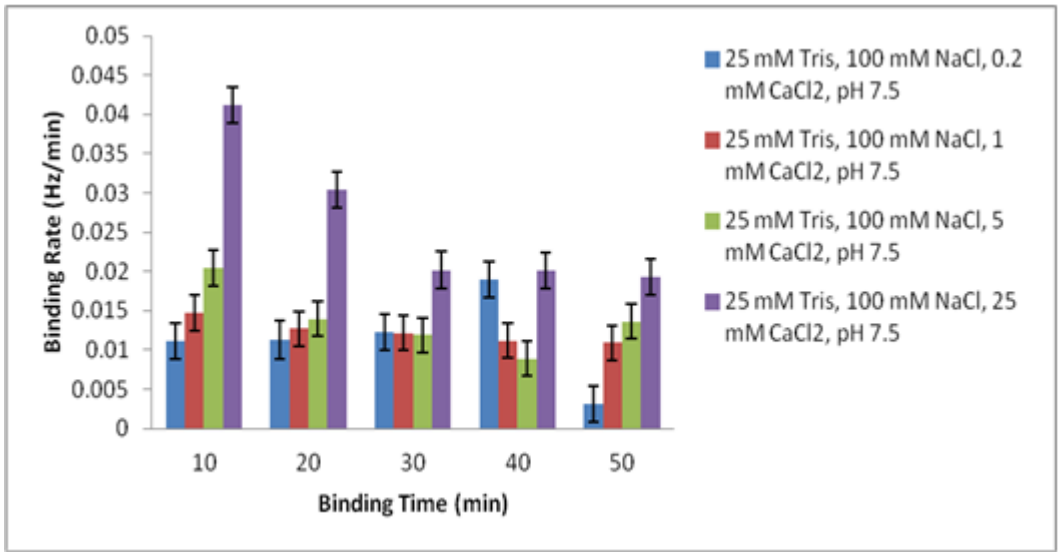

Fig.4.2.10. Binding Rates of yeast tRNA on silicon dioxide surface obtained every 10 min under binding buffer conditions, which included different concentration of $CaCl_2$: 25 mM Tris, 100 mM NaCl, 0.2 mM $CaCl_2$, pH 7.5 (blue bars), 25 mM Tris, 100 mM NaCl, 1 mM $CaCl_2$, pH 7.5 (red bars), 25 mM Tris, 100 mM NaCl, 5 mM $CaCl_2$, pH 7.5 (green bars), 25 mM Tris, 100 mM NaCl, 25 mM $CaCl_2$, pH 7.5 (purple bars).

4.2.3 Influence of Na^+ Concentration in Binding Buffers

QCM-D was used to measure the yeast tRNA binding abilities on silicon dioxide sensor surface with binding buffers containing different concentration of NaCl (25 mM, 100 mM, and 400 mM). 5 mM $MgCl_2$ was added in each binding buffer in order to make sure that the frequency shift signal was strong enough. The real-time frequency shift in the experiment of yeast tRNA binding on silicon dioxide surfaces was plotted in Fig.4.2.11. The rapid downward frequency shift at approximate 170 min in Fig.4.2.11 – Panel A was compatible with the frequency

shift at approximate 170 min in the corresponding 'blank' experiment (Fig.4.2.11-Panel B), indicating that it was only related to the buffer change from elution buffer – 25 mM Tris, 8 mM EDTA, pH 8.0 ('step 6' in Fig.4.2.11 – Panel A) to binding buffer – 25 mM Tris, 400 mM NaCl, 5 mM $MgCl_2$, pH 7.5 ('step 7' in Fig.4.2.11 – Panel A). Yeast tRNA did not show any significant binding on silicon dioxide surfaces with binding buffers containing low Na^+ concentration (25 mM) or high Na^+ concentration (400 mM) (see Fig.4.2.11 – Panel A). Since both the yeast tRNA phosphate background and silicon surface are negative charged, adding Na^+ in binding buffer can decrease the repulsive interaction between them and therefore enhance the yeast tRNA binding ability[58,59]. The binding ability of yeast tRNA on silicon dioxide surfaces increased significantly when increasing NaCl concentration from 25 mM to 100 mM. However, when increasing Na^+ concentration from 100 mM to 400 mM in binding buffers, the binding ability and the highest binding rate of yeast tRNA onto silicon dioxide surfaces decreased dramatically from (0.1393 ± 0.0029) Hz/min to (0.0193 ± 0.0033) Hz/min (Fig.4.2.12, Table S-5). This effect could be connected with the shielding of the negative charges at yeast tRNA surface as well as at silicon dioxide surfaces[21] . Therefore, in order to maximize the yeast tRNA binding ability on silicon dioxide surfaces, it is necessary to optimize the monovalent cation concentration in binding buffers. Based on the study stated previously, 100 mM

NaCl in binding buffer was the optimized concentration to enhance yeast tRNA binding on silicon dioxide surfaces.

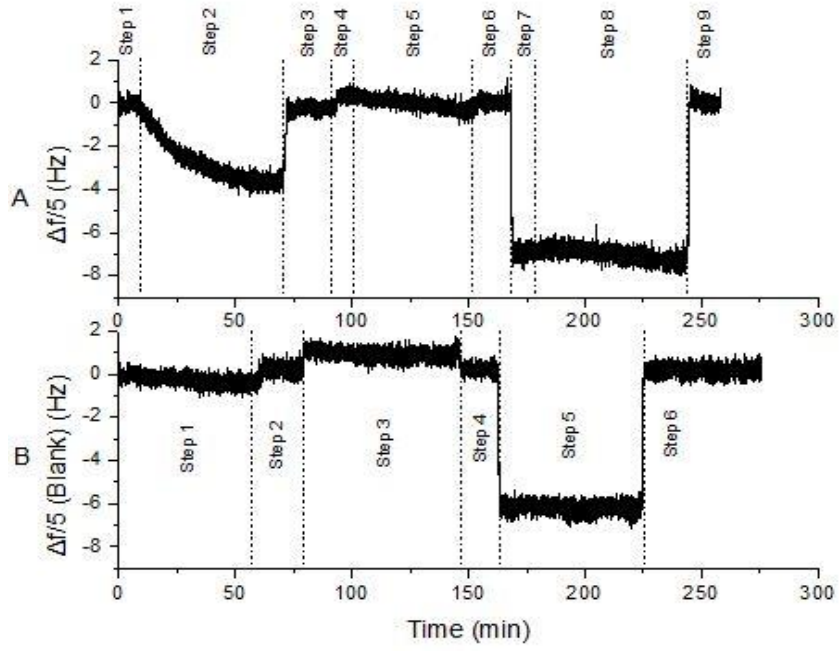

Fig.4.2.11. Frequency shift divided by the fifth overtone (Δf/5) as a function of time for yeast tRNA binding to silicon dioxide sensor under binding buffer conditions with different concentration of NaCl (25 mM, 100 mM, and 400 mM).
Panel A – Experiments with yeast tRNA solution: Step 1 - Binding buffer (25 mM Tris, 100 mM NaCl, 5 mM $MgCl_2$, pH 7.5); Step 2 – 5 μM yeast tRNA in same binding buffer as Step 1; Step 3 - Elution buffer (25 mM Tris, 8 mM EDTA, pH 8.0); Step 4 - Binding buffer (25 mM Tris, 25 mM NaCl, 5 mM $MgCl_2$, pH 7.5); Step 5 – 5 μM yeast tRNA in same binding buffer as Step 4; Step 6 (same as Step 3) - Elution buffer (25 mM Tris, 8 mM EDTA, pH 8.0); Step 7 - Binding buffer (25 mM Tris, 400 mM NaCl, 5 mM $MgCl_2$, pH 7.5); Step 8 – 5 μM yeast tRNA in same binding buffer as Step 7; Step 9 (same as Step 3) - Elution buffer (25 mM Tris, 8 mM EDTA, pH 8.0).

Panel B – 'Blank' experiments without any yeast tRNA: Step 1 - Binding buffer (25 mM Tris, 100 mM NaCl, 5 mM $MgCl_2$, pH 7.5); Step 2 - Elution buffer (25 mM Tris, 8 mM EDTA, pH 8.0); Step 3 - Binding buffer (25 mM Tris, 25 mM NaCl, 5 mM $MgCl_2$ pH 7.5); Step 4 (same as Step 2) - Elution buffer (25 mM Tris, 8 mM EDTA, pH 8.0); Step 5 - Binding buffer (25 mM Tris, 400 mM NaCl, 5 mM $MgCl_2$, pH 7.5); Step 6 (same as Step 2) - Elution buffer (25 mM Tris, 8 mM EDTA, pH 8.0).

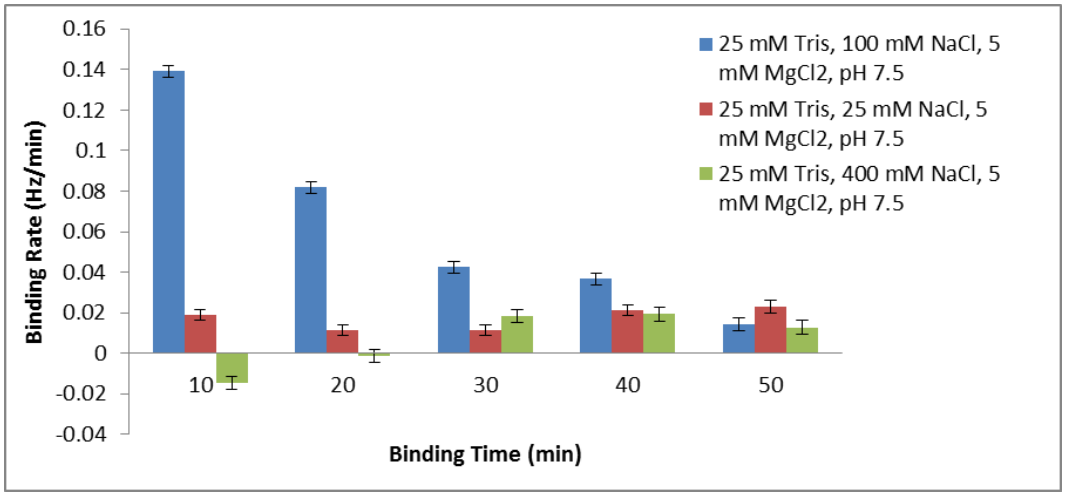

Fig.4.2.12. Binding Rates of yeast tRNA on silicon dioxide surface obtained every 10 min under binding buffer conditions, which included different concentration of NaCl: 25 mM Tris, 100 mM NaCl, 5 mM $MgCl_2$, pH 7.5 (blue bars), 25 mM Tris, 25 mM NaCl, 5 mM $MgCl_2$, pH 7.5 (red bars), 25 mM Tris, 400 mM NaCl, 5 mM $MgCl_2$, pH 7.5 (green bars).

4.2.4 Influence of Different Monovalent Cation in Binding Buffers

The effect of different monovalent salt in binding buffers on yeast tRNA binding ability to silicon dioxide surfaces was also measured by QCM-D. As shown in Fig.2.1, 59 % of the eight-five reviewed studies used NaCl as the only monovalent salt in binding buffers, while 25 % of them used KCl as monovalent salt instead. Although 15 % of the reviewed studies used both NaCl and KCl, the KCl concentration, mostly ranging from 2 mM to 5 mM, was quite small and negligible compared with NaCl concentration (ranging from 100 mM to 1000 mM) in binding buffers. The concentration of NaCl in binding buffer was optimized as

100 mM in Fig.4.2.11. QCM-D experiments were performed to measure the yeast tRNA binding ability on silicon dioxide sensor surfaces under two binding buffers – 25 mM Tris, 100 mM NaCl, 5 mM $MgCl_2$, pH 7.5, and 25 mM Tris, 100 mM KCl, 5 mM $MgCl_2$, pH 7.5. The yeast tRNA bond to bare silicon dioxide surface under both situation (see Fig.4.2.13 – Panel A). However, the binding rates of yeast tRNA in binding buffer with KCl were smaller than the ones in binding buffers with NaCl at the same concentration (Fig.4.2.14 and Table S-6). It is because Na^+ bound more tightly to yeast tRNA molecule[58,59]. Therefore, the yeast tRNA binding to silicon dioxide surfaces has preference with Na^+ as monovalent ion in binding buffers.

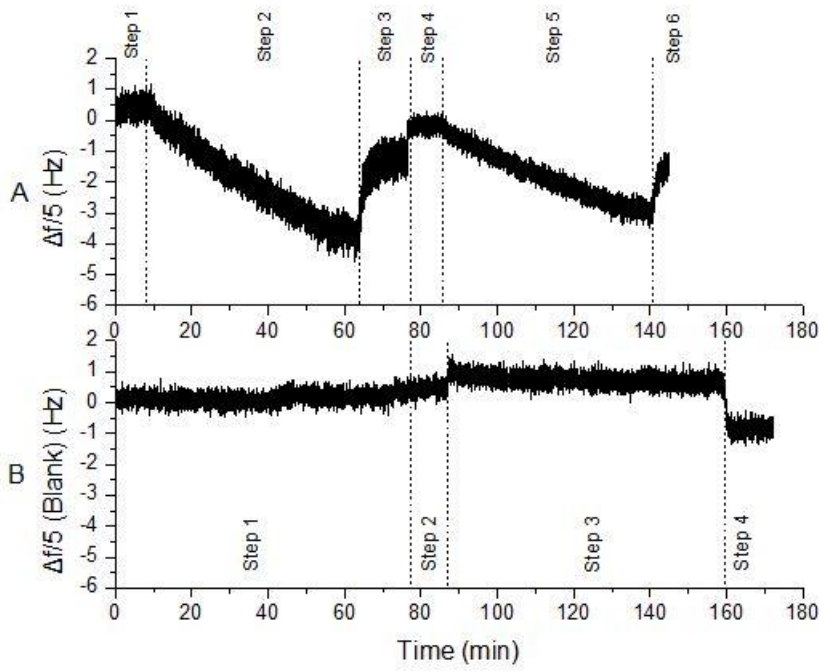

Fig.4.2.13. Frequency shift divided by the fifth overtone (Δf/5) as a function of time for yeast tRNA binding to silicon dioxide sensor under binding buffer conditions with different monovalent salt (NaCl or KCl) at 100 mM.
Panel A – Experiments with yeast tRNA solution: Step 1 - Binding buffer (25 mM Tris, 100 mM NaCl, 5 mM $MgCl_2$, pH 7.5); Step 2 – 5 μM yeast tRNA in same binding buffer as Step 1; Step 3 - Elution buffer (25 mM Tris, 8 mM EDTA, pH 8.0); Step 4 - Binding buffer (25 mM Tris, 100 mM KCl, 5 mM $MgCl_2$, pH 7.5); Step 5 – 5 μM yeast tRNA in same binding buffer as Step 4; Step 6 (same as Step 3) - Elution buffer (25 mM Tris, 8 mM EDTA, pH 8.0).

Panel B – 'Blank' experiments without any yeast tRNA: Step 1 - Binding buffer (25 mM Tris, 100 mM NaCl, 5 mM $MgCl_2$, pH 7.5); Step 2 - Elution buffer (25 mM Tris, 8 mM EDTA, pH 8.0); Step 3 - Binding buffer (25 mM Tris, 100 mM KCl, 5 mM $MgCl_2$ pH 7.5); Step 4 (same as Step 2) - Elution buffer (25 mM Tris, 8 mM EDTA, pH 8.0).

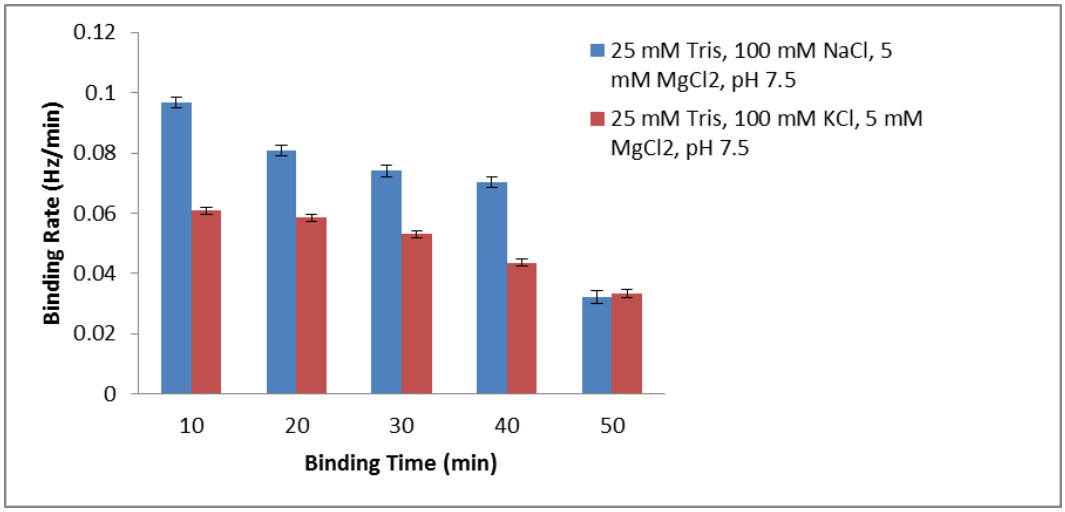

Fig.4.2.14. Binding Rates of yeast tRNA on silicon dioxide surface obtained every 10 min under binding buffer conditions, which included different monovalent salt: 25 mM Tris, 100 mM NaCl, 5 mM $MgCl_2$, pH 7.5 (blue bars), 25 mM Tris, 25 mM NaCl, 5 mM $MgCl_2$, pH 7.5 (red bars), 25 mM Tris, 400 mM NaCl, 5 mM $MgCl_2$, pH 7.5 (blue bars).

4.2.5 Influence of Different Binding Buffer pH

Ahmad *et al.*[17] found that the aptamer affinity was influenced by net charge of target protein, so that optimizing the binding buffer pH was significant to improve the selection efficiency. Moreover, Hianik *et al.*[21] found that different pH could influence the binding behavior of thrombin to aptamer immobilized on QCM-D sensor surface. The pH of binding buffer did not only influence single stranded aptamer binding to target, but also double strained DNA adsorption. As Cai *et al.*[28] pointed out, a marked decreasing of salmon sperm DNA adsorption was observed with the increased pH. In this study, measurements of yeast tRNA

binding ability to bare silicon dioxide surfaces in binding buffers with different pH were performed by QCM-D.

The measurements were performed continuously with following orders using QCM-D:

- 5 μM yeast tRNA in 25 mM Tris, 100 mM NaCl, 5 mM $MgCl_2$ pH 6.5;
- 5 μM yeast tRNA in 25 mM Tris, 100 mM NaCl, 5 mM $MgCl_2$ pH 7.5;
- 5 μM yeast tRNA in 25 mM Tris, 100 mM NaCl, 5 mM $MgCl_2$ pH 8.5.

After each single experiment, elution buffer – 25 mM Tris, 8 mM EDTA, pH 8.0 – was used to elute all the bond yeast tRNA from silicon dioxide sensor surface. As shown in Fig.4.2.15, after pumping elution buffer for approximate 10 min, the change of frequency was back to the point where elution buffer was in the corresponding 'blank' experiments. For instance, when elute the bond yeast tRNA in 'step 6' of Fig.4.2.15 – Panel A, the change of frequency went up to approximate -1 Hz, while the change of frequency was stabilized at about -1 Hz when changing from blank binding buffer ('step 3' in Fig.4.2.15 – Panel B) to elution buffer ('step 4' in Fig.4.2.15 – Panel B). That indicated all yeast tRNA was eluted from the silicon dioxide sensor surface with elution buffer.

In order to confirm that the only influence factor on yeast tRNA binding behavior was the binding buffer pH. All the other cations in binding buffers were

controlled at the same concentration. The measuring of yeast tRNA binding on silicon dioxide surfaces with pH 7.5 binding buffer was performed at both before and after the experiment with pH 8.5 binding buffer and pH 6.5 binding buffer (Fig.S-1 and Fig.S-2). The binding ability of yeast tRNA on silicon dioxide sensor surfaces did not change because of the order difference or lasting experiment time. Thus, the difference of yeast tRNA binding ability on silicon dioxide surfaces which were shown as different frequency shift in Fig.4.2.15 were only related to the pH of binding buffers.

Yeast tRNA only showed significant binding onto silicon dioxide surfaces when the binding buffer pH was neutral—7.5. Yeast tRNA rarely bound on silicon dioxide surfaces in acid (pH 6.5) buffer condition (Fig.4.2.15). Although it showed that yeast tRNA tended to bind a little in alkaline (pH 8.5) binding buffer condition, the binding rates of yeast tRNA in binding buffer with pH of 8.5, calculated every 10 min, were mostly half smaller compared with the binding rates of yeast tRNA at pH of 7.5 (see Fig.4.2.16 and Table S-7). Therefore, the yeast tRNA performed maximum binding on silicon dioxide surfaces when the pH of binding buffer is 7.5.

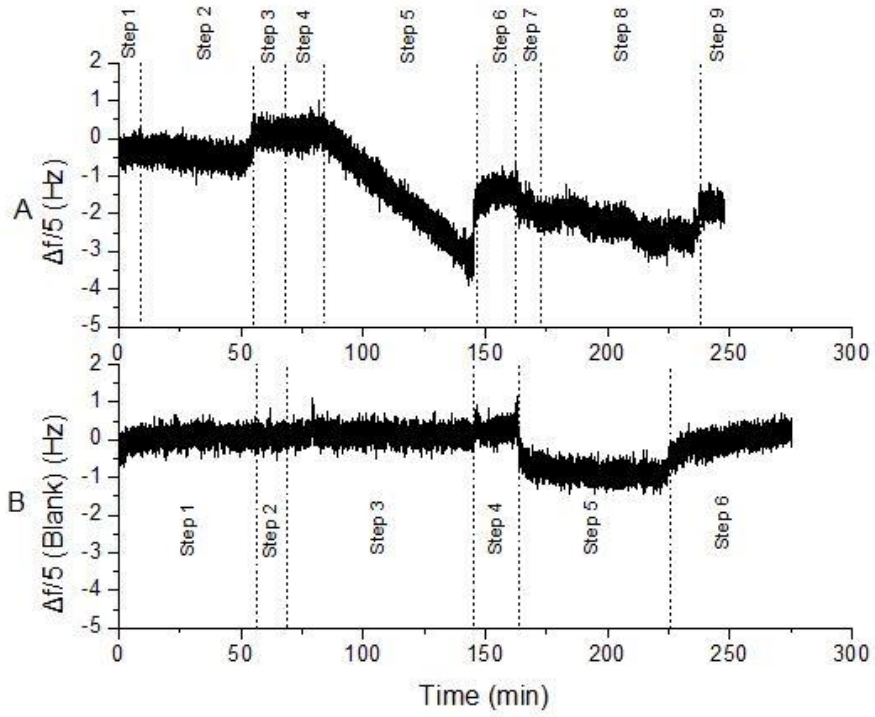

Fig.4.2.15. Frequency shift divided by the fifth overtone (Δf/5) as a function of time for yeast tRNA binding to silicon dioxide sensor under binding buffer conditions with different pH (6.5,7.5, and 8.5).
Panel A – Experiments with yeast tRNA solution: Step 1 - Binding buffer (25 mM Tris, 100 mM NaCl, 5 mM $MgCl_2$, pH 6.5); Step 2 – 5 μM yeast tRNA in same binding buffer as Step 1; Step 3 - Elution buffer (25 mM Tris, 8 mM EDTA, pH 8.0); Step 4 - Binding buffer (25 mM Tris, 100 mM NaCl, 5 mM $MgCl_2$, pH 7.5); Step 5 – 5 μM yeast tRNA in same binding buffer as Step 4; Step 6 (same as Step 3) - Elution buffer (25 mM Tris, 8 mM EDTA, pH 8.0); Step 7 - Binding buffer (25 mM Tris, 100 mM NaCl, 5 mM $MgCl_2$, pH 8.5); Step 8 – 5 μM yeast tRNA in same binding buffer as Step 7; Step 9 (same as Step 3) - Elution buffer (25 mM Tris, 8 mM EDTA, pH 8.0).

Panel B – 'Blank' experiments without any yeast tRNA: Step 1 - Binding buffer (25 mM Tris, 100 mM NaCl, 5 mM $MgCl_2$, pH 6.5); Step 2 - Elution buffer (25 mM Tris, 8 mM EDTA, pH 8.0); Step 3 - Binding buffer (25 mM Tris, 100 mM NaCl, 5 mM $MgCl_2$ pH 7.5); Step 4 (same as Step 2) - Elution buffer (25 mM Tris, 8 mM EDTA, pH 8.0); Step 5 - Binding buffer (25 mM Tris, 100 mM NaCl, 5 mM $MgCl_2$, pH 8.5); Step 6 (same as Step 2) - Elution buffer (25 mM Tris, 8 mM EDTA, pH 8.0).

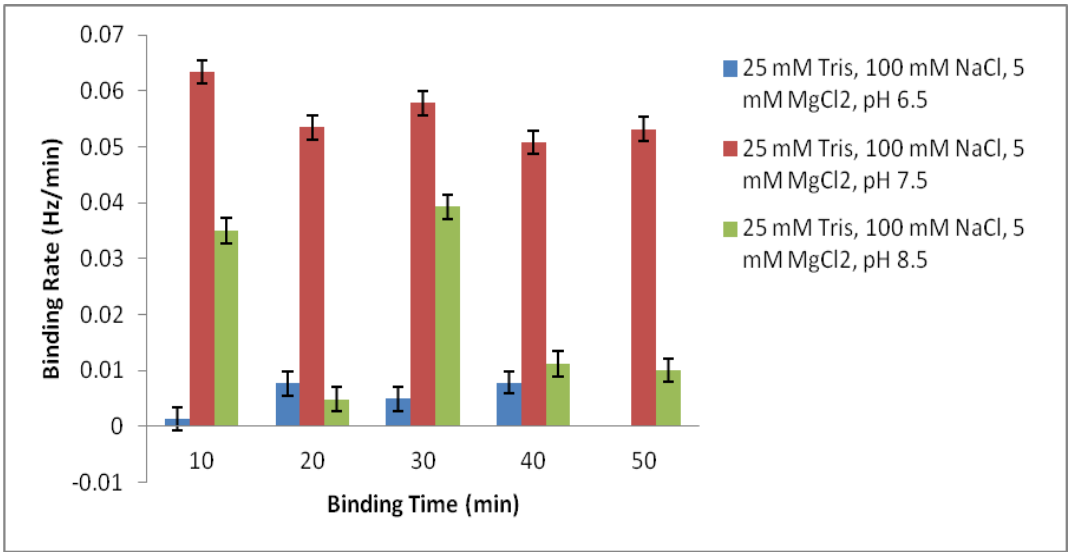

Fig.4.2.16. Binding Rates of yeast tRNA on silicon dioxide surface obtained every 10 min under binding buffer conditions, which included different pH: 25 mM Tris, 100 mM NaCl, 5 mM $MgCl_2$, pH 6.5 (blue bars), 25 mM Tris, 100 mM NaCl, 5 mM $MgCl_2$, pH 7.5 (red bars), 25 mM Tris, 100 mM NaCl, 5 mM $MgCl_2$, pH 8.5 (green bars).

The binding rates of yeast tRNA on silicon dioxide surfaces with binding buffer - 25 mM Tris, 100 mM NaCl, 5 mM $MgCl_2$, pH 7.5 – obtained from different measurements were compared in order to confirm its consistency. Even though the experiments were performed on different silicon dioxide QCM-D sensor surface at different time, yeast tRNA still showed similar binding rates (see Fig.4.2.17). It indicated that the results of yeast tRNA binding on silicon dioxide sensor surfaces obtained from QCM-D were repeatable and reliable. The yeast tRNA binding was only influenced by binding buffer conditons.

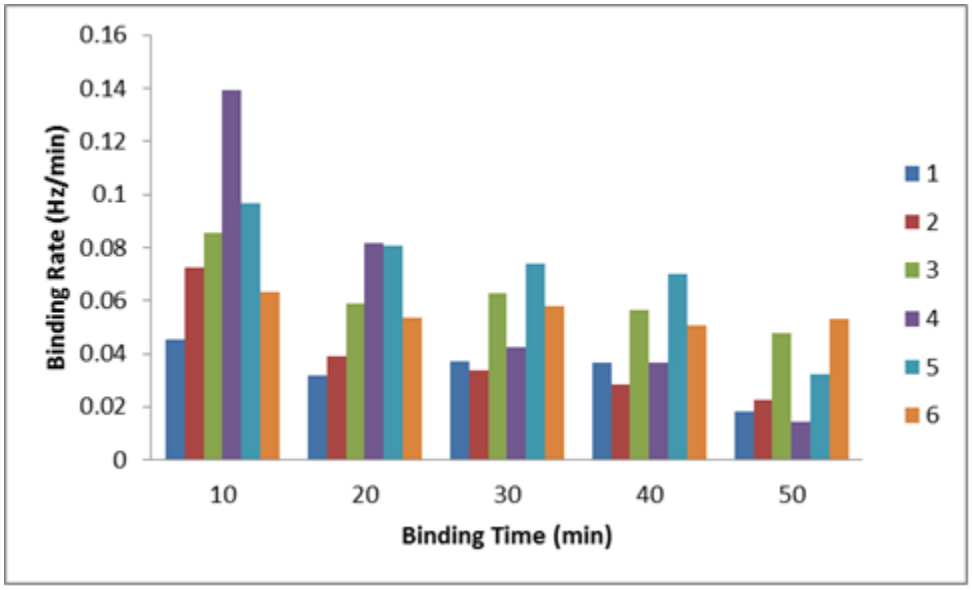

Fig.4.2.17. Binding Rates of yeast tRNA on silicon dioxide surface obtained every 10 min under binding buffer condition – 25 mM Tris, 100 mM NaCl, 5 mM $MgCl_2$, pH 7.5: Bars 1-measurement performed in step 2 of Fig.4.2.4, Bars 2-measurement performed in step 11 of Fig.4.2.4, Bars 3-measurement performed in step 8 of Fig.4.2.7, Bars 4-measurement performed in step 2 of Fig.4.2.11, Bars 5-measurement performed in step 2 of Fig.4.2.13, Bars 6-measurement performed in step 5 of Fig.4.2.15.

4.3 Verification of PET-G Sensor Surface with ATR

The PET-G coated QCM-D sensor surface was custom prepared by Q-sense. In order to confirm the chemical property of the transparent material coated on gold surface, attenuated total reflection (ATR) model of Fourier Transform Infrared Microscope HYPERION 3000 was used. As a comparison, the chemical property of PET-G (Fig.4.3.1) sheet (McMaster-Carr) and Acrylic (Fig.4.3.2)

sheet (McMaster-Carr) were tested with Fourier Transform Infrared Microscope HYPERION 3000 (Fig.4.3.3 and Fig.4.3.4) as well. While comparing the two spectra, the high peaks at 1700 cm^{-1} were consistent, showing the C=O group existing in both PET-G and Acrylic[60]. However, the relatively small peaks at 1505.51, 1340.58, and 871.86 cm^{-1} only appeared in PET-G measurement, which indicated the benzene group in PET-G[61]. In addition, there is clear difference in the large peaks ranging from 900 cm^{-1} to 1300 cm^{-1}, due to the different stretch force of C-H and C-O groups in PET-G and Acrylic[62]. Therefore, Fourier Transform Infrared Microscope HYPERION 3000 is a reliable instrument to verify the PET-G coated QCM-D sensor surface.

Fig 4.3.5 showed the measurement of PET-G coated QCM-D sensor by Fourier Transform Infrared Microscope HYPERION 3000. Compared with PET-G sheet spectrum, the main characteristic peaks at 1505.51, 1340.58, and 871.86 cm^{-1} are consistent, indicating both surface had benzene group. Moreover, the relative high peaks at 1700 cm^{-1} which represented the C=O group, and the multiple peeks under 1400 cm^{-1} were consistent as well. Therefore, the spectrum from Fourier Transform Infrared Microscope HYPERION 3000 verified that the transparent material coated onto QCM-D sensor surface was PET-G.

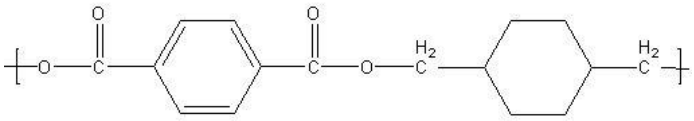

Fig.4.3.1. Chemical structure of PET-G

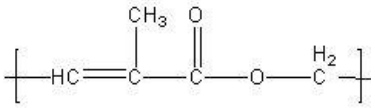

Fig.4.3.2. Chemical structure of Acrylic

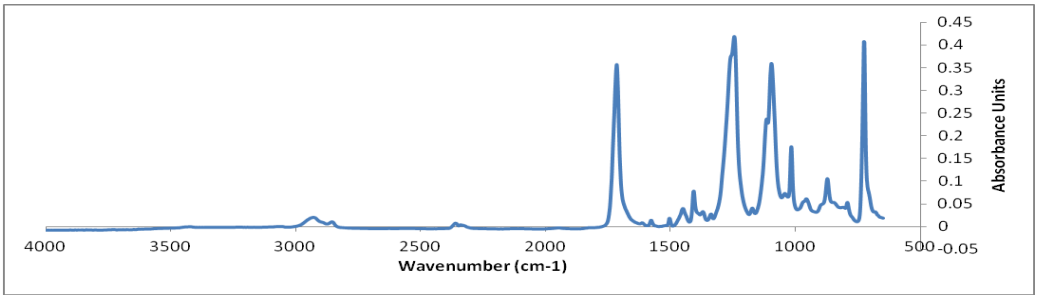

Fig.4.3.3. ATR spectrum of PET-G sheet measured by Fourier Transform Infrared Microscope HYPERION 3000.

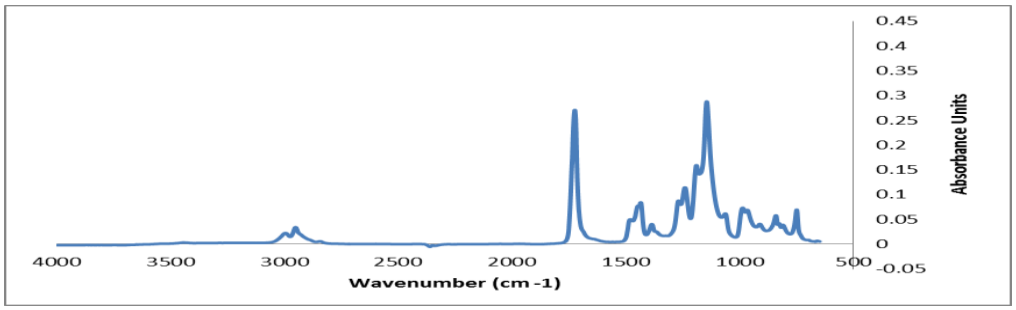

Fig.4.3.4. ATR spectrum of Acrylic sheet measured by Fourier Transform Infrared Microscope HYPERION 3000.

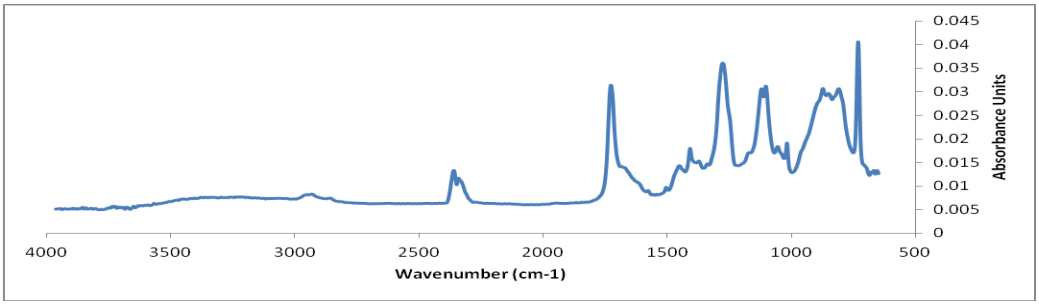

Fig.4.3.5. ATR spectrum of PET-G coated QCM-D sensor measured by Fourier Transform Infrared Microscope HYPERION 3000 (The y-axis scal is ten times smaller of the one in Fig.4.3.3 and Fig.4.3.4).

4.4 Yeast tRNA Binding Behavior on PET-G Surfaces

4.4.1 Influence of Different Divalent Cation in Binding Buffers

From previous measurements, divalent cation, especially Mg^{2+}, in binding buffers acted as significant 'bridge' to bring yeast tRNA binding onto silicon dioxide surfaces. Yeast tRNA in binding buffers with Mg^{2+} showed much stronger adsorption ability than the one in binding buffers without any divalent cation (Fig.4.2.6). Similar measurements were also performed on PET-G coated QCM-D sensors.

After obtained a stable baseline by pumping just binding buffer – 25 mM Tris, 100 mM NaCl, 5 mM $MgCl_2$, pH 7.5 – for the first approximate 10 min ('step 1' in Fig.4.4.1 – Panel A), 5 μM yeast tRNA in the same binding buffer was pumped into QCM-D system with the same binding buffer for approximate 50 min ('step 2'). The frequency quickly shifted down, which represented yeast tRNA bound to the surface. Then the valve was switched to pump elution buffer – 25 mM Tris, 10 mM EDTA, pH 8.5, so that the bounded yeast tRNA could be eluted from PET-G sensor surface.

In order to verify that the frequency shift actually represented that yeast tRNA was adsorbed onto PET-G sensor surfaces and then eluted from the surface with elution buffer. Gel electrophoresis was performed to measure a series of samples collected before binding and during elution process. The yeast tRNA

sample was collected from yeast tRNA in binding buffer (25 mM Tris, 100 mM NaCl, 5 mM $MgCl_2$, pH 7.5), and the pump waste outlet stream first immediately after switching to the elution buffer and then at 2 minute intervals; a total of eight samples were collected (Lanes 3 through 10 in Fig 4.4.3).The band intensity was kept the same as the one in binding buffer (25 mM Tris, 100 mM NaCl, 5 mM $MgCl_2$, pH 7.5) when just pumped elution buffer in QCM-D system, however, decreased gradually after running elution buffer for 2 min, 4 min, and 6 min. Yeast tRNA can be rarely detected after running elution buffer for 8 min, which appears to coincide with the change in frequency as measured by QCM-D.

Moreover, as shown in Fig 4.4.1 – Panel B, the frequency did not change if running just binding buffer – 25 mM Tris, 100 mM NaCl, 5 mM $MgCl_2$, pH 7.5 (‘step 1’ in Fig 4.4.1 – Panel B). Therefore, the binding of yeast tRNA to a PET-G sensor surface and elution of yeast tRNA from the surface could be both detected accurately using QCM-D in real time and showed as frequency shifts.

QCM-D experiments with yeast tRNA-free solutions were also conducted to examine whether the buffer effect is important for binding behavior measurements. The change in frequency (Fig.4.4.1 – Panel B) when the solutions were changed from binding buffer to elution buffer were compatible with the ones in the experiments containing yeast tRNA (Fig.4.4.1 – Panel A). For example, when the valve was switched from binding buffer (25 mM Tris, 100 mM NaCl, 5

mM $MgCl_2$, pH 7.5) containing 5 μM yeast tRNA ('step 2' in Fig.4.4.1-A) to elution buffer—25 mM Tris, 10 mM EDTA, pH 8.5 ('step 3' in Fig.4.4.1-A), the change of frequency went back to approximate 4 Hz. The frequency difference from the stable baseline ('step 1' in Fig.4.4.1 – Panel A) was about 3.5 Hz, which was compatible with the corresponding 'blank' experiments (Fig.4.4.1 – Panel B from 'step 1' to 'step 2'). Therefore, all bound yeast tRNA was eluted from PET-G surface with elution buffer and did not affect further experiment.

During the yeast tRNA binding experiment, the change of dissipation were less than 1.2×10^{-6} (Fig.4.4.2 – Panel A), indicating that yeast tRNA layer binding on the PET-G surfaces was stable and did not aggregate under the studied binding buffer condition[54]. Therefore, the frequency shift is proportional to the change of yeast tRNA deposited mass on surfaces which can be quantified by Sauerbrey equation (equation 1). Thus, the rate of frequency shift can represent the rate of yeast tRNA binding mass on surface, which can be quantified by equation 3.

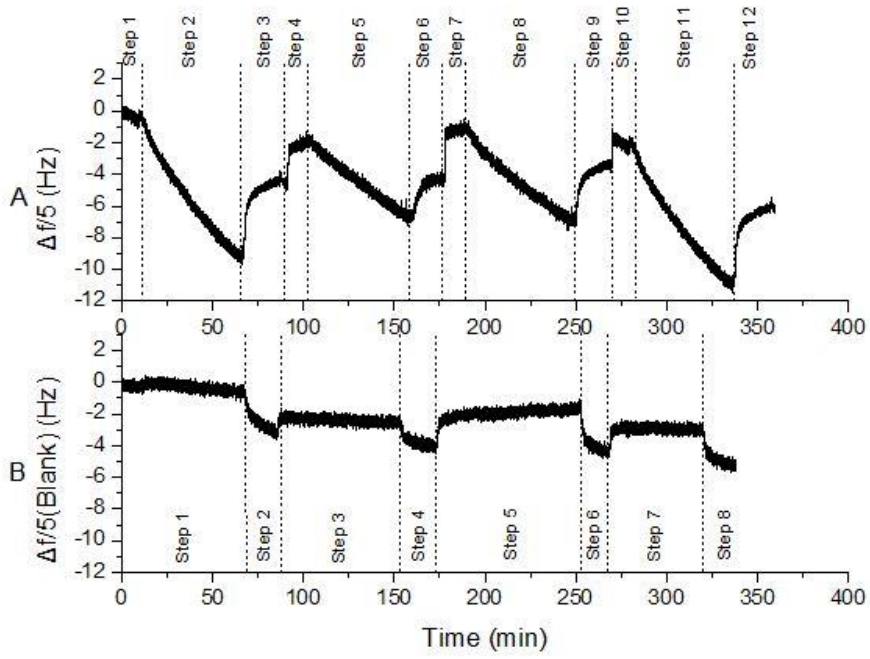

Fig.4.4.1. Frequency shift divided by the fifth overtone (Δf/5) as a function of time for yeast tRNA binding to PET-G sensor under binding buffer conditions with or without divalent salt ($CaCl_2$ or $MgCl_2$) at 5 mM concentration.
Panel A – Experiments with yeast tRNA solution: Step 1 - Binding buffer (25 mM Tris, 100 mM NaCl, 5 mM $MgCl_2$, pH 7.5); Step 2 – 5 μM yeast tRNA in same binding buffer as Step 1; Step 3 - Elution buffer (25 mM Tris, 10 mM EDTA, pH 8.5); Step 4 - Binding buffer (25 mM Tris, 100 mM NaCl, pH 7.5); Step 5 – 5 μM yeast tRNA in same binding buffer as Step 4; Step 6 (same as Step 3) - Elution buffer (25 mM Tris, 10 mM EDTA, pH 8.5); Step 7 - Binding buffer (25 mM Tris, 100 mM NaCl, 5 mM $CaCl_2$, pH 7.5); Step 8 – 5 μM yeast tRNA in same binding buffer as Step 7; Step 9 (same as Step 3) - Elution buffer (25 mM Tris, 10 mM EDTA, pH 8.5); Step 10 (same as Step 1) - Binding buffer (25 mM Tris, 100 mM NaCl, 5 mM $MgCl_2$, pH 7.5); Step 11 (same as Step 2) – 5 μM yeast tRNA in same binding buffer as Step 10; Step 12 (same as Step 3) - Elution buffer (25 mM Tris, 10 mM EDTA, pH 8.5).

Panel B – 'Blank' experiments without any yeast tRNA: Step 1 - Binding buffer (25 mM Tris, 100 mM NaCl, 5 mM $MgCl_2$ pH 7.5); Step 2 - Elution buffer (25 mM Tris, 10 mM EDTA, pH 8.5); Step 3 - Binding buffer (25 mM Tris, 100 mM NaCl, pH 7.5); Step 4 (same as Step 2) - Elution buffer (25 mM Tris, 10 mM EDTA, pH 8.5); Step 5 - Binding buffer (25 mM Tris, 100 mM NaCl, 5 mM $CaCl_2$, pH 7.5); Step 6 (same as Step 2) - Elution buffer (25 mM Tris, 10 mM EDTA, pH 8.5); Step 7 (same as Step 1) - Binding buffer (25 mM Tris, 100 mM NaCl, 5 mM $MgCl_2$, pH 7.5); Step 8 (same as Step 2) - Elution buffer (25 mM Tris, 10 mM EDTA, pH 8.5).

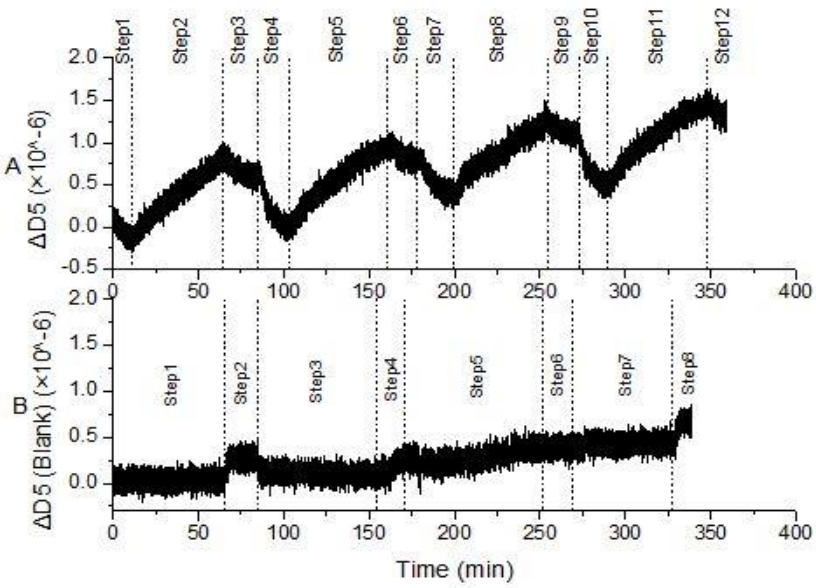

Fig.4.4.2. Associated dissipation shift (ΔD_5) as a function of time for the same experimental conditions as detailed in Fig 4.4.1.

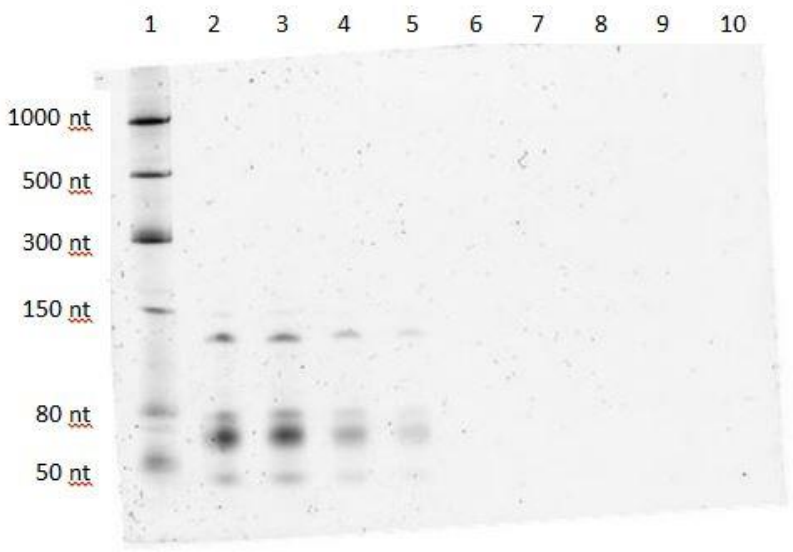

Fig.4.4.3. 8% denaturing gel electrophoresis image of samples collected during experiment corresponding to results in Fig 4.4.1 from step 1 to step 3. Lane 1 - 5 μL low range ssRNA ladder (NEB); Lane 2 – 5 μL of stock solution of 5 μM yeast tRNA solution in binding buffer (25 mM Tris, 100 mM NaCl, 5 mM $MgCl_2$, pH 7.5); Lane 3 - 5 μL of sample collected from pump waste after running elution buffer for 0 min; Lanes 4 through 10 - 5 μL of sample collected from pump waste after running elution buffer for 2, 4, 6, 8, 10, 12, and 14.

After eluted the bound yeast tRNA from PET-G surfaces using elution buffer—25 mM Tris, 10 mM EDTA, pH 8.5, the valve was switched to the binding buffer without any divalent salt (25 mM Tris, 100 mM NaCl, pH 7.5). Different from no binding as shown on silicon dioxide surfaces, yeast tRNA was gradually adsorbed on PET-G surfaces at smaller binding rates (Fig.4.4.4). As for the binding buffer with Ca^{2+} as divalent cation, the binding rates stayed similar as the ones in binding buffers without any divalent cations (see Fig.4.4.4 and Table S-8). Meanwhile, the measurement of yeast tRNA binding to PET-G surface in binding buffer with Mg^{2+} as divalent cation, which was measured at the end of series

experiments, performed similar adsorption ability and binding rates with the measurement at the beginning ('step 1' to 'step 3' in Fig.4.4.1 – Panel A). That indicated the difference of yeast tRNA binding behavior was only related to the different binding buffer conditions, but not related to order of the experiment.

Therefore, yeast tRNA binding ability on PET-G surfaces increased by adding Mg^{2+} in binding buffers. However, the process of yeast tRNA binding to PET-G surfaces was not preferable for every kind of divalent cation. Ca^{2+} did not enhance the binding ability of yeast tRNA on PET-G surfaces. Such results were compatible with the ones from yeast tRNA binding to silicon dioxide surface measurement.

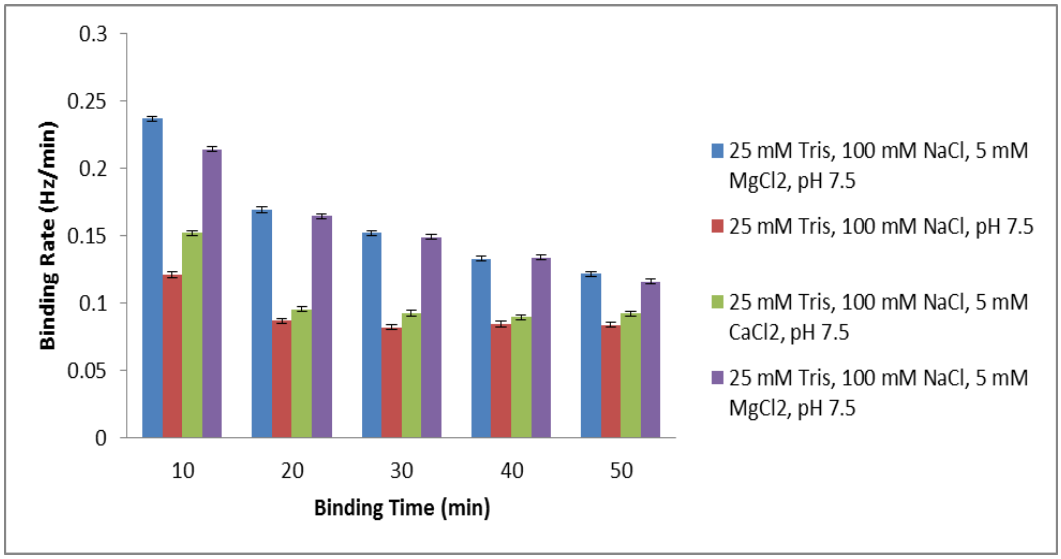

Fig.4.4.4. Binding Rates of yeast tRNA on PET-G surface obtained every 10 min under binding buffer conditions, which either included Mg^{2+} or Ca^{2+}, or did not contain any divalent cations: 25 mM Tris, 100 mM NaCl, 5 mM $MgCl_2$, pH 7.5 (blue bars and purple bars), 25 mM Tris, 100 mM NaCl, 5 mM $CaCl_2$, pH 7.5 (green bars), 25 mM Tris, 100 mM NaCl, pH 7.5 (red bars).

4.4.2 Influence of the Divalent Cation Concentration in Binding Buffers

From previous experiments in Fig.4.4.1, the adsorption of yeast tRNA on PET-G surfaces was highly enhanced by adding 5 mM $MgCl_2$ in binding buffer. The concentration of $MgCl_2$ in binding buffer was optimized through QCM-D. The other parameters of binding buffers were controlled as the same—25 mM Tris as the buffer base, 100 mM NaCl as monovalent salt. All the binding buffer pH was adjusted to 7.5 by HCl and NaOH in DEPC-H_2O. $MgCl_2$ concentration was ranged from 0.2 mM, 1 mM, 5 mM to 25 mM, which was compatible with

the measurements on silicon dioxide surfaces. As shown in Fig. 4.4.5 – Panel A, yeast tRNA bound to PET-G surfaces at any concentration of $MgCl_2$. The binding rates calculated every 10 min tended to increase with the increasing concentration of $MgCl_2$ from 0.2 mM to 5 mM (Fig.4.4.6 and Table S-9). However, the yeast tRNA binding ability on PET-G surfaces performed weaker in binding buffers containing 25 mM of $MgCl_2$ than in binding buffers containing 5 mM of $MgCl_2$. Therefore, the optimized concentration of $MgCl_2$ in binding buffer for yeast tRNA on PET-G surface was 5 mM based on the measurements. These results were compatible with the ones obtained from yeast tRNA binding to silicon dioxide surfaces. In order to maximize the yeast tRNA background blocking efficiency in aptamer SELEX process, the concentration of Mg^{2+} in binding buffer should be set at 5 mM.

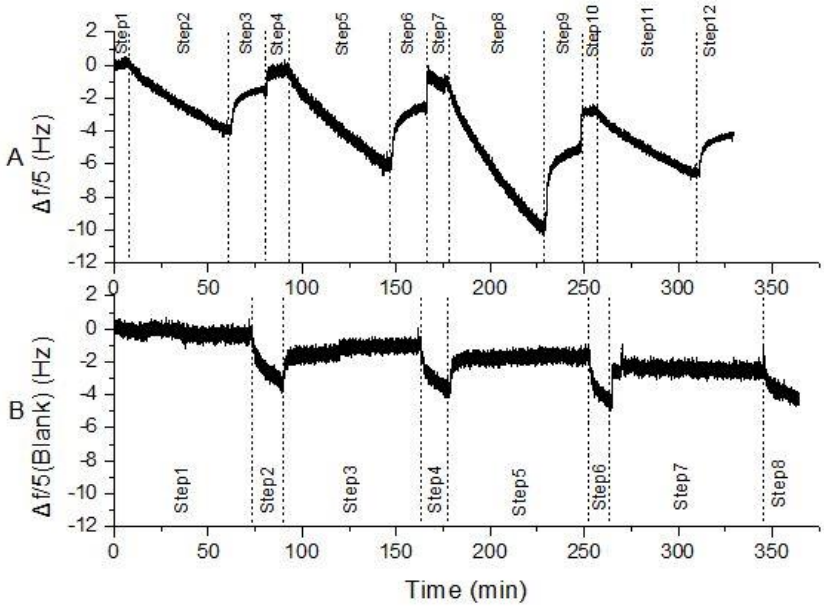

Fig.4.4.5. Frequency shift divided by the fifth overtone (Δf/5) as a function of time for yeast tRNA binding to PET-G sensor under binding buffer conditions with different concentration of $MgCl_2$ (0.2 mM, 1 mM, 5 mM, and 25 mM). Panel A – Experiments with yeast tRNA solution: Step 1 - Binding buffer (25 mM Tris, 100 mM NaCl, 0.2 mM $MgCl_2$, pH 7.5); Step 2 – 5 μM yeast tRNA in same binding buffer as Step 1; Step 3 - Elution buffer (25 mM Tris, 10 mM EDTA, pH 8.5); Step 4 - Binding buffer (25 mM Tris, 100 mM NaCl, 1 mM $MgCl_2$, pH 7.5); Step 5 – 5 μM yeast tRNA in same binding buffer as Step 4; Step 6 (same as Step 3) - Elution buffer (25 mM Tris, 10 mM EDTA, pH 8.5); Step 7 - Binding buffer (25 mM Tris, 100 mM NaCl, 5 mM $MgCl_2$, pH 7.5); Step 8 – 5 μM yeast tRNA in same binding buffer as Step 7; Step 9 (same as Step 3) - Elution buffer (25 mM Tris, 10 mM EDTA, pH 8.5); Step 10 (same as Step 1) - Binding buffer (25 mM Tris, 100 mM NaCl, 25 mM $MgCl_2$, pH 7.5); Step 11 (same as Step 2) – 5 μM yeast tRNA in same binding buffer as Step 10; Step 12 (same as Step 3) - Elution buffer (25 mM Tris, 10 mM EDTA, pH 8.5).

Panel B – 'Blank' experiments without any yeast tRNA: Step 1 - Binding buffer (25 mM Tris, 100 mM NaCl, 0.2 mM $MgCl_2$, pH 7.5); Step 2 - Elution buffer (25 mM Tris, 10 mM EDTA, pH 8.5); Step 3 - Binding buffer (25 mM Tris, 100 mM NaCl, 1 mM $MgCl_2$ pH 7.5); Step 4 (same as Step 2) - Elution buffer (25 mM Tris, 10 mM EDTA, pH 8.5); Step 5 - Binding buffer (25 mM Tris, 100 mM NaCl, 5 mM $MgCl_2$, pH 7.5); Step 6 (same as Step 2) - Elution buffer (25 mM Tris, 10 mM EDTA, pH 8.5); Step 7 (same as Step 1) - Binding buffer (25 mM Tris, 100 mM NaCl, 25 mM $MgCl_2$, pH 7.5); Step 8 (same as Step 2) - Elution buffer (25 mM Tris, 10 mM EDTA, pH 8.5).

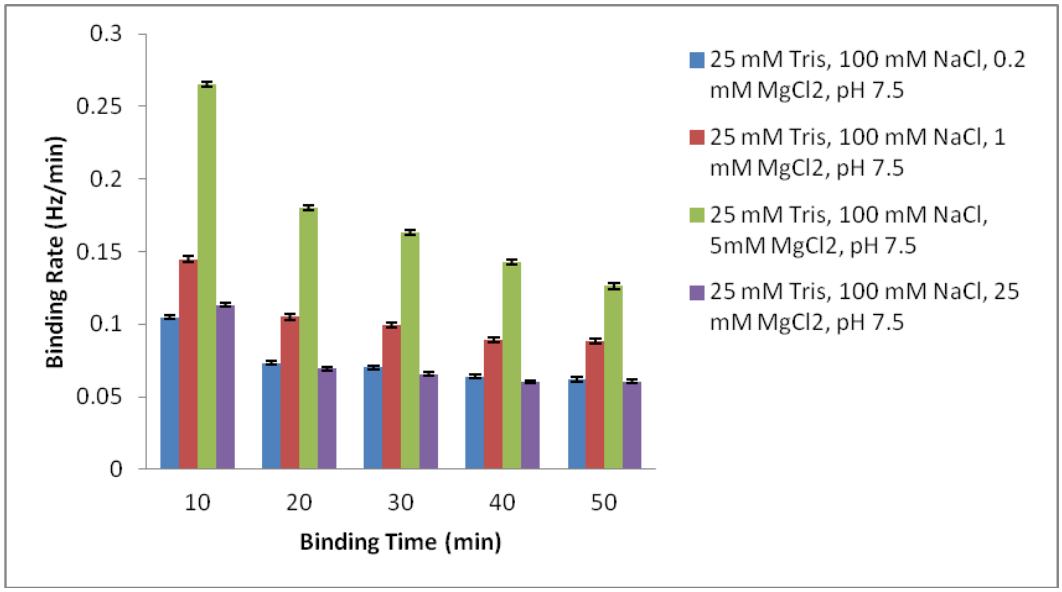

Fig.4.4.6. Binding Rates of yeast tRNA on PET-G surface obtained every 10 min under binding buffer conditions, which included different concentration of $MgCl_2$: 25 mM Tris, 100 mM NaCl, 0.2 mM $MgCl_2$, pH 7.5 (blue bars), 25 mM Tris, 100 mM NaCl, 1 mM $MgCl_2$, pH 7.5 (red bars), 25 mM Tris, 100 mM NaCl, 5 mM $MgCl_2$, pH 7.5 (green bars), 25 mM Tris, 100 mM NaCl, 25 mM $MgCl_2$, pH 7.5 (purple bars).

Although 5 mM of Ca^{2+} in the binding buffer did not enhance yeast tRNA binding behavior on PET-G surface significantly, measurements of yeast tRNA binding abilities on PET-G surfaces with different concentration of $CaCl_2$ were performed using QCM-D, to test whether lower or higher concentration of Ca^{2+} had different effect. The concentration of $CaCl_2$ in binding buffers were ranged from 0.2 mM, 1 mM, 5 mM, to 25 mM, while the other situation of binding buffers were kept the same as 25 mM Tris, 100 mM NaCl, and pH of 7.5. The frequency shifts were similar among measurements with binding buffers

containing different concentration of $CaCl_2$ (Fig.4.4.7). While the frequency shifts in Fig.4.4.7 – Panel A resulting from changing from elution buffer to binding buffer were compatible with the shifts appeared in corresponding 'blank' experiments without any yeast tRNA in the system (Fig.4.4.7 – Panel B), all the yeast tRNA adsorbed on PET-G surface were eluted from PET-G surface with elution buffer. Thus, the binding behavior of yeast tRNA on PET-G was only influenced by the concentration of $CaCl_2$. Moreover, the preferred binding rates calculated every 10 min during yeast tRNA binding to PET-G surface did not show significant difference with variance concentration of Ca^{2+} in the binding buffer (Fig.4.4.8 and Table S-10). The binding rates of yeast tRNA on PET-G surfaces in binding buffers with Ca^{2+} performed similar with the binding rates of yeast tRNA in binding buffers without any divalent salt (see Table S-9 and Table S-11). Therefore, the different concentration of Ca^{2+} in binding buffers did not result in different binding ability of yeast tRNA on PET-G surface. Ca^{2+} did not act as significant divalent cation to influence yeast tRNA binding on PET-G surface no matter at lower or higher concentration.

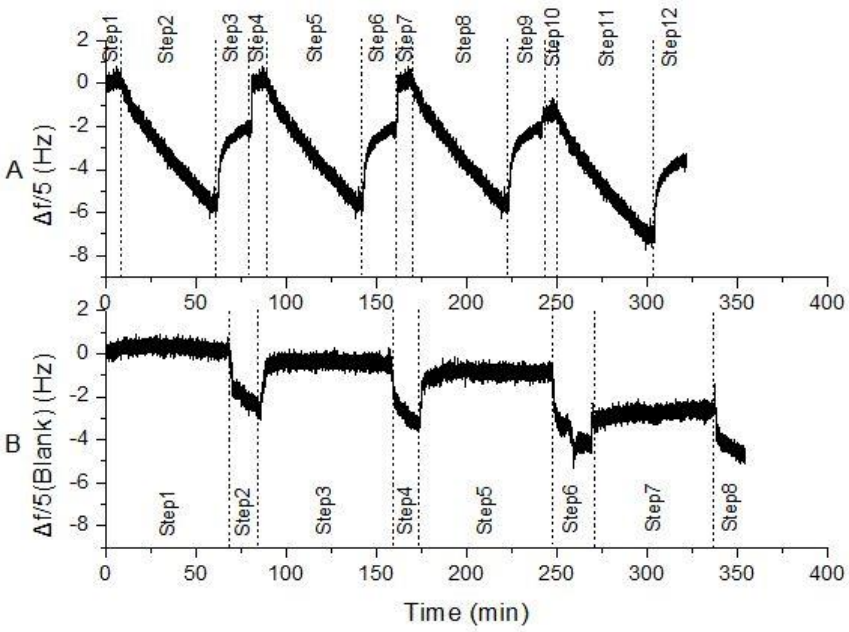

Fig.4.4.7. Frequency shift divided by the fifth overtone (Δf/5) as a function of time for yeast tRNA binding to PET-G sensor under binding buffer conditions with different concentration of $CaCl_2$ (0.2 mM, 1 mM, 5 mM, and 25 mM).
Panel A – Experiments with yeast tRNA solution: Step 1 - Binding buffer (25 mM Tris, 100 mM NaCl, 0.2 mM $CaCl_2$, pH 7.5); Step 2 – 5 μM yeast tRNA in same binding buffer as Step 1; Step 3 - Elution buffer (25 mM Tris, 10 mM EDTA, pH 8.5); Step 4 - Binding buffer (25 mM Tris, 100 mM NaCl, 1 mM $CaCl_2$, pH 7.5); Step 5 – 5 μM yeast tRNA in same binding buffer as Step 4; Step 6 (same as Step 3) - Elution buffer (25 mM Tris, 10 mM EDTA, pH 8.5); Step 7 - Binding buffer (25 mM Tris, 100 mM NaCl, 5 mM $CaCl_2$, pH 7.5); Step 8 – 5 μM yeast tRNA in same binding buffer as Step 7; Step 9 (same as Step 3) - Elution buffer (25 mM Tris, 10 mM EDTA, pH 8.5); Step 10 (same as Step 1) - Binding buffer (25 mM Tris, 100 mM NaCl, 25 mM $CaCl_2$, pH 7.5); Step 11 (same as Step 2) – 5 μM yeast tRNA in same binding buffer as Step 10; Step 12 (same as Step 3) - Elution buffer (25 mM Tris, 10 mM EDTA, pH 8.5).

Panel B – 'Blank' experiments without any yeast tRNA: Step 1 - Binding buffer (25 mM Tris, 100 mM NaCl, 0.2 mM $CaCl_2$, pH 7.5); Step 2 - Elution buffer (25 mM Tris, 10 mM EDTA, pH 8.5); Step 3 - Binding buffer (25 mM Tris, 100 mM NaCl, 1 mM $CaCl_2$ pH 7.5); Step 4 (same as Step 2) - Elution buffer (25 mM Tris, 10 mM EDTA, pH 8.5); Step 5 - Binding buffer (25 mM Tris, 100 mM NaCl, 5 mM $CaCl_2$, pH 7.5); Step 6 (same as Step 2) - Elution buffer (25 mM Tris, 10 mM EDTA, pH 8.5); Step 7 (same as Step 1) - Binding buffer (25 mM Tris, 100 mM NaCl, 25 mM $CaCl_2$, pH 7.5); Step 8 (same as Step 2) - Elution buffer (25 mM Tris, 10 mM EDTA, pH 8.5).

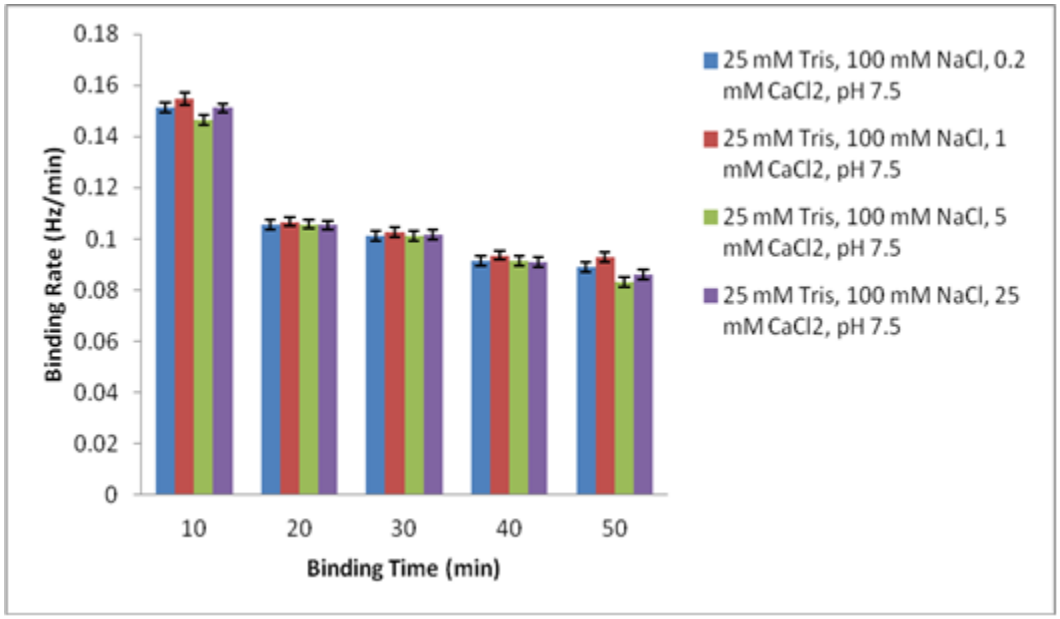

Fig.4.4.8. Binding Rates of yeast tRNA on PET-G surface obtained every 10 min under binding buffer conditions, which included different concentration of $CaCl_2$: 25 mM Tris, 100 mM NaCl, 0.2 mM $CaCl_2$, pH 7.5 (blue bars), 25 mM Tris, 100 mM NaCl, 1 mM $CaCl_2$, pH 7.5 (red bars), 25 mM Tris, 100 mM NaCl, 5 mM $CaCl_2$, pH 7.5 (green bars), 25 mM Tris, 100 mM NaCl, 25 mM $CaCl_2$, pH 7.5 (purple bars).

4.4.3 Influence of Different Monovalent Cation in Binding Buffers

QCM-D was used to test whether the different monovalent salt in binding buffer could affect the binding ability of yeast tRNA onto PET-G surfaces. Compatible with the measurements on silicon dioxide sensors, NaCl and KCl were chosen as the monovalent salt in binding buffers. The monovalent salt concentration was fixed at 100mM. In order to enhance the frequency shift results from QCM-D, 5 mM $MgCl_2$ was added in binding buffers as divalent salt, based

on previous measurements (see Fig.4.4.1). Buffer pH was adjusted to 7.5. As shown in Fig.4.4.9 – Panel A, yeast tRNA bound onto PET-G surfaces in binding buffers with either NaCl or KCl as monovalent salt. For each single binding experiment, the yeast tRNA binding rates calculated every 10 min decreased slightly with the increasing binding time. Moreover, the binding rates of yeast tRNA onto PET-G surfaces while K^+ was acting as the monovalent cation in binding buffer, were about one fourth smaller compared with the ones while Na^+ was acting as the monovalent cation in binding buffer at the same concentration (Fig.4.4.10 and Table S-11). Measurements of yeast tRNA binding on PET-G surface with Na^+ were performed both before and after the yeast tRNA binding with K^+ in binding buffer, which performed similar binding ability (Fig.4.4.9 – Panel A) and binding rates (Fig.4.4.10). It indicated that the binding behavior was only influenced by the binding buffer. Therefore, different monovalent salt in binding buffers did influence the binding behavior of yeast tRNA on PET-G surface, however, not significantly. The yeast tRNA binding to PET-G surfaces preferred Na^+ rather than K^+ as the monovalent salt in binding buffers. Such results were compatible with the ones obtained from testing on silicon dioxide sensor surface. Therefore, it is better to use Na^+ as the monovalent cation in binding buffers to enhance the yeast tRNA background pre-blocking ability in aptamer SELEX process.

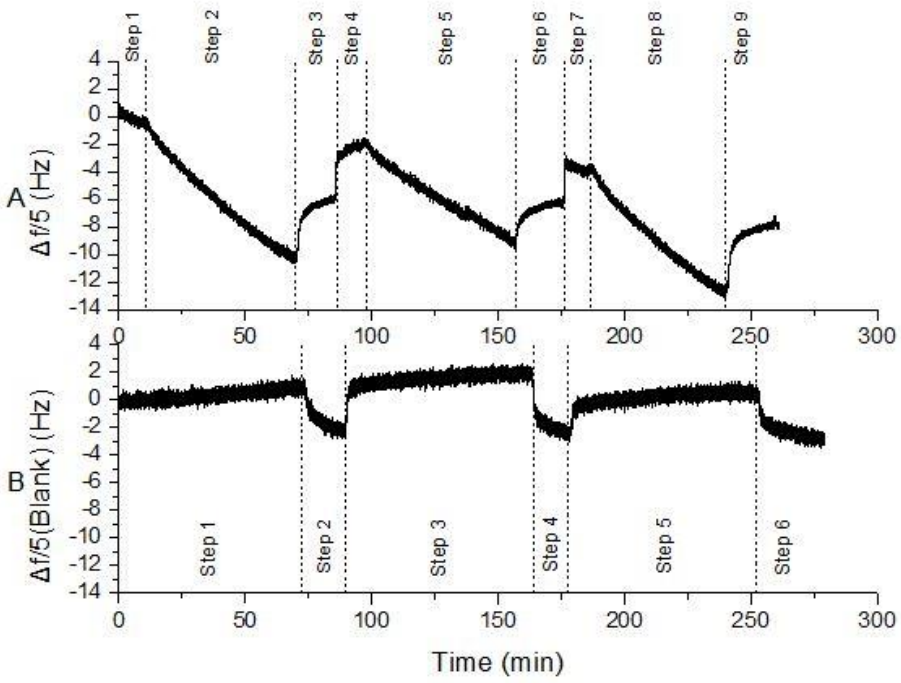

Fig.4.4.9. Frequency shift divided by the fifth overtone (Δf/5) as a function of time for yeast tRNA binding to PET-G sensor under binding buffer conditions with different monovalent salt (NaCl or KCl) at 100 mM.
Panel A – Experiments with yeast tRNA solution: Step 1 - Binding buffer (25 mM Tris, 100 mM NaCl, 5 mM $MgCl_2$, pH 7.5); Step 2 – 5 μM yeast tRNA in same binding buffer as Step 1; Step 3 - Elution buffer (25 mM Tris, 10 mM EDTA, pH 8.5); Step 4 - Binding buffer (25 mM Tris, 100 mM KCl, 5 mM $MgCl_2$, pH 7.5); Step 5 – 5 μM yeast tRNA in same binding buffer as Step 4; Step 6 (same as Step 3) - Elution buffer (25 mM Tris, 10 mM EDTA, pH 8.5); Step 7 - Binding buffer (25 mM Tris, 100 mM NaCl, 5 mM $MgCl_2$, pH 7.5); Step 8 – 5 μM yeast tRNA in same binding buffer as Step 7; Step 9 (same as Step 3) - Elution buffer (25 mM Tris, 10 mM EDTA, pH 8.5).

Panel B – 'Blank' experiments without any yeast tRNA: Step 1 - Binding buffer (25 mM Tris, 100 mM NaCl, 5 mM $MgCl_2$, pH 7.5); Step 2 - Elution buffer (25 mM Tris, 10 mM EDTA, pH 8.5); Step 3 - Binding buffer (25 mM Tris, 100 mM KCl, 5 mM $MgCl_2$ pH 7.5); Step 4 (same as Step 2) - Elution buffer (25 mM Tris, 10 mM EDTA, pH 8.5); Step 5 - Binding buffer (25 mM Tris, 100 mM NaCl, 5 mM $MgCl_2$, pH 7.5); Step 6 (same as Step 2) - Elution buffer (25 mM Tris, 10 mM EDTA, pH 8.5).

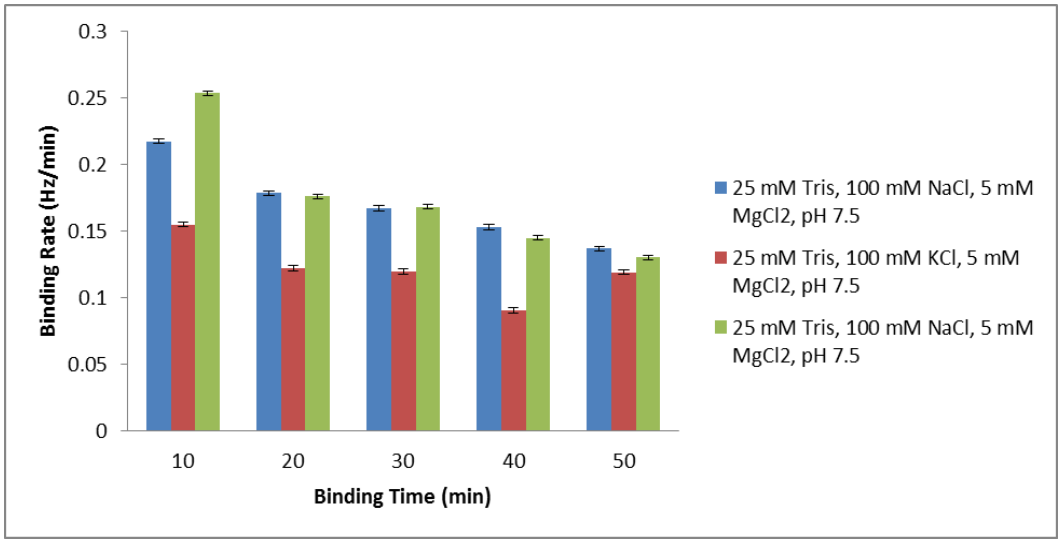

Fig.4.4.10. Binding Rates of yeast tRNA on PET-G surface obtained every 10 min under binding buffer conditions, which included different monovalent salt (NaCl or KCl) at 100 mM: 25 mM Tris, 100 mM NaCl, 5 mM $MgCl_2$, pH 7.5 (blue bars and green bars), 25 mM Tris, 100 mM KCl, 5 mM $MgCl_2$, pH 7.5 (red bars).

4.4.4 Influence of Different Concentration NaCl in Binding Buffers

Low monovalent salt concentration (25 mM NaCl) in binding buffer resulted in rarely adsorption of yeast tRNA on silicon dioxide surfaces because of the charge repulsion force between yeast tRNA and silicon dioxide surface. The adsorption of yeast tRNA on silicon dioxide surfaces was also hardly able to be detected by QCM-D in binding buffer with high concentration of monovalent salt (400 mM NaCl), because of the shielding of negative charges on yeast tRNA or silicon dioxide surface. As a significant influence factor, the concentration of NaCl in binding buffer for yeast tRNA binding on PET-G surfaces was optimized

using QCM-D. 5 mM $MgCl_2$ was used as divalent salt in binding buffers to ensure the possible maximize yeast tRNA adsorption. Compatible with the measurements performed on silicon dioxide sensors, three different concentration of NaCl were chosen as 25 mM, 100 mM, and 400 mM. From Fig.4.4.11 – Panel A, yeast tRNA hardly bound on PET-G sensor surfaces when the concentration of NaCl was either low as 25 mM or high as 400 mM. The rapid frequency shifts occurred at approximate 85 min and 170 min in Fig.4.4.11 – Panel A were due to the buffer effect when changing from binding buffer to elution buffer, because they were compatible with the ones detected in the 'blank' experiment performed without any yeast tRNA. Thus the binding behavior of yeast tRNA was only influenced by different binding buffer conditions. The binding rates of yeast tRNA in binding buffers containing 25 mM NaCl and 400 mM NaCl were much smaller than the ones in binding buffers with 100 mM NaCl (Fig.4.4.12 and Table S-12). They were even close to zero and could be ignored because of the instrument noise. Therefore, the concentration of NaCl performed significant influence on the binding ability of yeast tRNA on PET-G surface.

In order to emphasize the significance to optimize the concentration of NaCl in binding buffers, the yeast tRNA binding ability on PET-G surfaces with binding buffers containing different concentration of NaCl but no divalent salt were measured via QCM-D. The range of NaCl concentration was from 25 mM, 100 mM, to 400 mM. The QCM-D results indicated that yeast tRNA did not

adsorb on PET-G surfaces at either low NaCl concentration (25 mM) or high NaCl concentration (400 mM) (Fig.4.4.13 – Panel A). The yeast tRNA binding to PET-G surfaces only occurred when the concentration of NaCl in binding buffer was 100 mM. Moreover, the binding rates of yeast tRNA in binding buffer containing 100 mM of NaCl, which were calculated every 10 min, were much higher than the ones with high NaCl concentration and low NaCl concentration (Fig.4.4.14 and Table S-13). Therefore, the binding ability of yeast tRNA on PET-G surface mainly depended on the concentration of NaCl in binding buffer. The most proper concentration of NaCl to enhance yeast tRNA binding on PET-G surface is 100 mM.

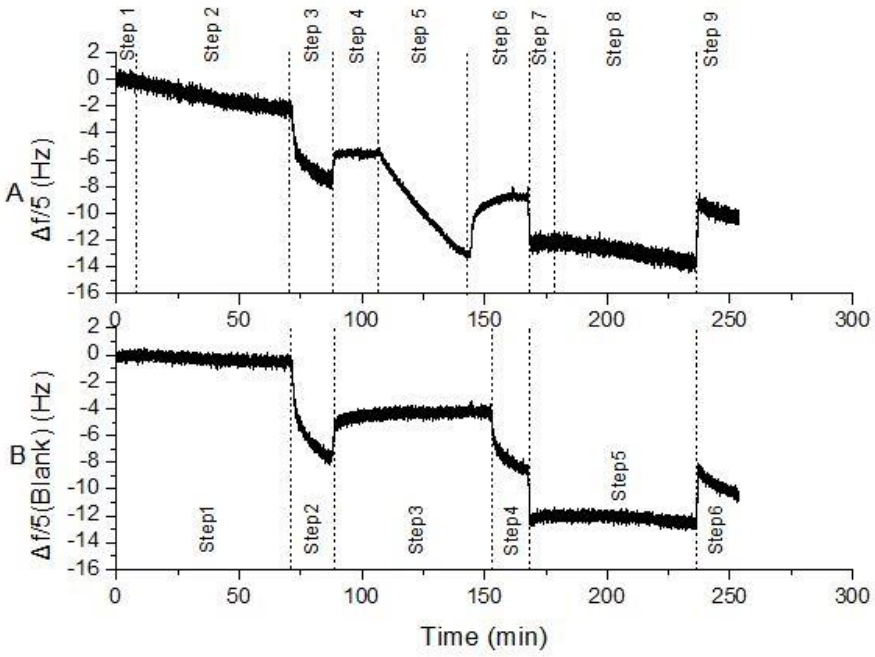

Fig.4.4.11. Frequency shift divided by the fifth overtone (Δf/5) as a function of time for yeast tRNA binding to PET-G sensor under binding buffer conditions with different concentration of NaCl (25 mM, 100 mM, and 400 mM) and 5 mM $MgCl_2$.
Panel A – Experiments with yeast tRNA solution: Step 1 - Binding buffer (25 mM Tris, 25 mM NaCl, 5 mM $MgCl_2$, pH 7.5); Step 2 – 5 μM yeast tRNA in same binding buffer as Step 1; Step 3 - Elution buffer (25 mM Tris, 10 mM EDTA, pH 8.5); Step 4 - Binding buffer (25 mM Tris, 100 mM NaCl, 5 mM $MgCl_2$, pH 7.5); Step 5 – 5 μM yeast tRNA in same binding buffer as Step 4; Step 6 (same as Step 3) - Elution buffer (25 mM Tris, 10 mM EDTA, pH 8.5); Step 7 - Binding buffer (25 mM Tris, 400 mM NaCl, 5 mM $MgCl_2$, pH 7.5); Step 8 – 5 μM yeast tRNA in same binding buffer as Step 7; Step 9 (same as Step 3) - Elution buffer (25 mM Tris, 10 mM EDTA, pH 8.5).

Panel B – 'Blank' experiments without any yeast tRNA: Step 1 - Binding buffer (25 mM Tris, 25 mM NaCl, 5 mM $MgCl_2$, pH 7.5); Step 2 - Elution buffer (25 mM Tris, 10 mM EDTA, pH 8.5); Step 3 - Binding buffer (25 mM Tris, 100 mM NaCl, 5 mM $MgCl_2$ pH 7.5); Step 4 (same as Step 2) - Elution buffer (25 mM Tris, 10 mM EDTA, pH 8.5); Step 5 - Binding buffer (25 mM Tris, 400 mM NaCl, 5 mM $MgCl_2$, pH 7.5); Step 6 (same as Step 2) - Elution buffer (25 mM Tris, 10 mM EDTA, pH 8.5).Finally, run binding buffer—25mM Tris, 400mM NaCl, 5mM $MgCl_2$, pH 7.5 (step 5), and change to elution buffer--25mM Tris, 10mM EDTA, pH 8.5 (step 6).

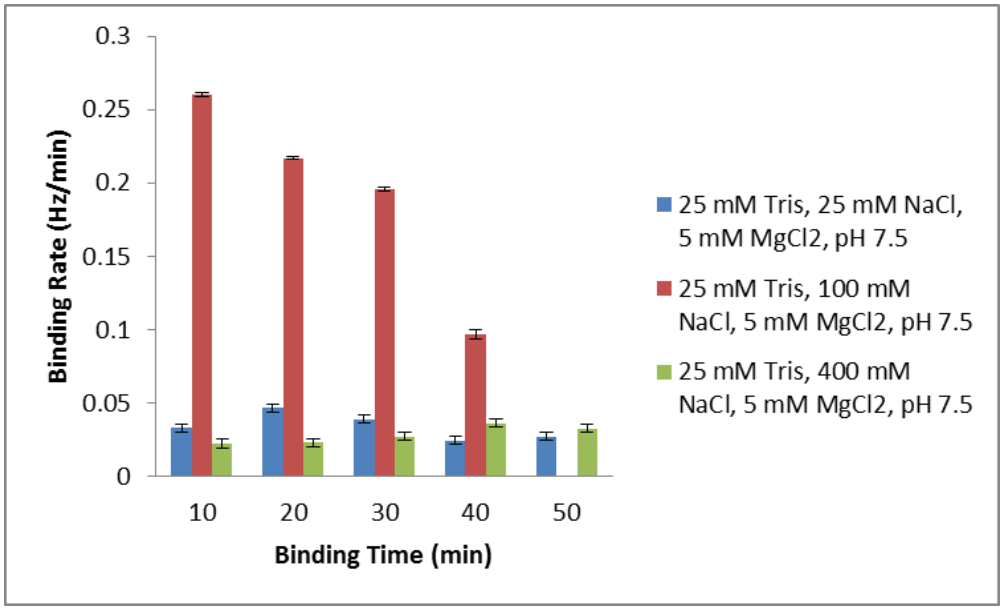

Fig.4.4.12. Binding Rates of yeast tRNA on PET-G surface obtained every 10 min under binding buffer conditions, which included different concentration of NaCl and 5 mM $MgCl_2$: 25 mM Tris, 25 mM NaCl, 5 mM $MgCl_2$, pH 7.5 (blue bars), 25 mM Tris, 100 mM NaCl, 5 mM $MgCl_2$, pH 7.5 (red bars), 25 mM Tris, 400 mM NaCl, 5 mM $MgCl_2$, pH 7.5 (green bars).

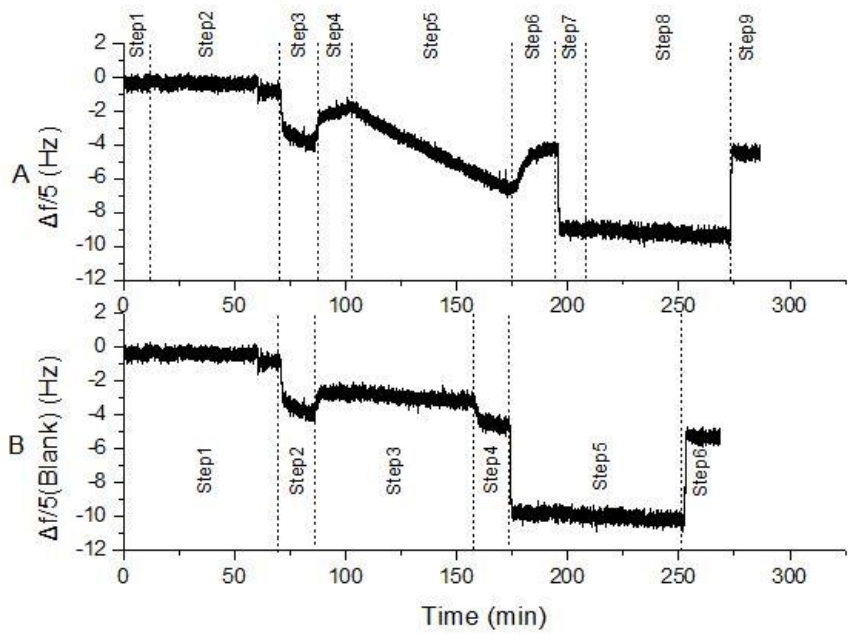

Fig.4.4.13. Frequency shift divided by the fifth overtone (Δf/5) as a function of time for yeast tRNA binding to PET-G sensor under binding buffer conditions with different concentration of NaCl (25 mM, 100 mM, and 400 mM).
Panel A – Experiments with yeast tRNA solution: Step 1 - Binding buffer (25 mM Tris, 25 mM NaCl, pH 7.5); Step 2 – 5 μM yeast tRNA in same binding buffer as Step 1; Step 3 - Elution buffer (25 mM Tris, 10 mM EDTA, pH 8.5); Step 4 - Binding buffer (25 mM Tris, 100 mM NaCl, pH 7.5); Step 5 – 5 μM yeast tRNA in same binding buffer as Step 4; Step 6 (same as Step 3) - Elution buffer (25 mM Tris, 10 mM EDTA, pH 8.5); Step 7 - Binding buffer (25 mM Tris, 400 mM NaCl, pH 7.5); Step 8 – 5 μM yeast tRNA in same binding buffer as Step 7; Step 9 (same as Step 3) - Elution buffer (25 mM Tris, 10 mM EDTA, pH 8.5).

Panel B – 'Blank' experiments without any yeast tRNA: Step 1 - Binding buffer (25 mM Tris, 25 mM NaCl, pH 7.5); Step 2 - Elution buffer (25 mM Tris, 10 mM EDTA, pH 8.5); Step 3 - Binding buffer (25 mM Tris, 100 mM NaCl, pH 7.5); Step 4 (same as Step 2) - Elution buffer (25 mM Tris, 10 mM EDTA, pH 8.5); Step 5 - Binding buffer (25 mM Tris, 400 mM NaCl, pH 7.5); Step 6 (same as Step 2) - Elution buffer (25 mM Tris, 10 mM EDTA, pH 8.5).

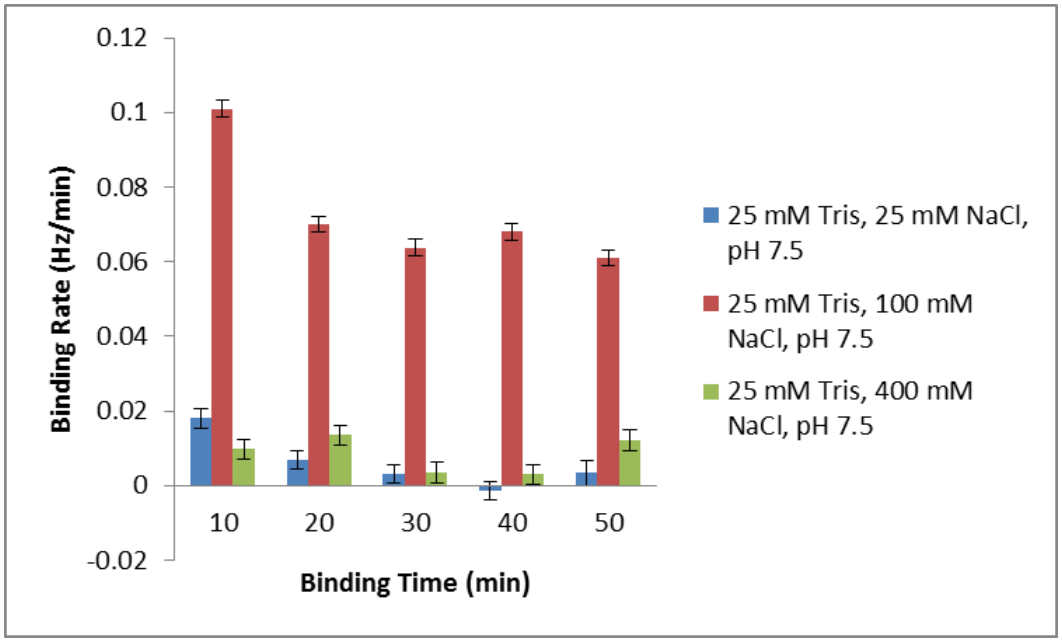

Fig.4.4.14. Binding Rates of yeast tRNA on PET-G surface obtained every 10 min under binding buffer conditions, which included different concentration of NaCl: 25 mM Tris, 25 mM NaCl, pH 7.5 (blue bars), 25 mM Tris, 100 mM NaCl, pH 7.5 (red bars), 25 mM Tris, 400 mM NaCl, pH 7.5 (green bars).

4.4.5 Influence of Different Concentration of KCl in Binding Buffers

Since the concentration of NaCl significantly influenced the binding ability of yeast tRNA on PET-G surface, the measurements under different concentration of KCl were further performed in order to identify whether each monovalent salt concentration could have dramatically influence. 5 mM of $MgCl_2$ was added to each binding buffer condition to maximize the yeast tRNA

adsorption on PET-G sensor surface. The frequency shift showed that yeast tRNA only bond to PET-G surface when the concentration of KCl in binding buffer was set to 100 mM (Fig.4.4.15 – Panel A). Furthermore, each frequency shift occurred when changing from elution buffer to binding buffer in Fig.4.4.15 – Panel A was compatible with the frequency shift occurred in corresponding 'blank' experiment without any yeast tRNA pumped into QCM-D. The binding rates calculated every 10 min were close to zero when the concentration of KCl was either too high (400 mM) or too low (25 mM) in Fig.4.4.16 (see Table S-14). It indicated that yeast tRNA hardly bound to PET-G surfaces under both buffer conditions. These results suggested that yeast tRNA only bound to PET-G surface in the presence of proper concentration of monovalent salt (either KCl or NaCl) in binding buffers.

In order to further confirm this conclusion, the yeast tRNA binding behavior on PET-G surface under binding buffers only containing different concentration of KCl (25 mM, 100 mM, and 400 mM) were measured. No divalent salt was involved in such experiments. The yeast tRNA was only detected adsorptions on PET-G surfaces when the binding buffer contained 100 mM KCl rather than 25 mM or 400 mM KCl (Fig.4.4.17 – Panel A). It indicated that yeast tRNA only showed countable binding rates under binding buffer with 100 mM of KCl (Fig.4.4.18 and Table S-15). Therefore, it is necessary and significant to optimize the concentration of monovalent salt in binding buffer

before performing the background pre-blocking using yeast tRNA during SELEX process.

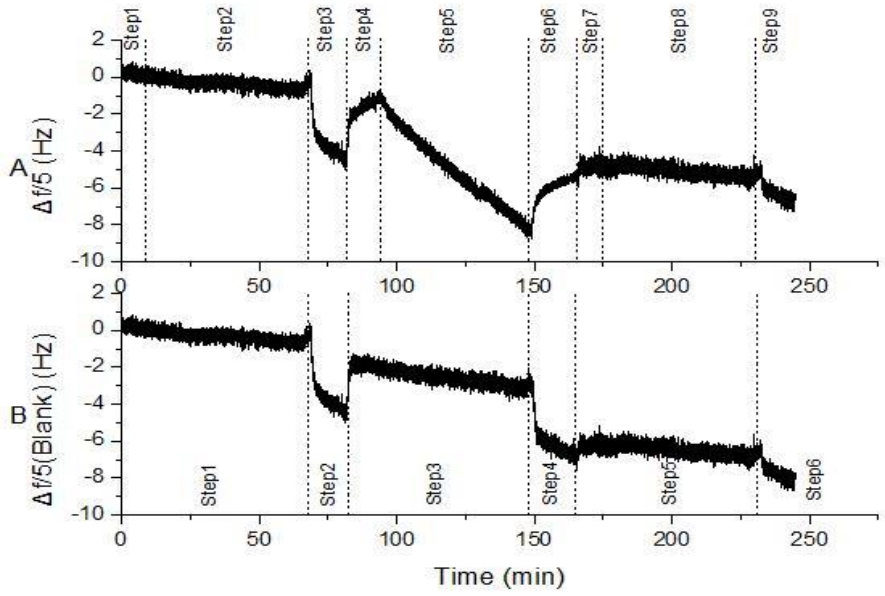

Fig.4.4.15. Frequency shift divided by the fifth overtone (Δf/5) as a function of time for yeast tRNA binding to PET-G sensor under binding buffer conditions with different concentration of KCl (25 mM, 100 mM, and 400 mM) and 5 mM $MgCl_2$.
Panel A – Experiments with yeast tRNA solution: Step 1 - Binding buffer (25 mM Tris, 25 mM KCl, 5 mM $MgCl_2$, pH 7.5); Step 2 – 5 μM yeast tRNA in same binding buffer as Step 1; Step 3 - Elution buffer (25 mM Tris, 10 mM EDTA, pH 8.5); Step 4 - Binding buffer (25 mM Tris, 100 mM KCl, 5 mM $MgCl_2$, pH 7.5); Step 5 – 5 μM yeast tRNA in same binding buffer as Step 4; Step 6 (same as Step 3) - Elution buffer (25 mM Tris, 10 mM EDTA, pH 8.5); Step 7 - Binding buffer (25 mM Tris, 400 mM KCl, 5 mM $MgCl_2$, pH 7.5); Step 8 – 5 μM yeast tRNA in same binding buffer as Step 7; Step 9 (same as Step 3) - Elution buffer (25 mM Tris, 10 mM EDTA, pH 8.5).

Panel B – 'Blank' experiments without any yeast tRNA: Step 1 - Binding buffer (25 mM Tris, 25 mM KCl, 5 mM $MgCl_2$, pH 7.5); Step 2 - Elution buffer (25 mM Tris, 10 mM EDTA, pH 8.5); Step 3 - Binding buffer (25 mM Tris, 100 mM KCl, 5 mM $MgCl_2$ pH 7.5); Step 4 (same as Step 2) - Elution buffer (25 mM Tris, 10 mM EDTA, pH 8.5); Step 5 - Binding buffer (25 mM Tris, 400 mM KCl, 5 mM $MgCl_2$, pH 7.5); Step 6 (same as Step 2) - Elution buffer (25 mM Tris, 10 mM EDTA, pH 8.5).

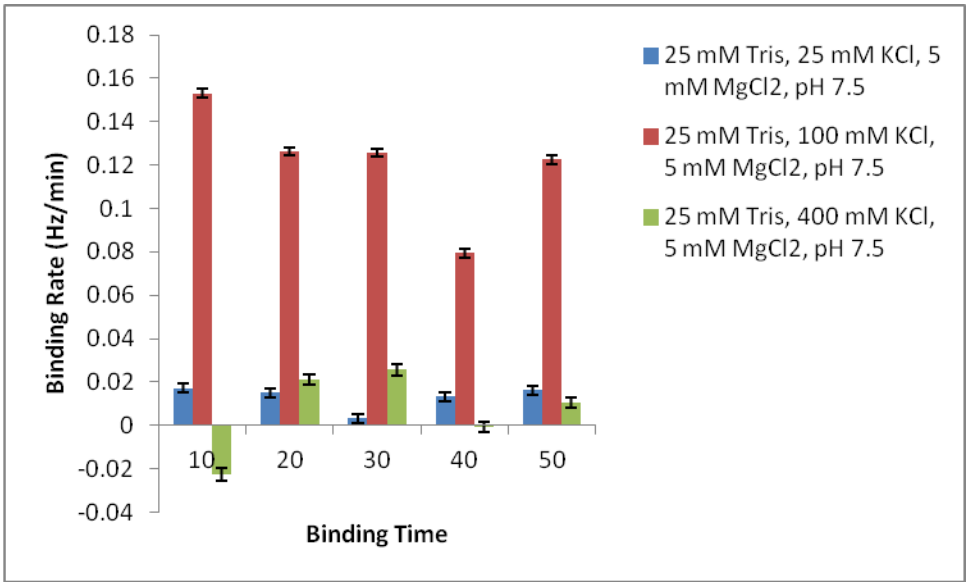

Fig.4.4.16. Binding Rates of yeast tRNA on PET-G surface obtained every 10 min under binding buffer conditions, which included different concentration of KCl and 5 mM $MgCl_2$: 25 mM Tris, 25 mM KCl, 5 mM $MgCl_2$, pH 7.5 (blue bars), 25 mM Tris, 100 mM KCl, 5 mM $MgCl_2$, pH 7.5 (red bars), 25 mM Tris, 400 mM KCl, 5 mM $MgCl_2$, pH 7.5 (green bars).

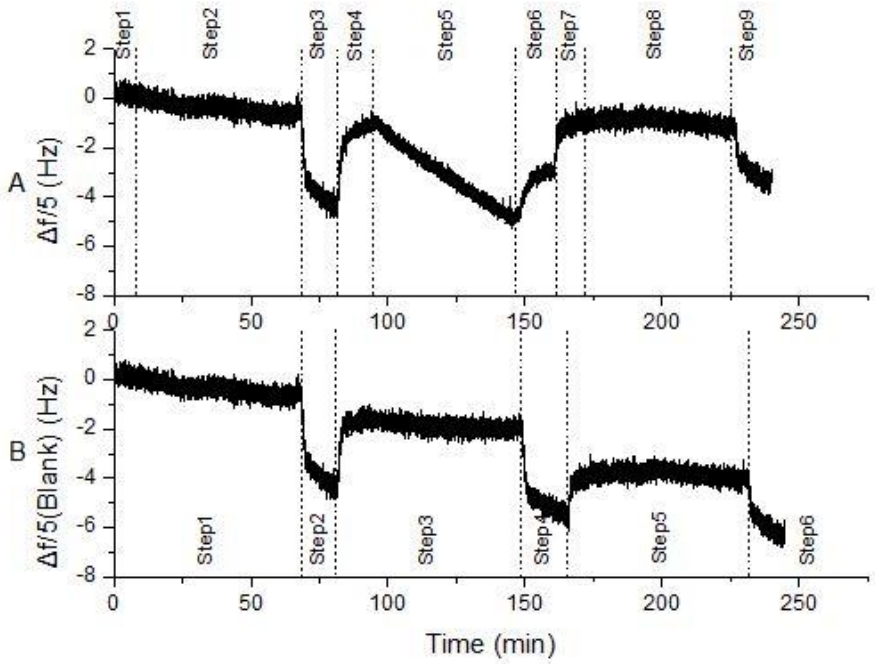

Fig.4.4.17. Frequency shift divided by the fifth overtone (Δf/5) as a function of time for yeast tRNA binding to PET-G sensor under binding buffer conditions with different concentration of KCl (25 mM, 100 mM, and 400 mM).
Panel A – Experiments with yeast tRNA solution: Step 1 - Binding buffer (25 mM Tris, 25 mM KCl, pH 7.5); Step 2 – 5 μM yeast tRNA in same binding buffer as Step 1; Step 3 - Elution buffer (25 mM Tris, 10 mM EDTA, pH 8.5); Step 4 - Binding buffer (25 mM Tris, 100 mM KCl, pH 7.5); Step 5 – 5 μM yeast tRNA in same binding buffer as Step 4; Step 6 (same as Step 3) - Elution buffer (25 mM Tris, 10 mM EDTA, pH 8.5); Step 7 - Binding buffer (25 mM Tris, 400 mM KCl, pH 7.5); Step 8 – 5 μM yeast tRNA in same binding buffer as Step 7; Step 9 (same as Step 3) - Elution buffer (25 mM Tris, 10 mM EDTA, pH 8.5).

Panel B – 'Blank' experiments without any yeast tRNA: Step 1 - Binding buffer (25 mM Tris, 25 mM KCl, pH 7.5); Step 2 - Elution buffer (25 mM Tris, 10 mM EDTA, pH 8.5); Step 3 - Binding buffer (25 mM Tris, 100 mM KCl, pH 7.5); Step 4 (same as Step 2) - Elution buffer (25 mM Tris, 10 mM EDTA, pH 8.5); Step 5 - Binding buffer (25 mM Tris, 400 mM KCl, pH 7.5); Step 6 (same as Step 2) - Elution buffer (25 mM Tris, 10 mM EDTA, pH 8.5).

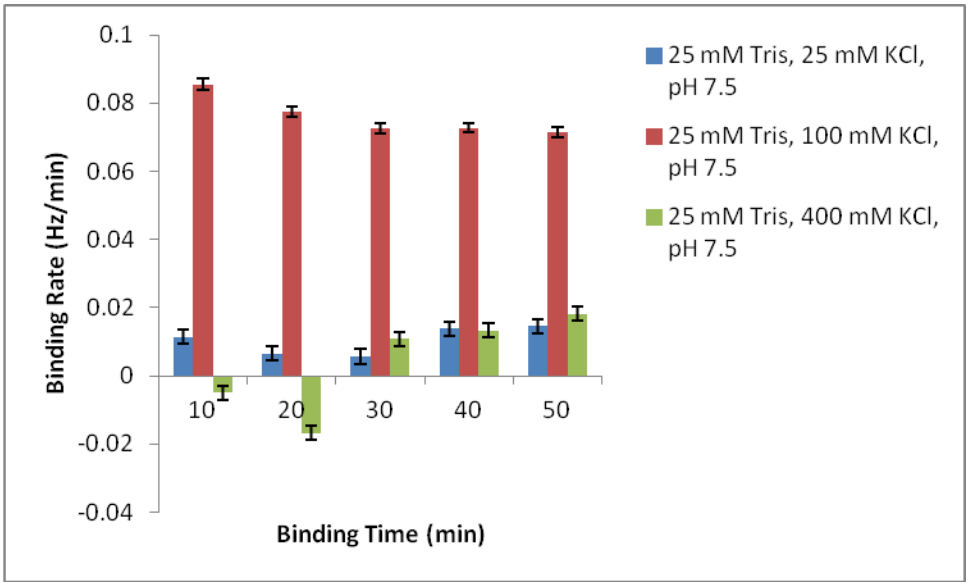

Fig.4.4.18. Binding Rates of yeast tRNA on PET-G surface obtained every 10 min under binding buffer conditions, which included different concentration of KCl: 25 mM Tris, 25 mM KCl, pH 7.5 (blue bars), 25 mM Tris, 100 mM KCl, pH 7.5 (red bars), 25 mM Tris, 400 mM KCl, pH 7.5 (green bars).

4.4.6 Influence of Binding Buffer pH

The pH of binding buffers influenced the binding ability of yeast tRNA on silicon dioxide surfaces significantly. Yeast tRNA was found only binding to silicon dioxide sensor surfaces when the pH of binding buffer was 7.5. Neither the binding buffer with pH of 6.5 nor with pH of 8.5 could result in yeast tRNA adsorption onto silicon dioxide surfaces. However, similar frequency shifts were observed while measuring the yeast tRNA binding abilities on PET-G surface with binding buffers of different pH (Fig.4.4.19 – Panel A). Containing equal

concentration of NaCl (100 mM) and $MgCl_2$ (5 mM) in Tris based buffers, yeast tRNA showed almost equally adsorption amount on PET-G surface with variety pH buffer conditions in approximate 60 min (Fig.4.4.19 – Panel A). Moreover, the frequency difference occurred when changing from elution buffer to binding buffer was compatible with the corresponding measurements performed in 'blank' experiments. That showed that all yeast tRNA was eluted from PET-G surface after pumping elution buffer into QCM-D, and did not influence the following measurement. Meanwhile, the binding rates calculated every 10 min did not have much difference among different pH values ranging from 6.5, 7.5, to 8.5 (Fig.4.4.20 and Table S-16).

Moreover, the frequency difference occurred when changing from elution buffer to binding buffer was compatible with the corresponding measurements performed in 'blank' experiments. That showed that all yeast tRNA was eluted from PET-G surface after pumping elution buffer into QCM-D, and did not influence the following measurement. In that case, the single variable quality in these experiments was the pH of binding buffer. Therefore, pH of binding buffer did not significantly influence the binding abillity of yeast tRNA on PET-G surfaces.

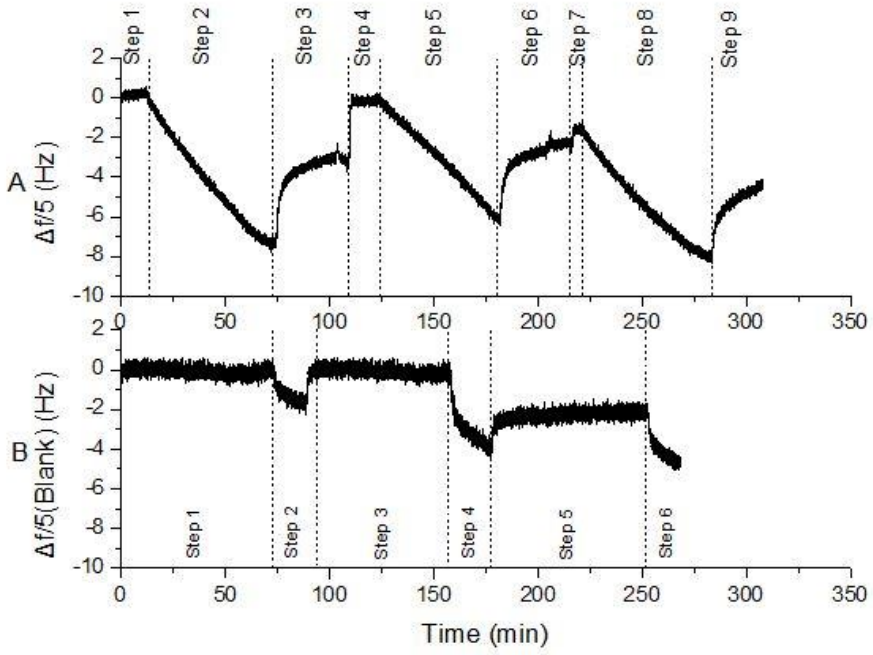

Fig.4.4.19. Frequency shift divided by the fifth overtone (Δf/5) as a function of time for yeast tRNA binding to PET-G sensor under binding buffer conditions with different pH (6.5,7.5, and 8.5).
Panel A – Experiments with yeast tRNA solution: Step 1 - Binding buffer (25 mM Tris, 100 mM NaCl, 5 mM $MgCl_2$, pH 6.5); Step 2 – 5 μM yeast tRNA in same binding buffer as Step 1; Step 3 - Elution buffer (25 mM Tris, 10 mM EDTA, pH 8.5); Step 4 - Binding buffer (25 mM Tris, 100 mM NaCl, 5 mM $MgCl_2$, pH 7.5); Step 5 – 5 μM yeast tRNA in same binding buffer as Step 4; Step 6 (same as Step 3) - Elution buffer (25 mM Tris, 10 mM EDTA, pH 8.5); Step 7 - Binding buffer (25 mM Tris, 100 mM NaCl, 5 mM $MgCl_2$, pH 8.5); Step 8 – 5 μM yeast tRNA in same binding buffer as Step 7; Step 9 (same as Step 3) - Elution buffer (25 mM Tris, 10 mM EDTA, pH 8.5).

Panel B – 'Blank' experiments without any yeast tRNA: Step 1 - Binding buffer (25 mM Tris, 100 mM NaCl, 5 mM $MgCl_2$, pH 6.5); Step 2 - Elution buffer (25 mM Tris, 10 mM EDTA, pH 8.5); Step 3 - Binding buffer (25 mM Tris, 100 mM NaCl, 5 mM $MgCl_2$ pH 7.5); Step 4 (same as Step 2) - Elution buffer (25 mM Tris, 10 mM EDTA, pH 8.5); Step 5 - Binding buffer (25 mM Tris, 100 mM NaCl, 5 mM $MgCl_2$, pH 8.5); Step 6 (same as Step 2) - Elution buffer (25 mM Tris, 10 mM EDTA, pH 8.5).

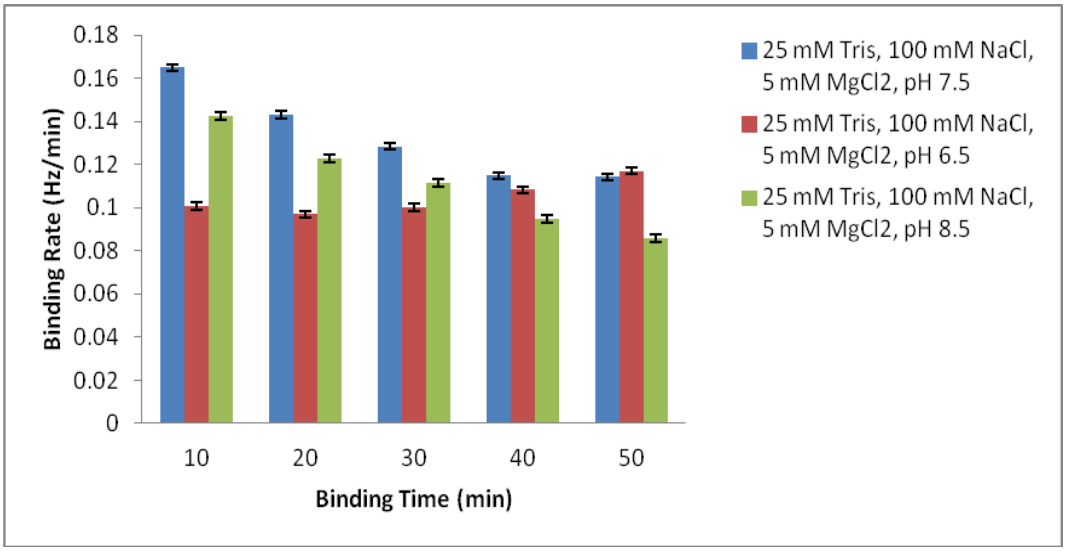

Fig.4.4.20. Binding Rates of yeast tRNA on PET-G surface obtained every 10 min under binding buffer conditions, which included different pH: 25 mM Tris, 100 mM NaCl, 5 mM $MgCl_2$, pH 6.5 (blue bars), 25 mM Tris, 100 mM NaCl, 5 mM $MgCl_2$, pH 7.5 (red bars), 25 mM Tris, 100 mM NaCl, 5 mM $MgCl_2$, pH 8.5 (green bars).

The binding rates of yeast tRNA on PET-G surfaces with binding buffer - 25 mM Tris, 100 mM NaCl, 5 mM $MgCl_2$, pH 7.5 – obtained from different measurements were compared in order to verify its consistency. Yeast tRNA still showed quite similar binding rates when the experiments were performed with different PET-G coated QCM-D sensor at different time (see Fig.4.4.21). It indicated that the QCM-D results of yeast tRNA binding on PET-G sensor surfaces were repeatable and reliable.

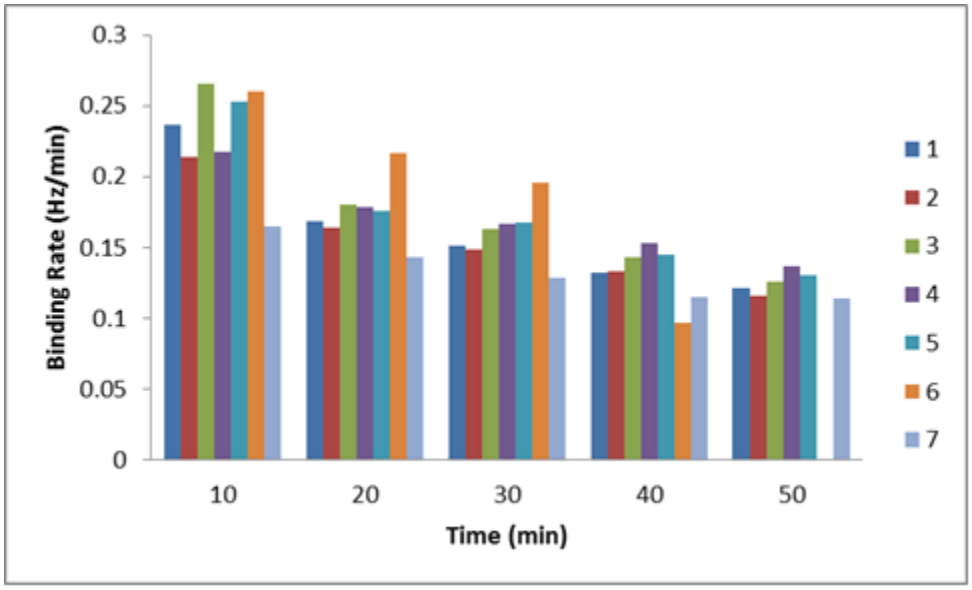

Fig.4.4.21. Binding Rates of yeast tRNA on PET-G surface obtained every 10 min under binding buffer condition – 25 mM Tris, 100 mM NaCl, 5 mM $MgCl_2$, pH 7.5: Bars 1-measurement performed in step 2 of Fig.4.4.1, Bars 2-measurement performed in step 11 of Fig.4.4.1, Bars 3-measurement performed in step 8 of Fig.4.4.5, Bars 4-measurement performed in step 2 of Fig.4.4.9, Bars 5-measurement performed in step 8 of Fig.4.4.9, Bars 6-measurement performed in step 5 of Fig.4.4.11, Bars 7-measurement performed in step 5 of Fig.4.4.19.

Chapter 5 Conclusions and Recommendations for Future Work

5.1 Conclusions

In this study, the yeast tRNA binding behaviour on both silicon dioxide surfaces and PET-G surfaces were studied under various binding buffer conditions using QCM-D.

The key findings from this study are summarized below:

- Yeast tRNA only bond to bare silicon dioxide surfaces when the binding buffers containing divalent salt, such as $MgCl_2$ and $CaCl_2$. Moreover, the presence of specific divalent cations, for example Mg^{2+} over Ca^{2+}, in the binding buffer greatly enhanced the binding of yeast tRNA on silicon dioxide surfaces.
- The concentration of $MgCl_2$ need to be optimized in order to increase the binding rates of yeast tRNA on silicon dioxide surface. The most proper concentration of $MgCl_2$ was 5 mM based on QCM-D measurement results.
- Monovalent salt in binding buffers influenced yeast tRNA binding ability on silicon dioxide surfaces as well. Yeast tRNA showed higher binding rates in binding buffers with NaCl other than with KCl at the same concentration.

- Yeast tRNA only bond on silicon dioxide surfaces with proper NaCl concentration (100 mM), and did not show any binding at lower (25 mM) or higher (400 mM) NaCl concentration.
- The binding of yeast tRNA on silicon dioxide surface also required strict pH condition. Yeast tRNA binding was only observed when the pH was adjusted to 7.5 other than 6.5 or 8.5.
- For PET-G surfaces, the presence of divalent salt, especially $MgCl_2$ over $CaCl_2$, improved yeast tRNA binding ability dramatically. However, different with silicon dioxide surfaces, yeast tRNA still bond to PET-G surfaces at relatively lower rates when binding buffer did not contain any divalent salt.
- The binding rates of yeast tRNA on PET-G surfaces increased with the increasing concentration of $MgCl_2$ (from 0.2 mM to 5 mM, but decreased if the concentration was too high (from 5 mM to 25 mM). The most proper concentration of $MgCl_2$ to enhance yeast tRNA binding on PET-G surfaces was 5 mM.
- The concentration of $CaCl_2$ did not influence the yeast tRNA binding ability on PET-G surfaces.
- The influence of different monovalent salt and different monovalent salt concentration on yeast tRNA binding ability to PET-G surfaces was also

measured. The results showed that yeast tRNA had higher binding rates when NaCl rather than KCl was the monovalent salt in binding buffers.

- Similar with binding behaviour on silicon dioxide, the concentration of monovalent salt, including both NaCl and KCl, influenced yeast tRNA binding on PET-G surfaces significantly. Yeast tRNA did not show any binding on PET-G surfaces at low concentration of monovalent salt (25 mM NaCl or 25 mM KCl) or high concentration of monovalent salt (400 mM NaCl or 400 mM KCl). Therefore, the concentration of monovalent salt had to be fixed at 100 mM.
- Binding buffer pH did not affect yeast tRNA binding ability on PET-G surface significantly.

Overall, the results have clearly quantified the influence of different binding buffer conditions on yeast tRNA binding on silicon dioxide surfaces and PET-G surfaces. These results provided initial quantitative information to guide the design of aptamer selection processes.

5.2 Recommendations for Future Works

Future studies should be designed to focus on actual aptamer selection process. Yeast tRNA binding behavior on PET-G sensor surfaces which were immobolized by Ni-NTA functional groups could be measured using QCM-D.

After identifying which is the optimized binding buffer condition for yeast tRNA to block the possible binding spots on surface, measurements could be further performed on PET-G sensor surface coated with targets. Quantity analysis could be done to confirm whether the modified binding buffer condition (25 mM Tris, 100 mM NaCl, 5 mM $MgCl_2$, pH 7.5) is the optimized binding buffer. After pre-blocking every possible background binding spots with yeast tRNA, RNA aptamer library in the same binding buffer can be pumped into QCM-D system. Therefore, the QCM-D frequency shift could represent how much aptamer bound to the sensor surface after pre-blocking.Compared with the one without pumping any yeast tRNA, the efficiency of yeast tRNA pre-blocking can be quantified.

Furthermore, quantitative polymerize chain reaction (qPCR) is an advanced technique to quantity analysis the background binding after pre-blocking with yeast tRNA. Yeast tRNA in binding buffer (25 mM Tris, 100 mM NaCl, 5 mM $MgCl_2$, pH 7.5) can be injected into empty PET-G substrate microcolumns via a standard syringe pump. After yeast tRNA blocking any possible binding sites on the surface, certain concentration of RNA library will be injected afterwards. By analyzing RNA library concentration in outlet solutions via qPCR, the quantity of RNA aptamer bound on PET-G surface can be calculated. Repeat the experiment with another binding buffer condition, compared with which can verify whether binding buffer with 25 mM Tris, 100 mM NaCl, 5 mM $MgCl_2$, pH 7.5 is the optimized condition.

References

[1] Jayasena, S. D. (1999). Aptamers: an emerging class of molecules that rival antibodies in diagnostics. Clinical Chemistry, 45(9), 1628-1650.

[2] Ng, E. W., Shima, D. T., Calias, P., Cunningham, E. T., Guyer, D. R., & Adamis, A. P. (2006). Pegaptanib, a targeted anti-VEGF aptamer for ocular vascular disease. Nature Reviews Drug Discovery, 5(2), 123-132.

[3] Keefe, A. D., Pai, S., & Ellington, A. (2010). Aptamers as therapeutics. Nature Reviews Drug Discovery, 9(7), 537-550.

[4] Cerchia, L., Ducongé, F., Pestourie, C., Boulay, J., Aissouni, Y., Gombert, K., & Libri, D. (2005). Neutralizing aptamers from whole-cell SELEX inhibit the RET receptor tyrosine kinase. Plos Biology, 3(4), e123.

[5] McCauley, T. G., Hamaguchi, N., & Stanton, M. (2003). Aptamer-based biosensor arrays for detection and quantification of biological macromolecules. Analytical Biochemistry, 319(2), 244-250.

[6] Xiao, Y., Lubin, A. A., Heeger, A. J., & Plaxco, K. W. (2005). Label-free electronic detection of thrombin in blood serum by using an aptamer-based sensor. Angewandte Chemie International Edition, 44(34), 5456-5459.

[7] Swensen, J. S., Xiao, Y., Ferguson, B. S., Lubin, A. A., Lai, R. Y., Heeger, A. J., & Soh, H. T. (2009). Continuous, real-time monitoring of cocaine in undiluted blood serum via a microfluidic, electrochemical aptamer-based sensor. Journal of the American Chemical Society, 131(12), 4262-4266.

[8] Romig, T. S., Bell, C., & Drolet, D. W. (1999). Aptamer affinity chromatography: combinatorial chemistry applied to protein purification. Journal of Chromatography B: Biomedical Sciences and Applications, 731(2), 275-284.

[9] Cho, S., Lee, S. H., Chung, W. J., Kim, Y. K., Lee, Y. S., & Kim, B. G. (2004). Microbead-based affinity chromatography chip using RNA aptamer modified with photocleavable linker. Electrophoresis, 25(21-22), 3730-3739.

[10] Ellington, A. D., & Szostak, J. W. (1990). *In vitro* selection of RNA molecules that bind specific ligands. Nature, 346(6287), 818-822.

[11] Tuerk, C., & Gold, L. (1990). Systematic evolution of ligands by exponential enrichment: RNA ligands to bacteriophage T4 DNA polymerase. Science, 249(4968), 505-510.

[12] Stoltenburg, R., Reinemann, C., & Strehlitz, B. (2007). SELEX—a evolutionary method to generate high-affinity nucleic acid ligands. Biomolecular Engineering, 24(4), 381-403.

[13] Gopinath, S. C. B. (2007). Methods developed for SELEX. Analytical and Bioanalytical Chemistry, 387(1), 171-182.

[14] Hamula, C. L., Guthrie, J. W., Zhang, H., Li, X. F., & Le, X. C. (2006). Selection and analytical applications of aptamers. TrAC Trends in Analytical Chemistry, 25(7), 681-691.
[15] Cox, J. C., & Ellington, A. D. (2001). Automated selection of anti-protein aptamers. Bioorganic & Medicinal Chemistry, 9(10), 2525-2531.
[16] Aquino-Jarquin, G., & Toscano-Garibay, J. D. (2011). RNA aptamer evolution: two decades of selection. International Journal of Molecular Sciences, 12(12), 9155-9171.
[17] Ahmad, K. M., Oh, S. S., Kim, S., McClellen, F. M., Xiao, Y., & Soh, H. T. (2011). Probing the limits of aptamer affinity with a microfluidic SELEX platform. Plos One, 6(11), e27051.
[18] Bridonneau, P., Chang, Y. F., O'Connell, D., Gill, S. C., Snyder, D. W., Johnson, L., & Parma, D. H. (1998). High-affinity aptamers selectively inhibit human nonpancreatic secretory phospholipase A2 (hnps-PLA2). Journal of Medicinal Chemistry, 41(6), 778-786.
[19] Carothers, J. M., Goler, J. A., Kapoor, Y., Lara, L., & Keasling, J. D. (2010). Selecting RNA aptamers for synthetic biology: investigating magnesium dependence and predicting binding affinity. Nucleic Acids Research, gkq082.
[20] Topp, S., & Gallivan, J. P. (2010). Emerging applications of riboswitches in chemical biology. ACS Chemical Biology, 5(1), 139-148.
[21] Hianik, T., Ostatná, V., Sonlajtnerova, M., & Grman, I. (2007). Influence of ionic strength, pH and aptamer configuration for binding affinity to thrombin. Bioelectrochemistry, 70(1), 127-133.
[22] Krauss, I. R., Merlino, A., Randazzo, A., Novellino, E., Mazzarella, L., & Sica, F. (2012). High-resolution structures of two complexes between thrombin and thrombin-binding aptamer shed light on the role of cations in the aptamer inhibitory activity. Nucleic Acids Research, 40(16), 8119-8128.
[23] Cho, E. J., Collett, J. R., Szafranska, A. E., & Ellington, A. D. (2006). Optimization of aptamer microarray technology for multiple protein targets. Analytica Chimica ACTA, 564(1), 82-90.
[24] Baaske, P., Wienken, C. J., Reineck, P., Duhr, S., & Braun, D. (2010). Optical thermophoresis for quantifying the buffer dependence of aptamer binding. Angewandte Chemie International Edition, 49(12), 2238-2241.
[25] Vandeventer, P. E., Lin, J. S., Zwang, T. J., Nadim, A., Johal, M. S., & Niemz, A. (2012). Multiphasic DNA adsorption to silica surfaces under varying buffer, pH, and ionic strength conditions. The Journal of Physical Chemistry B, 116(19), 5661-5670.

[26] Nguyen, T. H., & Elimelech, M. (2007). Plasmid DNA adsorption on silica: kinetics and conformational changes in monovalent and divalent salts. Biomacromolecules, 8(1), 24-32.

[27] Franchi, M., Ferris, J. P., & Gallori, E. (2003). Cations as mediators of the adsorption of nucleic acids on clay surfaces in prebiotic environments. Origins of Life and Evolution of the Biosphere, 33(1), 1-16.

[28] Cai, P., Huang, Q., Zhang, X., & Chen, H. (2006). Adsorption of DNA on clay minerals and various colloidal particles from an Alfisol. Soil Biology and Biochemistry, 38(3), 471-476.

[29] Shen, Y., Kim, H., Tong, M., & Li, Q. (2011). Influence of solution chemistry on the deposition and detachment kinetics of RNA on silica surfaces. Colloids and Surfaces B: Biointerfaces, 82(2), 443-449.

[30] Wang, J., Rudzinski, J. F., Gong, Q., Soh, H. T., & Atzberger, P. J. (2012). Influence of target concentration and background binding on *in vitro* selection of affinity reagents. Plos One, 7(8), e43940.

[31] Latulippe, D. R., Szeto, K., Ozer, A., Duarte, F. M., Kelly, C. V., Pagano, J. M., & Craighead, H. G. (2013). Multiplexed microcolumn-based process for efficient selection of RNA aptamers. Analytical Chemistry, 85(6), 3417-3424.

[32] Höök, F., Kasemo, B., Nylander, T., Fant, C., Sott, K., & Elwing, H. (2001). Variations in coupled water, viscoelastic properties, and film thickness of a Mefp-1 protein film during adsorption and cross-linking: a quartz crystal microbalance with dissipation monitoring, ellipsometry, and surface plasmon resonance study. Analytical Chemistry, 73(24), 5796-5804.

[33] Sato, T., Ali, M. M., Pelton, R., & Cranston, E. D. (2012). DNA stickers promote polymer adsorption onto cellulose. Biomacromolecules, 13(10), 3173-3180.

[34] Michanek, A., Kristen, N., Höök, F., Nylander, T., & Sparr, E. (2010). RNA and DNA interactions with zwitterionic and charged lipid membranes—a DSC and QCM-D study. Biochimica et Biophysica Acta (BBA)-Biomembranes, 1798(4), 829-838.

[35] Fukusho, S., Furusawa, H., & Okahata, Y. (2002). *In vitro* selection and evaluation of RNA aptamers that recognize arginine-rich-motif model peptide on a quartz-crystal microbalance. Chemical Communications, (1), 88-89.

[36] Furusawa, H., Murakawa, A., Fukusho, S., & Okahata, Y. (2003). *In vitro* selection of N-Peptide-Binding RNA on a Quartz Crystal Microbalance to study a sequence specific interaction between the peptide and loop RNA. ChemBioChem, 4(2-3), 217-220.

[37] Li, Z., Rajendran, B., Kamins, T. I., Li, X., Chen, Y., & Williams, R. S. (2005). Silicon nanowires for sequence-specific DNA sensing: device fabrication and simulation. Applied Physics A, 80(6), 1257-1263.

[38] Kambhampati, D. K., Jakob, T. A., Robertson, J. W., Cai, M., Pemberton, J. E., & Knoll, W. (2001). Novel silicon dioxide sol-gel films for potential sensor applications: a surface plasmon resonance study. Langmuir, 17(4), 1169-1175.

[39] Christel, L. A., Petersen, K., McMillan, W., & Northrup, M. A. (1999). Rapid, automated nucleic acid probe assays using silicon microstructures for nucleic acid concentration. Journal of Biomechanical Engineering, 121(1), 22-27.

[40] Indest, T., Laine, J., Kleinschek, K. S., & Zemljič, L. F. (2010). Adsorption of human serum albumin (HSA) on modified PET films monitored by QCM-D, XPS and AFM. Colloids and Surfaces A: Physicochemical and Engineering Aspects, 360(1), 210-219.

[41] Pyle, A. (2002). Metal ions in the structure and function of RNA. JBIC Journal of Biological Inorganic Chemistry, 7(7-8), 679-690.

[42] Rogers, S. O., & Bendich, A. J. (1985). Extraction of DNA from milligram amounts of fresh, herbarium and mummified plant tissues. Plant Molecular Biology, 5(2), 69-76.

[43] Brouwer, N., Van Dijken, H., Ruiters, M. H., Van Willigen, J. D., & Ter Horst, G. J. (1992). Localization of dopamine D_2 receptor mRNA with non-radioactive in situ hybridization histochemistry. Neuroscience Letters, 142(2), 223-227.

[44] Simmons, D. M., Arriza, J. L., & Swanson, L. W. (1989). A complete protocol for in situ hybridization of messenger RNAs in brain and other tissues with radio-labeled single-stranded RNA probes. Journal of Histotechnology, 12(3), 169-181.

[45] Tombelli, S., Minunni, M., Luzi, E., & Mascini, M. (2005). Aptamer-based biosensors for the detection of HIV-1 Tat protein. Bioelectrochemistry, 67(2), 135-141.

[46] Vaughan, P., & Macreadie, I. G. (2007). Yeasts. Kirk-Othmer Encyclopedia of Chemical Technology.

[47] Lehrach, H., Diamond, D., Wozney, J. M., & Boedtker, H. (1977). RNA molecular weight determinations by gel electrophoresis under denaturing conditions, a critical reexamination. Biochemistry, 16(21), 4743-4751.

[48] Q-Sense: http://www.biolinscientific.com/q-sense/products/

[49] Sauerbrey, Z. (1959). Use of quartz crystal vibrator for weighting thin films on a microbalance. Phys. 155, 206-222.

[50] Quevedo, I. R., & Tufenkji, N. (2009). Influence of solution chemistry on the deposition and detachment kinetics of a CdTe quantum dot examined

using a quartz crystal microbalance. Environmental Science & Technology, 43(9), 3176-3182.

[51] Singer, B. S., Shtatland, T., Brown, D., & Gold, L. (1997). Libraries for genomic SELEX. Nucleic Acids Research, 25(4), 781-786.

[52] Walls, D. J. (1991). Application of ATR-IR to the analysis of surface structure and orientation in uniaxially drawn poly (ethyleneterephthalate). Applied Spectroscopy, 45(7), 1193-1198.

[53] Wilfinger, W. W., Mackey, K., & Chomczynski, P. (1997). Effect of pH and ionic strength on the spectrophotometric assessment of nucleic acid purity. BioTechniques, 22(3), 474-481.

[54] Notley, S. M., Eriksson, M., & Wågberg, L. (2005). Visco-elastic and adhesive properties of adsorbed polyelectrolyte multilayers determined in situ with QCM-D and AFM measurements. Journal of Colloid and Interface Science, 292(1), 29-37.

[55] Feiler, A. A., Sahlholm, A., Sandberg, T., & Caldwell, K. D. (2007). Adsorption and viscoelastic properties of fractionated mucin (BSM) and bovine serum albumin (BSA) studied with quartz crystal microbalance (QCM-D). Journal of Colloid and Interface science, 315(2), 475-481.

[56] Malmström, J., Agheli, H., Kingshott, P., & Sutherland, D. S. (2007). Viscoelastic modeling of highly hydrated laminin layers at homogeneous and nanostructured surfaces: quantification of protein layer properties using QCM-D and SPR. Langmuir, 23(19), 9760-9768.

[57] Chowrira, B. M., Berzal-Herranz, A., & Burke, J. M. (1993). Ionic requirements for RNA binding, cleavage, and ligation by the hairpin ribozyme. Biochemistry, 32(4), 1088-1095.

[58] Uplinger, J., Thomas, B., Rollings, R., Fologea, D., McNabb, D., & Li, J. (2012). K^+, Na^+, and Mg^{2+} on DNA translocation in silicon nitride nanopores. Electrophoresis, 33(23), 3448-3457.

[59] Albrechts, B., Hautzinger, D. S., Kruger, M., Elwenspoek, M. C., Muller, K. M., & Korvink, J. G. (2010). Adsorption studies of DNA origami on silicon dioxide.

[60] Lin, S. Y., Chen, K. S., & Liang, R. C. (1999). Thermal micro ATR/FT-IR spectroscopic system for quantitative study of the molecular structure of poly (N-isopropylacrylamide) in water. Polymer, 40(10), 2619-2624.

[61] Delgado-Macuil, R., Rojas-López, M., Gayou, V. L., Orduña-Díaz, A., & Díaz-Reyes, J. (2007). ATR spectroscopy applied to photochromic polymer analysis. Materials Characterization, 58(8), 771-775.

[62] Urbaniak-Domagala, W. (2012). The Use of the Spectrometric Technique FTIR-ATR to Examine the Polymers Surface. Chapter 3.

[63] Allen, P., Worland, S., & Gold, L. (1995). Isolation of high-affinity RNA ligands to HIV-1 integrase from a random pool. Virology, 209(2), 327-336.

[64] Bartel, D. P., Zapp, M. L., Green, M. R., & Szostak, J. W. (1991). HIV-1 Rev regulation involves recognition of non-Watson-Crick base pairs in viral RNA. Cell, 67(3), 529-536.

[65] Bruno, J. G., & Kiel, J. L. (2002). Research report use of magnetic beads in selection and detection of biotoxin aptamers by electrochemiluminescence and enzymatic methods. BioTechniques, 32(1), 178-183.

[66] Stoltenburg, R., Reinemann, C., & Strehlitz, B. (2005). FluMag-SELEX as an advantageous method for DNA aptamer selection. Analytical and Bioanalytical Chemistry, 383(1), 83-91.

[67] Rhode, H., Schulze, M., Cumme, G. A., Göhlert, A., Blume, E., Bublitz, R., & Horn, A. (2000). Glycosylphosphatidylinositol-specific phospholipase D of human serum activity modulation by naturally occurring amphiphiles. Biological Chemistry, 381(5-6), 471-485.

[68] Gopinath, S. C., Sakamaki, Y., Kawasaki, K., & Kumar, P. K. (2006). An efficient RNA aptamer against human influenza B virus hemagglutinin. Journal of Ciochemistry, 139(5), 837-846.

[69] Gopinath, S. C., Misono, T. S., Kawasaki, K., Mizuno, T., Imai, M., Odagiri, T., & Kumar, P. K. (2006). An RNA aptamer that distinguishes between closely related human influenza viruses and inhibits haemagglutinin-mediated membrane fusion. Journal of General Virology, 87(3), 479-487.

[70] Dobbelstein, M., & Shenk, T. (1995). *In vitro* selection of RNA ligands for the ribosomal L22 protein associated with Epstein-Barr virus-expressed RNA by using randomized and cDNA-derived RNA libraries. Journal of Virology, 69(12), 8027-8034.

[71] Weiss, S., Proske, D., Neumann, M., Groschup, M. H., Kretzschmar, H. A., Famulok, M., & Winnacker, E. L. (1997). RNA aptamers specifically interact with the prion protein PrP. Journal of Virology, 71(11), 8790-8797.

[72] Elenbaas, B., Dobbelstein, M., Roth, J., Shenk, T., & Levine, A. J. (1996). The MDM2 oncoprotein binds specifically to RNA through its RING finger domain. Molecular Medicine, 2(4), 439.

[73] Kim, S. J., Kim, M. Y., Lee, J. H., You, J. C., & Jeong, S. (2002). Selection and stabilization of the RNA aptamers against the human immunodeficiency virus type-1 nucleocapsid protein. Biochemical and Biophysical Research Communications, 291(4), 925-931.

[74] Ciesiolka, J., Gorski, J., & Yarus, M. (1995). Selection of an RNA domain that binds Zn^{2+}. RNA, 1(5), 538-550.

[75] Nieuwlandt, D., Wecker, M., & Gold, L. (1995). *In vitro* selection of RNA ligands to substance P. Biochemistry, 34(16), 5651-5659.

[76] Li, Y., Geyer, R., & Sen, D. (1996). Recognition of anionic porphyrins by DNA aptamers. Biochemistry, 35(21), 6911-6922.

[77] Holeman, L. A., Robinson, S. L., Szostak, J. W., & Wilson, C. (1998). Isolation and characterization of fluorophore-binding RNA aptamers. Folding and Design, 3(6), 423-431.

[78] Yang, Q., Goldstein, I. J., Mei, H. Y., & Engelke, D. R. (1998). DNA ligands that bind tightly and selectively to cellobiose. Proceedings of the National Academy of Sciences, 95(10), 5462-5467.

[79] Bruno, J. G., & Kiel, J. L. (1999). *In vitro* selection of DNA aptamers to anthrax spores with electrochemiluminescence detection. Biosensors and Bioelectronics, 14(5), 457-464.

[80] Tok, J. B. H., Cho, J., & Rando, R. R. (2000). RNA aptamers that specifically bind to a 16S ribosomal RNA decoding region construct. Nucleic Acids Research, 28(15), 2902-2910.

[81] Smith, D., Kirschenheuter, G. P., Charlton, J., Guidot, D. M., & Repine, J. E. (1995). *In vitro* selection of RNA-based irreversible inhibitors of human neutrophil elastase. Chemistry & Biology, 2(11), 741-750.

[82] Goodman, S. D., Velten, N. J., Gao, Q., Robinson, S., & Segall, A. M. (1999). *In vitro* selection of integration host factor binding sites. Journal of Bacteriology, 181(10), 3246-3255.

[83] Zhang, F., & Anderson, D. (1998). *In vitro* selection of bacteriophage φ29 prohead RNA aptamers for prohead binding. Journal of Biological Chemistry, 273(5), 2947-2953.

[84] Rhie, A., Kirby, L., Sayer, N., Wellesley, R., Disterer, P., Sylvester, I., ... & Tahiri-Alaoui, A. (2003). Characterization of 2′-fluoro-RNA aptamers that bind preferentially to disease-associated conformations of prion protein and inhibit conversion. Journal of Biological Chemistry, 278(41), 39697-39705.

[85] Misono, T. S., & Kumar, P. K. (2005). Selection of RNA aptamers against human influenza virus hemagglutinin using surface plasmon resonance. Analytical Biochemistry, 342(2), 312-317.

[86] Blank, M., Weinschenk, T., Priemer, M., & Schluesener, H. (2001). Systematic evolution of a DNA aptamer binding to rat brain tumor microvessels selective targeting of endothelial regulatory protein pigpen. Journal of Biological Chemistry, 276(19), 16464-16468.

[87] Tuerk, C., MacDougal, S., & Gold, L. (1992). RNA pseudoknots that inhibit human immunodeficiency virus type 1 reverse transcriptase. Proceedings of the National Academy of Sciences, 89(15), 6988-6992.

[88] Schneider, D., Tuerk, C., & Gold, L. (1992). Selection of high affinity RNA ligands to the bacteriophage R17 coat protein. Journal of Molecular Biology, 228(3), 862-869.

[89] Giver, L., Bartel, D., Zapp, M., Pawul, A., Green, M., & Ellington, A. D. (1993). Selective optimization of the Rev-binding element of HIV-1. Nucleic Acids Research, 21(23), 5509-5516.

[90] Chen, H., & Gold, L. (1994). Selection of high-affinity RNA ligands to reverse transcriptase: inhibition of cDNA synthesis and RNase H activity. Biochemistry, 33(29), 8746-8756.

[91] Kubik, M. F., Stephens, A. W., Schneider, D., Marlar, R. A., & Tasset, D. (1994). High-affinity RNA ligands to human α-thrombin. Nucleic Acids Research, 22(13), 2619-2626.

[92] Jensen, K. B., Atkinson, B. L., Willis, M. C., Koch, T. H., & Gold, L. (1995). Using *in vitro* selection to direct the covalent attachment of human immunodeficiency virus type 1 Rev protein to high-affinity RNA ligands. Proceedings of the National Academy of Sciences, 92(26), 12220-12224.

[93] Pan, W., Craven, R. C., Qiu, Q., Wilson, C. B., Wills, J. W., Golovine, S., & Wang, J. F. (1995). Isolation of virus-neutralizing RNAs from a large pool of random sequences. Proceedings of the National Academy of Sciences, 92(25), 11509-11513.

[94] Berglund, J. A., Charpentier, B., & Rosbash, M. (1997). A high affinity binding site for the HIV-1 nucleocapsid protein. Nucleic acids research, 25(5), 1042-1049.

[95] Kumar, P. K. R., Machida, K., Urvil, P. T., Kakiuchi, N., Vishnuvardhan, D., Shimotohno, K., & Nishikawa, S. (1997). Isolation of RNA aptamers specific to the NS3 protein of hepatitis C virus from a pool of completely random RNA. Virology, 237(2), 270-282.

[96] Houser-Scott, F., Ansel-McKinney, P., Cai, J. M., & Gehrke, L. (1997). *In vitro* genetic selection analysis of alfalfa mosaic virus coat protein binding to 3'-terminal AUGC repeats in the viral RNAs. Journal of Virology, 71(3), 2310-2319.

[97] Lochrie, M. A., Waugh, S., Pratt, D. G., Clever, J., Parslow, T. G., & Polisky, B. (1997). *In vitro* selection of RNAs that bind to the human immunodeficiency virus type-1 gag polyprotein. Nucleic Acids Research, 25(14), 2902-2910.

[98] Baskerville, S., Zapp, M., & Ellington, A. D. (1999). Anti-Rex aptamers as mimics of the Rex-binding element. Journal of Virology, 73(6), 4962-4971.

[99] Hirao, I., Madin, K., Endo, Y., Yokoyama, S., & Ellington, A. D. (2000). RNA aptamers that bind to and inhibit the ribosome-inactivating protein, pepocin. Journal of Biological Chemistry, 275(7), 4943-4948.

[100] Kawakami, J., Imanaka, H., Yokota, Y., & Sugimoto, N. (2000). *In vitro* selection of aptamers that act with Zn^{2+}. Journal of Inorganic Biochemistry, 82(1), 197-206.

[101] Shtatland, T., Gill, S. C., Javornik, B. E., Johansson, H. E., Singer, B. S., Uhlenbeck, O. C., & Gold, L. (2000). Interactions of Escherichia coli RNA with bacteriophage MS2 coat protein: genomic SELEX. Nucleic Acids Research, 28(21), e93-e93.

[102] Fukuda, K., Vishnuvardhan, D., Sekiya, S., Hwang, J., Kakiuchi, N., Taira, K., Nishikawa, S. (2000). Isolation and characterization of RNA aptamers specific for the hepatitis C virus nonstructural protein 3 protease. European Journal of Biochemistry, 267(12), 3685-3694.

[103] Brunel, C., Ehresmann, B., Ehresmann, C., & McKeown, M. (2001). Selection of genomic target RNAs by iterative screening. Bioorganic & Medicinal Chemistry, 9(10), 2533-2541.

[104] Rusconi, C. P., Scardino, E., Layzer, J., Pitoc, G. A., Ortel, T. L., Monroe, D., & Sullenger, B. A. (2002). RNA aptamers as reversible antagonists of coagulation factor IXa. Nature, 419(6902), 90-94.

[105] Chi-hong, B. C., Chernis, G. A., Hoang, V. Q., & Landgraf, R. (2003). Inhibition of heregulin signaling by an aptamer that preferentially binds to the oligomeric form of human epidermal growth factor receptor-3. Proceedings of the National Academy of Sciences, 100(16), 9226-9231.

[106] White, R. R., Shan, S., Rusconi, C. P., Shetty, G., Dewhirst, M. W., Kontos, C. D., & Sullenger, B. A. (2003). Inhibition of rat corneal angiogenesis by a nuclease-resistant RNA aptamer specific for angiopoietin-2. Proceedings of the National Academy of Sciences, 100(9), 5028-5033.

[107] Kumarevel, T. S., Gopinath, S. C. B., Nishikawa, S., Mizuno, H., & Kumar, P. K. R. (2004). Identification of important chemical groups of the hut mRNA for HutP interactions that regulate the hut operon in Bacillus subtilis. Nucleic Acids Research, 32(13), 3904-3912.

[108] Sekiya, S., Noda, K., Nishikawa, F., Yokoyama, T., Kumar, P. K., & Nishikawa, S. (2006). Characterization and application of a novel RNA aptamer against the mouse prion protein. Journal of Biochemistry, 139(3), 383-390.

[109] Mann, D., Reinemann, C., Stoltenburg, R., & Strehlitz, B. (2005). *In vitro* selection of DNA aptamers binding ethanolamine. Biochemical and Biophysical Research Communications, 338(4), 1928-1934.

[110] Tang, J., Xie, J., Shao, N., & Yan, Y. (2006). The DNA aptamers that specifically recognize ricin toxin are selected by two *in vitro* selection methods. Electrophoresis, 27(7), 1303-1311.

[111] Mannironi, C., Di Nardo, A., Fruscoloni, P., & Tocchini-Valentini, G. P. (1997). *In vitro* selection of dopamine RNA ligands. Biochemistry, 36(32), 9726-9734.

[112] Meli, M., Vergne, J., Décout, J. L., & Maurel, M. C. (2002). Adenine-Aptamer Complexes A bioartite RNA site that binds the adenine nucleic base. Journal of Biological Chemistry, 277(3), 2104-2111.
[113] Huizenga, D. E., & Szostak, J. W. (1995). A DNA aptamer that binds adenosine and ATP. Biochemistry, 34(2), 656-665.
[114] Kiga, D., Futamura, Y., Sakamoto, K., & Yokoyama, S. (1998). An RNA aptamer to the xanthine/guanine base with a distinctive mode of purine recognition. Nucleic Acids Research, 26(7), 1755-1760.
[115] Koizumi, M., & Breaker, R. R. (2000). Molecular recognition of cAMP by an RNA aptamer. Biochemistry, 39(30), 8983-8992.
[116] Lorsch, J. R., & Szostak, J. W. (1994). *In vitro* selection of RNA aptamers specific for cyanocobalamin. Biochemistry, 33(4), 973-982.
[117] Lauhon, C. T., & Szostak, J. W. (1995). RNA aptamers that bind flavin and nicotinamide redox cofactors. Journal of the American Chemical Society, 117(4), 1246-1257.
[118] Burke, D. H., & Gold, L. (1997). RNA aptamers to the adenosine moiety of S-adenosyl methionine: structural inferences from variations on a theme and the reproducibility of SELEX. Nucleic Acids Research, 25(10), 2020-2024.
[119] Gebhardt, K., Shokraei, A., Babaie, E., & Lindqvist, B. H. (2000). RNA aptamers to S-adenosylhomocysteine: kinetic properties, divalent cation dependency, and comparison with anti-S-adenosylhomocysteine antibody. Biochemistry, 39(24), 7255-7265.
[120] Wilson, C., Nix, J., & Szostak, J. (1998). Functional requirements for specific ligand recognition by a biotin-binding RNA pseudoknot. Biochemistry, 37(41), 14410-14419.
[121] Boiziau, C., Dausse, E., Yurchenko, L., & Toulmé, J. J. (1999). DNA Aptamers selected against the HIV-1trans-activation-responsive RNA element form RNA-DNA kissing complexes. Journal of Biological Chemistry, 274(18), 12730-12737.
[122] Scarabino, D., Crisari, A., Lorenzini, S., Williams, K., & Tocchini-Valentini, G. P. (1999). tRNA prefers to kiss. The EMBO Journal, 18(16), 4571-4578.
[123] Geiger, A., Burgstaller, P., von der Eltz, H., Roeder, A., & Famulok, M. (1996). RNA aptamers that bind L-arginine with sub-micromolar dissociation constants and high enantioselectivity. Nucleic Acids Research, 24(6), 1029-1036.
[124] Famulok, M. (1994). Molecular recognition of amino acids by RNA-aptamers: an L-citrulline binding RNA motif and its evolution into an L-arginine binder. Journal of the American Chemical Society, 116(5), 1698-1706.

[125] Lozupone, C., Changayil, S., Majerfeld, I., & Yarus, M. (2003). Selection of the simplest RNA that binds isoleucine. RNA, 9(11), 1315-1322.
[126] Famulok, M., & Szostak, J. W. (1992). Stereospecific recognition of tryptophan agarose by *in vitro* selected RNA. Journal of the American Chemical Society, 114(10), 3990-3991.
[127] Vianini, E., Palumbo, M., & Gatto, B. (2001). *In vitro* selection of DNA aptamers that bind L-tyrosinamide. Bioorganic & Medicinal Chemistry, 9(10), 2543-2548.
[128] Majerfeld, I., Puthenvedu, D., & Yarus, M. (2005). RNA affinity for molecular L-histidine; genetic code origins. Journal of Molecular Evolution, 61(2), 226-235.
[129] Jeong, S., Eom, T. Y., Kim, S. J., Lee, S. W., & Yu, J. (2001). *In vitro* selection of the RNA aptamer against the Sialyl Lewis X and its inhibition of the cell adhesion. Biochemical and Biophysical Research Communications, 281(1), 237-243.
[130] Fukusaki, E. I., Kato, T., Maeda, H., Kawazoe, N., Ito, Y., Okazawa, A., & Kobayashi, A. (2000). DNA aptamers that bind to chitin. Bioorganic & Medicinal Chemistry letters, 10(5), 423-425.
[131] Mehedi Masud, M., Kuwahara, M., Ozaki, H., & Sawai, H. (2004). Sialyllactose-binding modified DNA aptamer bearing additional functionality by SELEX. Bioorganic & Medicinal Chemistry, 12(5), 1111-1120.
[132] Srisawat, C., Goldstein, I. J., & Engelke, D. R. (2001). Sephadex-binding RNA ligands: rapid affinity purification of RNA from complex RNA mixtures. Nucleic Acids Research, 29(2), e4-e4.
[133] Lato, S. M., Boles, A. R., & Ellington, A. D. (1995). *In vitro* selection of RNA lectins: using combinatorial chemistry to interpret ribozyme evolution. Chemistry & Biology, 2(5), 291-303.
[134] Wallace, S. T., & Schroeder, R. E. N. É. E. (1998). *In vitro* selection and characterization of streptomycin-binding RNAs: recognition discrimination between antibiotics. RNA, 4(1), 112-123.
[135] Wallis, M. G., von Ahsen, U., Schroeder, R., & Famulok, M. (1995). A novel RNA motif for neomycin recognition. Chemistry & Biology, 2(8), 543-552.
[136] Wang, Y., & Rando, R. R. (1995). Specific binding of aminoglycoside antibiotics to RNA. Chemistry & Biology, 2(5), 281-290.
[137] Lato, S. M., & Ellington, A. D. (1996). Screening chemical libraries for nucleic-acid-binding drugs by *in vitro* selection: a test case with lividomycin. Molecular Diversity, 2(1-2), 103-110.

[138] Schürer, H., Stembera, K., Knoll, D., Mayer, G., Blind, M., Förster, H. H., & Hahn, U. (2001). Aptamers that bind to the antibiotic moenomycin A. Bioorganic & Medicinal Chemistry, 9(10), 2557-2563.
[139] Berens, C., Thain, A., & Schroeder, R. (2001). A tetracycline-binding RNA aptamer. Bioorganic & Medicinal Chemistry, 9(10), 2549-2556.
[140] Burke, D. H., Hoffman, D. C., Brown, A., Hansen, M., Pardi, A., & Gold, L. (1997). RNA aptamers to the peptidyl transferase inhibitor chloramphenicol. Chemistry & Biology, 4(11), 833-843.

Appendix

Table S-1 Binding Buffers for Aptamer SELEX Process

Target	Binding Buffer	Reference
Arginine	10 mM HEPES, 100 mM NaCl, pH 7.5,	[35]
HIV-1 Integrase	50 mM Na-HEPES, 250/500 mM NaCl, 2 mM DTT, 10 mM $MnCl_2$, 5 mM CHAPS, pH 7.5	[63]
HIV-1-REV	45 mM Tris, 50 mM KCl, 2.5 mM DTT, 400 U/mL RNAsin, pH 8	[64]
Biotoxin	10 mM Tris-HCl, 500 mM NaCl, 1 mM $MgCl_2$, pH 7.5	[65]
Lysozyme	20 mM Tris, 100 mM NaCl, 5 mM $MgCl_2$, pH 7.5	[15]
Steptavidin	20 mM Tris-HCl, 100 mM NaCl, 5 mM KCl, 2 mM $MgCl_2$, 1 mM $CaCl_2$, 0.02% Tween 20, pH 7.6	[66]
Human oncostatin M	20 mM HEPES, 110 mM NaCl, 5 mM KCl, 1 mM $MgCl_2$, 1 mM $CaCl_2$, pH 7.0	[67]
B/Johannesburg influenza virus	50 mM Tris-HCl, 25 mM NaCl, 5 mM $MgCl_2$, pH 7.5	[68]
A/Panama influenza virus	20 mM HEPES, 105 mM NaCl, pH 7.4	[69]
Ribosomal protein L22	20 mM Tris-HCl,250 mM NaCl, 1 mM $MgCl_2$, 1 mM DTT, 1 mM EDTA, 0.05% Nonidet, pH 7.5	[70]
Prion	8 mM Na_2HPO_4, 0.87 mM KH_2PO_4, 136 mM NaCl, 112.6 mM KCl, 2 mM MgCl2, 2 mM DTT	[71]
MDM2	20 mM Tris, 150 mM NaCl, 5 mM $MgCl_2$, 1 mM DTT, 50 μM $ZnCl_2$, 0.10% Nonidet, 2% polyethylene glycol, pH 7.5	[72]
Nucleocapsid of HIV-1	50 mM Tris-HCl, 1 mM $MgCl_2$, 10 mM DTT,30 μM $ZnCl_2$, pH 7.5	[73]
Zinc	20 mM HEPES-Na, 400 mM NaCl, 1 mM $MgCl_2$, pH 7.0	[74]
Tachykinin substance P	10 mM HEPES, 150 mM NaCl, 5 mM KCl, 5 mM $CaCl_2$, pH 7.0	[75]

N-methylmesoporphyrin IX	100 mM Tris-acetate, 200 mM NaCl, 10 mM $MgCl_2$, 25 mM KOAc, 0.50% Triton X-100, 5% dimethyl sulfoxide, pH 7.4	[76]
Sulforhodamine B	10 mM Na-HEPES, 100 mM KCl, 5 mM $MgCl_2$, pH 7.4	[77]
Cellobiose	20 mM Tris, 100 mM NaCl, 5 mM $MgCl_2$, pH 7.5	[78]
Spores of B. antracis	40 mM Tris-HCl, 1 M NaCl, 2 mM $MgCl_2$, pH 7.5	[79]
A site of 16S rRNA	50 mM Tris-HCl, 1 M NaCl, 3 mM $MgCl_2$, pH 7.4	[80]
Neutrophil elastase	25 mM Tris, pH 7.5	[81]
Host factor (IHF)	50 mM Tris-Cl, 50 mM KCl, 1 mM EDTA, pH 7.8	[82]
Prohead	50 mM Tris-HCl, 10 mM $MgCl_2$, pH 7.8	[83]
Prion	20 mM HEPES, 100 mM NaCl, 50 mM KCl, 10 mM $MgCl_2$, pH 7.2	[84]
A/Panama influenza virus	0.01 M HEPES, 0.15 mM NaCl, 0.01% Tween 20, 3 mM EDTA, pH 7.4	[85]
YPEN-1 rat endothelial cells	50 mM TriszHCl, 100 mM NaCl, 5 mM KCl, pH 7.4	[86]
Reverse transcriptase (HIV-1)	50 mM Tris, 200 mM KOAc, 10 mM DTT, pH 7.7	[87]
Bacteriophage R17 coat protein	50 mM Tris, 100 mM KOAc, 10 mM DTT, pH 7.5	[88]
Rev-binding element of HIV-1	50 mM Tris-Cl, 50 mM KCl, pH 8.0	[89]
Reverse transcriptase	50 mM Tris-HC1, 200 mM KOAc, 10 mM DTT, pH 7.7	[90]
Human α-thrombin	50 mM Tris-HCl, 100 mM NaCl, 1 mM $MgCl_2$, 1 mM DTT, pH 7.7	[91]
HIV-1 Rev	50 mM TrisOAc, 200 mM KOAc, 10 mM DTT, pH 7.7	[92]
Rous sarcoma virus	20 mM Tris-HCl, 100 mM NaCl, 2.5 mM $MgCl_2$, pH 7.5	[93]
Nucleo capsid (NC) protein of HIV-1	50 mM Tris,100 mM NaCl, 1 mM $MgCl_2$, 10 mM DTT, 30 μM $ZnCl_2$, pH 7.5	[94]
NS3 of hepatitis C virus	50 mM Tris–HCl, 30 mM NaCl, 5 mM $CaCl_2$, 10 mM DTT, pH 7.7	[95]

Coat protein of alfalfa mosaic virus	10 mM Tris-HCl, 50 mM NaCl, 1 mM DTT, 1 mM EDTA, pH 7.5	[96]
HIV-1 gag polyprotein	50 mM Tris, 200 mM KOAc, 5 mM $MgCl_2$, 1 mM DTT, pH 7.5	[97]
Human nonpancreatic secretory phospholipaseA2	25 mM Tris, 150 mM NaCl, pH 5.8, 6.8, 7.4, 8.0, or 8.5	[18]
Rex fusion protein	50 mM Tris-HCl, 50 mM KCl, pH 8.0	[98]
Ribosome-inactivating protein	3 mM Tris-HCl, 45 mM NaCl, 3 mM $MgCl_2$, 0.15 mM DTT, 2.5 mM EDTA,3 mM Na_3PO_4, pH 7.5	[99]
HIV-1 Tat	2.5 mMTris–HCl, 100 mM NaCl, 2 mM $MgCl_2$, pH 7.6	[100]
Bacteriophage MS2 coat protein	100 mM HEPES-KOH, 80 mM KCl, 10 mM $MgCl_2$, pH 7.5	[101]
Hepatitis C virus nonstructural protein 3	50 mM Tris-HCl,30 mM NaCl, 5 mM $CaCl_2$, 10 mM DTT, pH 7.8	[102]
Drosophila transformer 2	50 mM Tris-HCl, 145 mM KCl, 3.2 mM $MgCl_2$, pH 8	[103]
Human coagulation factor IXa	20 mM HEPES, 50 mM NaCl, 2 mM $CaCl_2$, 0.01% sodium azide pH 7.4	[104]
Human epidermal growth factor receptor-3	10 mM HEPES, 100 mM NaCl, 2.5 mM $MgCl_2$, pH 7.4	[105]
Angiopoietin-2	20 mM HEPES, 150 mM NaCl, 2 mM $CaCl_2$, 0.01% sodium azide, pH 7.4	[106]
Histidine utilizing protein (HutP)	15 mM HEPES, 30 mM NaCl, 5 mM $MgCl_2$, pH 7.5	[107]
Histidine utilizing protein (HutP)	20 nM HEPES, 105 mM NaCl, pH 7.4	[69]
Mouse prion protein	20 mM Tris-HCl, 100 mM NaCl, pH 7	[108]
Ethanolamine	20 mM Tris-HCl, 200 mM NaCl, 5 mM KCl, 2 mM $MgCl_2$, 1 mM $CaCl_2$, 0.02% Tween 20, pH 7.6	[109]
Organic dyes	20 mM Tris-HCl, 500 mM KCl, pH 7.6	[10]
Ricin toxin	20 mM HEPES, 250 mM NaCl, 5 mM KCl, 1 mM $MgCl_2$, 1 mM $CaCl_2$, pH 7.35	[110]
Dopamine	50 mM Tris-HCl, 150 mM NaCl, 5 mM $MgCl_2$, pH 7.4,	[111]

Adenine	100 mM HEPES, 500 mM NaCl, 5 mM $MgCl_2$, pH 7.3	[112]
ATP	20 mM Tris, 300 mM NaCl, 5 mM $MgCl_2$, pH 7.6	[113]
Xanthine	20 mM Tris–HCl, 300 mM NaCl, 5 mM $MgCl_2$, pH 7.5	[114]
cAMP	20 mM Tris-HCl, 450 mM NaCl, 100 mM KCl, 10 mM $MgCl_2$, 5 mM $CaCl_2$, 1 mM $MnCl_2$, pH 7.5	[115]
Cyanocobalamin	25 mM HEPES, 1 M NaCl, 5 mM $MgCl_2$, pH 7.4	[116]
Riboflavin	20 mM HEPES, 300 mM KCl, 5 mM $MgCl_2$, pH 7.5	[117]
S-adenosyl methionine	50 mM Bis-Tris–HCl, 200 mM NaCl, 10 mM $MgCl_2$, pH 6.4	[118]
S-adenosyl homocysteine	25 mM Tris, 300 mM NaCl, 5 mM $MgCl_2$, pH 7.6	[119]
Biotin	10 mM NaHEPES, 100 mM KCl, 5 mM $MgCl_2$, pH 7.4	[120]
TAR RNA element of HIV-1	10 mM Tris-HCl, 50 mM NaCl, 10 mM $MgCl_2$, 1 mM DTT, pH 7.5	[121]
Yeast phenylalanine tRNA	50 mM Tris-HCl, 250 mM NaCl, 10 mM $MgCl_2$, 0.2 mM EDTA, pH 7.5	[122]
L-Arginine	50 mM Tris–HCl, 250 mM NaCl, 5 mM $MgCl_2$, pH 7.6	[123]
L-Citrulline	50 mM Tris-HCI, 250 mM NaCl, 5 mM $MgCl_2$, pH 7.6	[124]
L-Isoleucine	50 mM HEPES, 300 mM NaCl, 7.5 mM $MgCl_2$, 100 μM $ZnCl_2$, (pH7.0)	[125]
D-Tryptophan	50 mM Tris, 250 mM NaCl, 4 mM $MgCl_2$, pH 7.6	[126]
L-tyrosinamide	20 mM Tris, 300 mM NaCl, 5 mM $MgCl_2$, pH 7.6	[127]
L-histidine	50 mM Hepes, 250 mM NaCl, 5 mM $MgCl_2$, 5 mM $CaCl_2$, (pH 7.0)	[128]
Sialyl Lewis X	20 mM HEPES, 150 mM NaCl, 1 mM LiCl, 1 mM $MgCl_2$, pH 7.4	[129]
Chitin	50 mM Tris acetate, 100 mM NaCl, 100 mM KCl, 5 mM $MgCl_2$, pH 8.0	[130]
Sialyllactose	50 mM Tris–HCl, 250 mM NaCl, 5 mM $MgCl_2$, pH 7.6	[131]

Sephadex	50 mM HEPES, 100 mM NaCl, 10 mM $MgCl_2$, pH 7.4	[132]
Kanamycin A	50 mM Tris-HCl, 500 mM NaCl, pH 7.6	[133]
Streptomycin	50 mM Tris-HCl, 250 mM NaCl, 5 mM $MgCl_2$, pH 7.6	[134]
Neomycin	50 mM Tris-HCl, 250 mM NaCl, 5 mM $MgCl_2$, pH 7.6	[135]
Tobramycin	20 mM Tris acetate, 140 mM NaCl, 5 mM KCl, 1 mM $MgCl_2$, 1 mM $CaCl_2$, pH 7.4	[136]
Lividomycin	50 mM Tris-HC1, 500 mM NaCl, pH 7.6	[137]
Moenomycin A	20 mM HEPES, 150 mM NaCl, 5 mM $MgCl_2$, pH 7.4	[138]
Tetracycline	10 mM Tris–HCl, 250 mM NaCl, 5 mM $MgCl_2$, pH 7.6	[139]
Chloramphenicol	100 mM Bis-Tris–HCl, 400 mM NaCl, 20 mM $MgCl_2$, pH 6.4	[140]

Table S-2 Binding rates of yeast tRNA on silicon dioxide surfaces (with divalent salt and without divalent salt)

	Binding Rates (Hz/min)			
Binding time (min)	25 mM Tris, 100 mM NaCl, 5 mM MgCl2, pH 7.5	25 mM Tris, 100 mM NaCl, pH 7.5	25 mM Tris, 100 mM NaCl, 5 mM CaCl2, pH 7.5	25 mM Tris, 100 mM NaCl, 5 mM MgCl2, pH 7.5
10	0.0452 ±0.0033	0.0089 ±0.0027	0.0228 ±0.0029	0.0722 ±0.0030
20	0.0316 ±0.0026	0.0379 ±0.0029	0.0196 ±0.00314	0.0390 ±0.0030
30	0.0369 ±0.0031	0.0045 ±0.0033	0.0288 ±0.0029	0.0338 ±0.0031
40	0.0365 ±0.0028	0.0169 ±0.0032	0.0186 ±0.0029	0.0283 ±0.0029
50	0.0182 ±0.0027		0.0097 ±0.0031	0.0226 ±0.0030

Table S-3 Binding rates of yeast tRNA on silicon dioxide surfaces (different $MgCl_2$ concentration)

	Binding Rates (Hz/min)			
Binding time (min)	25 mM Tris, 100 mM NaCl, 0.2 mM MgCl2, pH 7.5	25 mM Tris, 100 mM NaCl, 1 mM MgCl2, pH 7.5	25 mM Tris, 100 mM NaCl, 5 mM MgCl2, pH 7.5	25 mM Tris, 100 mM NaCl, 25 mM MgCl2, pH 7.5
10	0.0015 ±0.0014	0.0126 ±0.0013	0.0866 ±0.0014	0.0217 ±0.0015
20	0.0004 ±0.0015	0.0603 ±0.0022	0.0599 ±0.0022	0.0168 ±0.0018
30	0.0007 ±0.0015	0.0544 ±0.0022	0.0633 ±0.0022	0.0136 ±0.0021
40	0.0008 ±0.0015	0.0477 ±0.0022	0.0563 ±0.0022	0.0061 ±0.0018
50		0.0421 ±0.0022	0.0488 ±0.0022	0.0108 ±0.0017

Table S-4 Binding rates of yeast tRNA on silicon dioxide surface (different $CaCl_2$ concentration)

	Binding Rates (Hz/min)			
Binding time (min)	25 mM Tris, 100 mM NaCl, 0.2 mM CaCl2, pH 7.5	25 mM Tris, 100 mM NaCl, 1 mM CaCl2, pH 7.5	25 mM Tris, 100 mM NaCl, 5 mM CaCl2, pH 7.5	25 mM Tris, 100 mM NaCl, 25 mM CaCl2, pH 7.5
10	0.0111 ±0.0023	0.0148 ±0.0023	0.0205 ±0.0023	0.0412 ±0.0023
20	0.0113 ±0.0024	0.0127 ±0.0022	0.0139 ±0.0022	0.0304 ±0.0023
30	0.0123 ±0.0023	0.0122 ±0.0023	0.0119 ±0.0022	0.0202 ±0.0024
40	0.0189 ±0.0023	0.0112 ±0.0022	0.0089 ±0.0021	0.0201 ±0.0024
50	0.0032 ±0.0023	0.0109 ±0.002256	0.0136 ±0.0023	0.0193 ±0.0023

Table S-5 Binding rates of yeast tRNA on silicon dioxide surface (different NaCl concentration)

	Binding Rates (Hz/min)		
Binding time (min)	25 mM Tris, 100 mM NaCl, 5 mM MgCl2, pH 7.5	25 mM Tris, 25 mM NaCl, 5 mM MgCl2, pH 7.5	25 mM Tris, 400 mM NaCl, 5 mM MgCl2, pH 7.5
10	0.1393 ±0.0029	0.0191 ±0.0026	-0.0144 ±0.0032
20	0.0818 ±0.0027	0.0115 ±0.0026	-0.0012 ±0.0031
30	0.0425 ±0.0028	0.0116 ±0.0027	0.0184 ±0.0033
40	0.0367 ±0.0030	0.0215 ±0.0026	0.0194 ±0.0033
50	0.0143 ±0.0033	0.0230 ±0.0031	0.0128 ±0.0035

Table S-6 Binding rates of yeast tRNA on silicon dioxide surfaces (different monovalent salt)

	Binding Rates (Hz/min)	
Binding time (min)	25 mM Tris, 100 mM NaCl, 5 mM MgCl2, pH 7.5	25 mM Tris, 100 mM KCl, 5 mM MgCl2, pH 7.5
10	0.0967 ±0.0018	0.0608 ±0.0012
20	0.0807 ±0.0017	0.0584 ±0.0012
30	0.0740 ±0.0018	0.0530 ±0.0012
40	0.0702 ±0.0018	0.0435 ±0.0012
50	0.0323 ±0.0021	0.0334 ±0.0013

Table S-7 Binding rates of yeast tRNA on silicon dioxide surface (different pH)

	Binding Rates (Hz/min)		
Binding time (min)	25 mM Tris, 100 mM NaCl, 5 mM MgCl2, pH 6.5	25 mM Tris, 100 mM NaCl, 5 mM MgCl2, pH 7.5	25 mM Tris, 100 mM NaCl, 5 mM MgCl2, pH 8.5
10	0.0012 ±0.0021	0.0633 ±0.0021	0.0350 ±0.0023
20	0.0076 ±0.0022	0.0534 ±0.0022	0.0048 ±0.0022
30	0.0049 ±0.0021	0.0578 ±0.0021	0.0393 ±0.0022
40	0.0078 ±0.0020	0.0508 ±0.0021	0.0112 ±0.0023
50	0.0012 ±0.0022	0.0532 ±0.0021	0.0100 ±0.0021

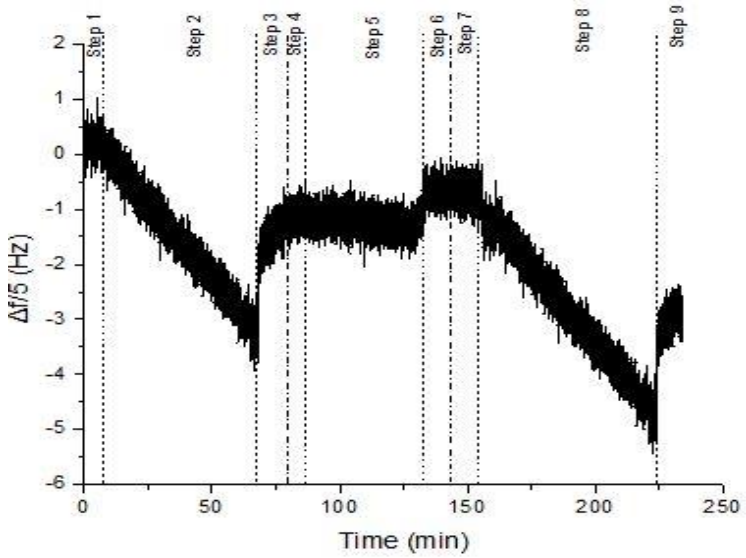

Fig.S-1. Frequency shift divided by the fifth overtone (Δf/5) as a function of time for yeast tRNA binding to silicon dioxide sensor under binding buffer conditions with different pH (6.5 and 7.5): Step 1 - Binding buffer (25 mM Tris, 100 mM NaCl, 5 mM $MgCl_2$, pH 7.5); Step 2 – 5 μM yeast tRNA in same binding buffer as Step 1; Step 3 - Elution buffer (25 mM Tris, 8 mM EDTA, pH 8.0); Step 4 - Binding buffer (25 mM Tris, 100 mM NaCl, 5 mM $MgCl_2$, pH 6.5); Step 5 – 5 μM yeast tRNA in same binding buffer as Step 4; Step 6 (same as Step 3) - Elution buffer (25 mM Tris, 8 mM EDTA, pH 8.0); Step 7 - Binding buffer (25 mM Tris, 100 mM NaCl, 5 mM $MgCl_2$, pH 7.5); Step 8 – 5 μM yeast tRNA in same binding buffer as Step 7; Step 9 (same as Step 3) - Elution buffer (25 mM Tris, 8 mM EDTA, pH 8.0).

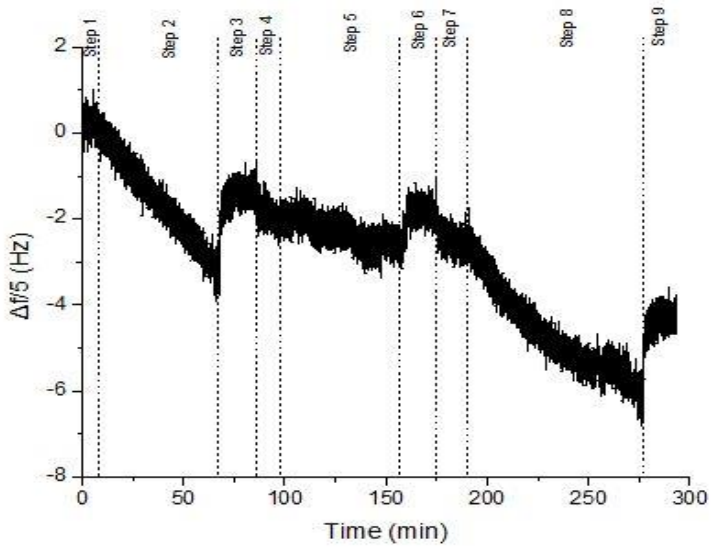

Fig.S-2. Frequency shift divided by the fifth overtone (Δf/5) as a function of time for yeast tRNA binding to silicon dioxide sensor under binding buffer conditions with different pH (8.5 and 7.5): Step 1 - Binding buffer (25 mM Tris, 100 mM NaCl, 5 mM $MgCl_2$, pH 7.5); Step 2 – 5 μM yeast tRNA in same binding buffer as Step 1; Step 3 - Elution buffer (25 mM Tris, 8 mM EDTA, pH 8.0); Step 4 - Binding buffer (25 mM Tris, 100 mM NaCl, 5 mM $MgCl_2$, pH 8.5); Step 5 – 5 μM yeast tRNA in same binding buffer as Step 4; Step 6 (same as Step 3) - Elution buffer (25 mM Tris, 8 mM EDTA, pH 8.0); Step 7 - Binding buffer (25 mM Tris, 100 mM NaCl, 5 mM $MgCl_2$, pH 7.5); Step 8 – 5 μM yeast tRNA in same binding buffer as Step 7; Step 9 (same as Step 3) - Elution buffer (25 mM Tris, 8 mM EDTA, pH 8.0).

Table S-8 Binding rates of yeast tRNA on PET-G surfaces (with divalent salt and without divalent salt)

	Binding Rates (Hz/min)			
Binding time (min)	25 mM Tris, 100 mM NaCl, 5 mM MgCl2, pH 7.5	25 M Tris, 100 mM NaCl, pH 7.5	25 mM Tris, 100 mM NaCl, 5 mM CaCl2, pH 7.5	25 mM Tris, 100 mM NaCl, 5 mM MgCl2, pH 7.5
10	0.2364 ±0.0019	0.1205 ±0.0019	0.1515 ±0.0020	0.2136 ±0.0019
20	0.1689 ±0.0019	0.0865 ±0.0019	0.0952 ±0.0020	0.1643 ±0.0019
30	0.1515 ±0.0018	0.0818 ±0.00196	0.0922 ±0.0020	0.1488 ±0.0018
40	0.1325 ±0.0018	0.0839 ±0.0019	0.0890 ±0.0020	0.1334 ±0.0018
50	0.1214 ±0.0019	0.0836 ±0.0020	0.0919 ±0.0017	0.1155 ±0.0016

Table S-9 Binding rates of yeast tRNA on PET-G surfaces (different $MgCl_2$ concentration)

	Binding Rates (Hz/min)			
Binding time (min)	25 mM Tris, 100 mM NaCl, 0.2 mM MgCl2, pH 7.5	25 mM Tris, 100 mM NaCl, 1 mM MgCl2, pH 7.5	25 mM Tris, 100 mM NaCl, 5 mM MgCl2, pH 7.5	25 mM Tris, 100 mM NaCl, 25 mM MgCl2, pH 7.5
10	0.1046 ±0.0014	0.1447 ±0.0019	0.2654 ±0.0019	0.1131 ±0.0013
20	0.0731 ±0.0013	0.1050 ±0.0019	0.1800 ±0.0018	0.0692 ±0.0012
30	0.0704 ±0.0013	0.0992 ±0.0019	0.1630 ±0.0018	0.0657 ±0.0013
40	0.0638 ±0.0013	0.0892 ±0.0019	0.1430 ±0.0018	0.0603 ±0.0012
50	0.0620 ±0.0014	0.0883 ±0.0020	0.1262 ±0.0018	0.0606 ±0.0012

Table S-10 Binding rates of yeast tRNA on PET-G surfaces (different $CaCl_2$ concentration)

	Binding Rates (Hz/min)			
Binding time (min)	25 mM Tris, 100 mM NaCl, 0.2 mM CaCl2, pH 7.5	25 mM Tris, 100 mM NaCl, 1 mM CaCl2, pH 7.5	25 mM Tris, 100 mM NaCl, 5 mM CaCl2, pH 7.5	25 mM Tris, 100 mM NaCl, 25 mM CaCl2, pH 7.5
10	0.1515 ±0.0020	0.1548 ±0.0023	0.1466 ±0.0019	0.1511 ±0.0019
20	0.1056 ±0.0019	0.1067 ±0.0019	0.1058 ±0.0019	0.1053 ±0.0019
30	0.1014 ±0.0019	0.1025 ±0.0019	0.1013 ±0.0019	0.1016 ±0.0019
40	0.0916 ±0.0018	0.0935 ±0.0018	0.0914 ±0.0018	0.0909 ±0.0018
50	0.0890 ±0.0019	0.0928 ±0.0019	0.0830 ±0.0019	0.0859 ±0.0019

Table S-11 Binding rates of yeast tRNA on PET-G surfaces (different monovalent salt)

	Binding Rates (Hz/min)		
Binding time (min)	25 mM Tris, 100 mM NaCl, 5 mM MgCl2, pH 7.5	25 mM Tris, 100 mM KCl, 5 mM MgCl2, pH 7.5	25 mM Tris, 100 mM NaCl, 5 mM MgCl2, pH 7.5
10	0.2172 ±0.0020	0.1547 ±0.0021	0.2531 ±0.0019
20	0.1782 ±0.0016	0.1218 ±0.0019	0.1757 ±0.0019
30	0.1667 ±0.0019	0.1194 ±0.0019	0.1679 ±0.0018
40	0.1526 ±0.0019	0.0902 ±0.0023	0.1448 ±0.0018
50	0.1365 ±0.0019	0.1189 ±0.0019	0.1300 ±0.0018

Table S-12 Binding rates of yeast tRNA on PET-G surfaces (different NaCl concentration with 5mM $MgCl_2$)

	Binding Rates (Hz/min)		
Binding time (min)	25 mM Tris, 25 mM NaCl, 5 mM MgCl2, pH 7.5	25 mM Tris, 100 mM NaCl, 5 mM MgCl2, pH 7.5	25 mM Tris, 400 mM NaCl, 5 mM MgCl2, pH 7.5
10	0.0330 ±0.0026	0.2601 ±0.0013	0.0227 ±0.0032
20	0.0466 ±0.0026	0.2171 ±0.0013	0.0230 ±0.0028
30	0.0389 ±0.0026	0.1957 ±0.0013	0.0271 ±0.0028
40	0.0246 ±0.0025	0.0966 ±0.0031	0.0364 ±0.0027
50	0.0271 ±0.0026		0.0327 ±0.0028

Table S-13 Binding rates of yeast tRNA on PET-G surfaces (different NaCl concentration)

	Binding Rates (Hz/min)		
Binding time (min)	25 mM Tris, 25 mM NaCl, pH 7.5	25 mM Tris, 100 mM NaCl, pH 7.5	25 mM Tris, 400 mM NaCl, pH 7.5
10	0.0180 ±0.0026	0.1010 ±0.0022	0.0097 ±0.0026
20	0.0068 ±0.0024	0.0700 ±0.0022	0.0135 ±0.0027
30	0.0031 ±0.0024	0.0638 ±0.0022	0.0033 ±0.0028
40	-0.0015 ±0.0024	0.0681 ±0.0022	0.0029 ±0.0028
50	0.0034 ±0.0034	0.0610 ±0.0022	0.0122 ±0.0027

Table S-14 Binding rates of yeast tRNA on PET-G surfaces (different KCl concentration with 5mM $MgCl_2$)

	Binding Rates (Hz/min)		
Binding time (min)	25 mM Tris, 25 mM KCl, 5 mM MgCl2, pH 7.5	25 mM Tris, 100 mM KCl, 5 mM MgCl2, pH 7.5	25 mM Tris, 400 mM KCl, 5 mM MgCl2, pH 7.5
10	0.0171 ±0.0020	0.1531 ±0.0019	-0.0227 ±0.0028
20	0.0151 ±0.0021	0.1264 ±0.0018	0.0210 ±0.0025
30	0.0031 ±0.0021	0.1259 ±0.0018	0.0256 ±0.0025
40	0.0133 ±0.0020	0.0794 ±0.0021	-0.0009 ±0.0023
50	0.0161 ±0.0020	0.1225 ±0.0018	0.0105 ±0.0023

Table S-15 Binding rates of yeast tRNA on PET-G surfaces (different KCl concentration)

	Binding Rates (Hz/min)		
Binding time (min)	25 mM Tris, 25 mM KCl, pH 7.5	25 mM Tris, 100 mM NaCl, pH 7.5	25 mM Tris, 400 mM NaCl, pH 7.5
10	0.0114 ±0.0020	0.0855 ±0.0018	-0.0050 ±0.0020
20	0.0065 ±0.0020	0.0773 ±0.0015	-0.0169 ±0.0021
30	0.0056 ±0.0021	0.0726 ±0.0015	0.0108 ±0.0020
40	0.0138 ±0.0020	0.0728 ±0.0015	0.0133 ±0.0020
50	0.0146 ±0.0020	0.0714 ±0.0015	0.0182 ±0.0021

Table S-16 Binding rates of yeast tRNA on PET-G surfaces (different pH)

	Binding Rates (Hz/min)		
Binding time (min)	25 mM Tris, 100 mM NaCl, 5 mM MgCl2, pH 7.5	25 mM Tris, 100 mM NaCl, 5 mM MgCl2, pH 6.5	25 mM Tris, 100 mM NaCl, 5 mM MgCl2, pH 8.5
10	0.1649 ±0.0017	0.1009 ±0.0017	0.1427 ±0.0017
20	0.1431 ±0.0016	0.0969 ±0.0016	0.1228 ±0.0016
30	0.1284 ±0.0017	0.1002 ±0.0016	0.1115 ±0.0018
40	0.1149 ±0.0016	0.1083 ±0.0016	0.0949 ±0.0018
50	0.1143 ±0.0017	0.1171 ±0.0016	0.0857 ±0.0017